

Department of Building Physics and Services

Fire Behaviour of Vertical Green System Vegetation: An Experimental and Computational Analysis

by

A.M. Schouten

MSC THESIS - 45 ECTS

Assessment committee

Member 1 (chair): Hooft, T.A.J. van
Member 2: Herpen, R.A.P. van
Member 3: Kramer, R.P.

Graduation

Program: Built Environment
Capacity group: Fire Safety
Supervisor: Herpen, R.
Date of defense: March 24, 2025
Student ID: 0990046
Study load (ECTS): 45
Track: Building Physics and Services

This thesis is public and Open Access.

This thesis has been realized in accordance with the regulations as stated in the TU/e Code of Scientific Conduct.

Disclaimer: the Department of Built Environment of Eindhoven University of Technology accepts no responsibility for the contents of MSc theses or practical training reports.

Contents

1 Abstract	1
2 Introduction	2
2.1 Problem Description	2
2.2 Relevance of this Research	2
2.3 Research Goals	4
2.3.1 Objectives	4
2.4 Fundamentals Fire Dynamics	4
2.5 Fundamentals Fire Safety	5
2.6 Types of VGS	6
2.7 Method	8
3 Experiments	9
3.1 The Aim	9
3.2 Peutz	9
3.3 Mobilane	10
3.3.1 samples	10
3.4 Method	11
3.4.1 intermediate fire test ISO 13785	11
3.4.2 Experimental setup	12
3.5 Results	16
3.6 Conclusion	22
4 Validation Study	26
4.1 Computational Domain and Geometry	26
4.2 CFD Software Type	26
4.3 Grid discretization	27
4.3.1 Grid levels	27
4.3.2 Calculation Lines	29
4.3.3 Grid Convergence Index (GCI)	29
4.4 Combustion model	30
4.4.1 Lagrangian particle model	32
4.5 Result Validation Study	33
4.6 Conclusion	37
5 Application Studies	38
5.1 Different Application Studies Conducted	38
5.2 Assessment Criteria/Method	39
5.3 Results	40
5.3.1 Different Moisture Content	40
5.3.2 Different plant density	41
5.3.3 Different leaf area	43
5.3.4 Lower Ignition Temperature	44
5.3.5 Removing lineburner	44
5.3.6 All Simulations	45
5.4 Elementary Effects Analysis	48
5.5 Conclusion	50
6 Discussion	52
7 Conclusion	53
8 Future Research	54

A Experiments	59
A.1 Experimental samples	60
A.2 Experimental Results	60
A.2.1 Test 1	60
A.2.2 Test 2	65
A.2.3 Test 3	67
A.2.4 Test 4	70
A.2.5 Overall Results	72
B Validation Study	73
B.1 Validation Study FDS Code	73
B.2 GCI Calculation Code Matlab	77
B.3 Matlab Code for Creating Average Temperature Image	82
C Application Studies	84
C.1 Moisture Simulations	84
C.2 Leaf Area Simulations	86
C.3 Vegetation Density	88
C.4 Lower Ignition Temperature	88
C.5 Removing Line Burner	88
C.6 Elementary Effects Matlab Code	89

List of Figures

1	Heat flux over 4 days of a bare Concrete wall and Concrete wall with a VGS [1]	3
2	Temperatures over 4 days of a bare Concrete wall and Concrete wall with a VGS [1]	3
3	Main and Sub-research Objectives	4
4	Fire Triangle	5
5	Natural Fire Curve [2]	5
6	Performance Based Fire Safety Engineering [3]	6
7	VGS types [4]	7
8	Most Common VGS plant types	7
9	Peutz Firesafety Lab [5]	9
10	MobiGreenFence Wall Planter VGS [6]	10
11	VGS Samples	11
12	Setup ISO 13785 (intermediate facade test) [7]	12
13	Setup 1	13
14	Setup back view	14
15	Numberering of thermocouples front view	14
16	Data logger setup	15
17	Specimen in setup 1	15
18	Final Setup 1 with Specimen	15
19	Test 1	16
20	Mass loss regression trend test 1	17
21	Test 2	18
22	Mass loss trend test 2	18
23	Test 3	19
24	Mass loss trend test 3	20
25	Test 4	20
26	Mass loss trend test 4	21
27	Median Temperatures of each Thermocouple per Test	22
28	Maximum Temperatures of each Thermocouple per Test	22
29	Samples after testing	24
30	Temperature ranges 80% datapoints per test per thermocouple	25
31	Validation study test domain	27
33	Grid levels	28
32	Allowed meshes in FDS from [8]	28
34	Calculations Lines Validation Study	29
35	Pine Needle Validation Study FDS [8]	32
36	Validation study setup	33
37	Median temperatures per thermocouple	33
38	Simulated and experimental temperatures	34
40	Average temperature recorded image	35
41	Maximum temperatures recorded per thermocouple	36
42	Boxplots Experiments and Validation Study	36
43	Temperatures at t=600	36
44	Different moisture Content Results	40
45	Average temperature image different moisture levels	42
46	Results different leaf area simulation	43
47	Results different leaf area simulation	44
49	Different moisture Content Results	45
50	Pyrolysis Gas Production All Simulations, With Gaussian Smoothing	47
51	Median Temperature at x=0 all simulations, With Gaussian Smoothing	47
52	Temperature over time of x=0 1m high	47
53	Normalized mass loss all Application Simulations	48
54	SBI-test Setup from [9]	59

55	Intermediate-fire test setup from [7]	60
56	Hook Supports for the Samples	61
57	Sample attached and cavity shown	61
58	Setup Experiment no Specimen	61
65	Temperature of thermocouples for test 1	62
59	Test 1 at t=0	62
60	Test 1 at t=3:45	62
61	Test 1 at t=10:00	62
62	Test 1 at t=13:45	62
63	Test 1 at t=25:00	62
64	Test 1 at t=30:00	62
66	Temperature of thermocouples for test 1, smoothed with gaussian	63
67	Temperature of thermocouples for test 1 per side, smoothed with gaussian	63
68	Setup 2	65
69	Test 2 at t=0:00	66
70	Test 2 at t=5:00	66
71	Test 2 at t=11:20	66
72	Test 2 at t=15:00	66
73	Test 2 at t=25:00	66
74	Test 2 at t=30:00	66
75	Temperature of thermocouples for test 2	66
76	Temperature of thermocouples for test 2, smoothed with gaussian	67
77	Temperature of thermocouples for test 2 per side, smoothed with gaussian	67
78	Setup 3	68
79	Test 3 at t=0:00	69
80	Test 3 at t=7:00	69
81	Test 3 at t=13:45	69
82	Test 3 at t=18:40	69
83	Test 3 at t=20:00	69
84	Test 3 at t=30:00	69
85	Temperature of thermocouples for test 3	69
86	Temperature of thermocouples for test 3, smoothed with gaussian	70
87	Temperature of thermocouples for test 3 per side, smoothed with gaussian	70
88	Test 4 at t=0:00	70
89	Test 4 at t=2:00	70
90	Test 4 at t=8:50	70
91	Test 4 at t=14:00	71
92	Test 4 at t=18:40	71
93	Test 4 at t=25:00	71
94	Temperature of thermocouples for test 4	71
95	Temperature of thermocouples for test 4, smoothed with gaussian	71
96	Temperature of thermocouples for test 4 per side, smoothed with gaussian	72
97	Boxplots of Temperatures per thermocouple per test	72
98	Average Temperatures Recorded along x=0	84
99	Average temperature image different moisture levels	84
103	Average temperature image different moisture levels	86

List of Tables

1	Overview mass loss and heat production	23
2	The median temperature recorded all thermocouples over the whole test time	23
3	Standard Deviation per Thermocouple all Simulations	24
4	Mesh sizing, number of cells [x, y, z] direction	28

5	Standard Deviation per Thermocouple	46
6	the total formed pyrolysis gas during the simulation	48
7	enthalpy of formation	64

1 Abstract

There is an increasing implementation of Vertical Green Systems (VGS) in urban environments which necessitates a thorough understanding of their fire behaviour to ensure fire safety. While VGS vegetation offer numerous benefits, their role as additional fire load in building facades remains insufficiently explored. This study aims to evaluate the fire behaviour of the vegetation of VGS through a combination of experimental fire tests and Computational Fluid Dynamics (CFD) using Fire Dynamic Simulator (FDS). The experiments were conducted in a controlled fire lab with the help of experts, and provided empirical data to validate the numerical models. The results indicate that vegetation alone does not generate extreme temperatures during combustion unless in direct contact with flames. Mass loss, caused by moisture evaporation and pyrolysis, occurred predominantly in areas exposed to direct ignition sources, with self-sustaining combustion being rare. The most influential parameters affecting fire behaviour were vegetation density and leaf geometry. Higher-density vegetation led to increased heat flux and prolonged burning duration. Whereas higher moisture content delayed ignition. Additionally, the experiments confirmed that a larger cavity between the VGS and the wall resulted in lower temperatures. The findings suggest that the fire risk associated with the vegetation of VGS can be effectively mitigated through appropriate vegetation selection, regular maintenance and the use of fire-resistant building materials. This study contributes to the body of knowledge by providing quantitative insights into the fire behaviour of the vegetation of VGS by using validated numerical models.

2 Introduction

2.1 Problem Description

The existing body of knowledge regarding green facades or vertical green systems (VGS) in the context of fire safety primarily focuses on their fire classification. Whilst this is valuable knowledge, there are still a lot of unknowns pertaining to vegetation of VGS and their fire behaviour. There is currently a lack of standards and guidelines pertaining to fire safety of VGS and due to the rising popularity of these systems it is of great importance to ensure that these systems are safe for the built environment.

To assess the potential fire safety risks posed by the vegetation of VGS with a non-combustible supporting system without introducing an extra cavity to the external wall, it is essential to examine how these systems influence fire behaviour. This includes analysing the impact of the additional fire load introduced by VGS, as well as understanding how various types of vegetation may affect burning characteristics.

2.2 Relevance of this Research

Over the last years green facades have been gaining popularity and are becoming more commonly used especially in cities. The world is urbanizing with over half the world's population, over 4 billion people, now living in urban areas. In the past few centuries and especially during the more recent decades, there has been a large shift from rural living to urban areas [10]. This transition in living type has also created a new set of problems for urban inhabitants, which are not as prevalent in rural situations.

This, however, is not the only shift that the world has encountered in recent decades. The impact of climate change has become more prevalent over the years and it is imperative to start thinking long-term when making impactful decisions, such as building construction is. The building sector is responsible for a large amount of the final energy consumption of Europe, in total about 40% [11]. There is a lot of focus on reducing the CO₂ emissions caused by the building sector. However, less attention is paid to the increasing temperatures over the world and the impact this has on the living comfort of its inhabitants [12]. As a consequence of rising temperatures, there is an increasing probability among the populace of overheating, which could lead to health problems, particularly for those who are vulnerable and of weaker health.[13]. In urban areas overheating is more likely to occur due to an effect called the urban heat island effect which can have disastrous effects for the inhabitants of cities [14, 15]. With the urbanization mentioned above of the world, it is important to start designing to mitigate the onset of this phenomenon.

VGS have gained traction over the last years for several different reasons. The first being that architects enjoy the green and environmentally friendly aesthetics that these green facades bring with them in a world in which it is becoming more important to be sustainable and environmentally friendly. Moreover, multiple studies have shown that having greenery in the vicinity of people's homes can be linked to improved overall mental health and well-being [16]. In urban areas where floor space is scarce and mostly utilized in functional ways, there is not a lot of space for greenery. This is why VGS would be a great solution for implementing more greenery whilst not losing usable living space.

Additionally, VGS helps with overall noise reduction. Which is important as long exposure to noise has been found to raise stress levels and impact peoples health [17]. Whilst not all VGS are evenly effective some have been found to have a reduction of around 5-10 dB whilst others range more from the 2.0 - 3.9 dB. Furthermore, studies indicate that reverberation time increases as the density of greenery coverage on VGS decreases. A similar positive correlation is observed with sound absorption, where an increase in greenery coverage leads to a higher sound absorption coefficient [18]. Moreover, VGS can reduce street noise by 2-3 dB and help minimize internal reverberation between building facades on opposite sides of a street [16].

Furthermore, studies have shown that VGS can help reduce the urban heat island effect [19, 20], by lowering the temperatures close to the wall by an average of 0.65 °C. This is due to the VGS evaporating moisture into the air which cools the overall temperature [19]. The implementation of green facades in urban areas can also help to broaden the biodiversity of the neighbourhoods [21, 22, 23].

In addition, VGS have been known to act as natural insulators for the buildings that they have been attached to, which would help to lower the overall energy use of the inhabitants. Cheng et al. [1] found that the addition of a VGS could significantly lower the overall heat flux of a concrete wall compared to a bare concrete wall in the same situation. Furthermore, they found that the VGS had an insulating effect. This is shown in Figure 2. Due to the VGS, the interior concrete surface fluctuated less in temperature compared to the interior wall of bare concrete [1]. The same conclusion was reached by Widiastuti et al. who conducted an experiment that looked at the temperature flux and the heat transfer of an exterior wall that had different amounts of leaf coverage from a VGS as well as a bare concrete wall as a control group [24].

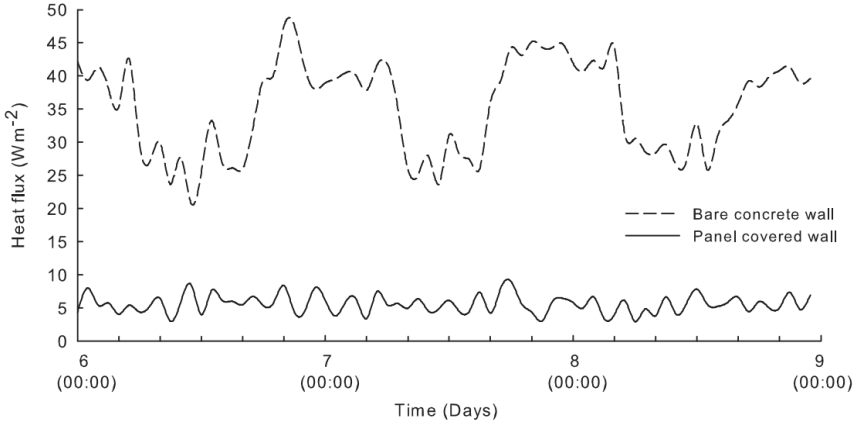


Figure 1: Heat flux over 4 days of a bare Concrete wall and Concrete wall with a VGS [1]

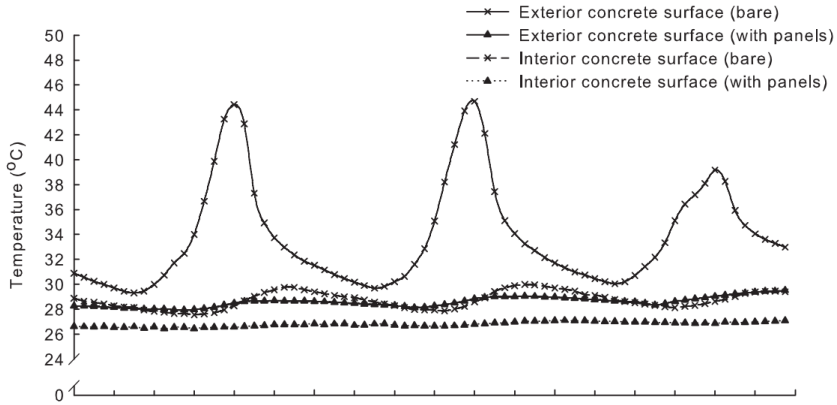


Figure 2: Temperatures over 4 days of a bare Concrete wall and Concrete wall with a VGS [1]

Moreover, green facades are great for catching fine particles matter such as heavy metals lead and calcium. These particles are collected on the leaves and generally washed off during the rain ending up in the soil. Not all particles wash off, as a part is absorbed and stored in the plant. Much like CO_2 which can also be absorbed by the plant which can help to improve the overall air quality of an urban environment [25, 26].

Overall, there are many positive aspects to implementing VGS in urban environments in the future. However, it should be done safely, and due to the newness of these facade types, there is not a lot of safety regulation regarding the fire safety of these facades. There have also not been many fires recorded in buildings which had a green facade in which the consequences of the fire could be viewed. Therefore, it is imperative to do research in this field to gain an understanding of how these systems would act in a fire and what the potential consequences could be. This way one can prevent disastrous situations from occurring due to a lack of knowledge and understanding of these VGS.

Whilst some research about the topic of VGS regarding their fire safety has been completed it is very little. Considering that there are also many different types of systems there are a lot of unknowns regarding these systems and their fire safety. As these systems are becoming more implemented over the world the fire risk due to the added load of the vegetation and the systems themselves should be taken into consideration and the building should be adapted correctly to ensure the safety of everyone.

2.3 Research Goals

In response to the previously mentioned issue, the following research goal has been defined:

To broaden the current body of knowledge concerning VGS and their impact on the fire behaviour of the building, with the aim to investigate whether the introduction of VGS may lead to unsafe situations.

Due to the wide scope of the above-mentioned research goal, a more specific research goal is formulated as follows:

To systematically assess the impact of vegetation on fire behaviour through a combination of experimental fire testing and validated Computational Fluid Dynamics (CFD) simulations, with the aim of quantifying its influence on combustion dynamics, heat transfer, and fire propagation characteristics.

2.3.1 Objectives

To help to fulfil the above-stated research goal the following main research objective has been established as can be seen in Figure 3. This figure also shows the sub-objectives which have been defined to help systematically answer the main research question.

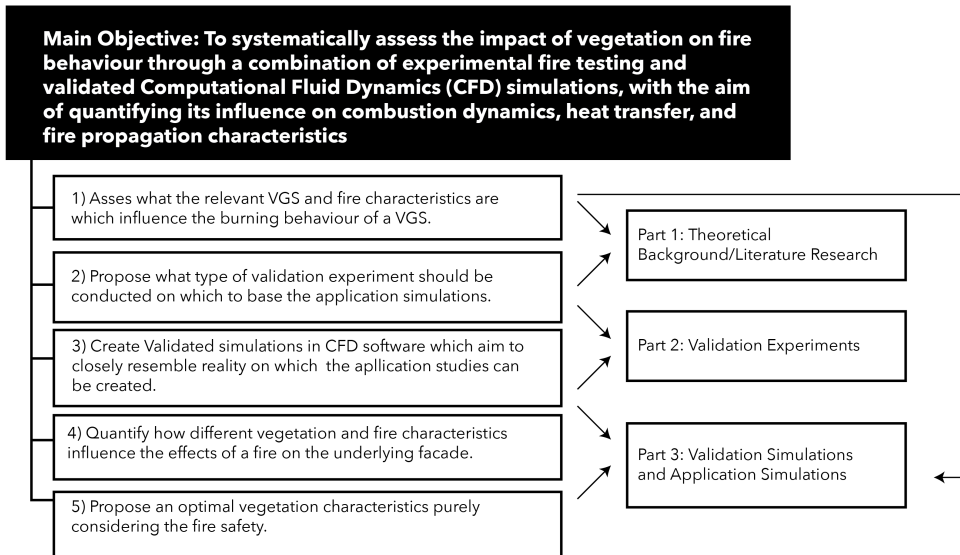


Figure 3: Main and Sub-research Objectives

2.4 Fundamentals Fire Dynamics

For a fire to burn successfully 3 different things are needed: heat, oxygen and fuel. These three elements make up the fire triangle, see Figure 4. With all of these three elements present, a fire will burn and keep burning successfully [27]. When one of the elements is removed fire will die out. Fire can be either fuel-controlled, meaning that the combustion is limited due to the amount of fuel that is available. A fire



Figure 4: Fire Triangle

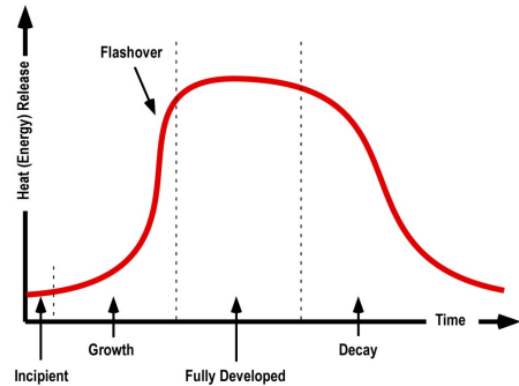


Figure 5: Natural Fire Curve [2]

is usually fuel-controlled during the growth phase. A fire can also be ventilation-controlled, which refers to there being a limited amount of oxygen available. And due to this limitation, it can't grow bigger, this is generally the case during the developed phase [2]. During a fire in a compartment, the fire follows the natural fire curve as seen in Figure 5. When a fire is ignited it will start as a fuel-controlled fire and after enough growth, flashover will occur which causes a big spike in the heat release rate (HRR). This is also when a fire becomes ventilation-controlled, meaning that the fire will be controlled by the amount of oxygen present in the compartment. Due to the closed nature of the compartment, there will most likely be a lack of oxygen which will cause the fire to die out. However, during this research, the fire which is analysed will be outside and thus will not be restricted by the amounts of oxygen present.

Furthermore, while flashover can theoretically occur in outdoor environments, the chance of this happening are minuscule. Flashover occurs due to a build-up of pyrolysis gasses within a confined space which when reaching a certain temperature spontaneously ignites. When this happens there is a big spike in HRR, as shown in Figure 5. As the gasses can dissipate in an outdoor environment these critical concentrations of pyrolysis gasses are most often not reached. Meaning, the natural fire curve will not necessarily be true for outdoor/exterior fires. The natural fire curve is not accurate for outdoor situations and whilst the theory should be understood it is not of great importance to this particular research. When biomass undergoes combustion, it engages in a singular chemical reaction where the fuel oxidizes, releasing thermal energy [28].

Heat is transferred through three primary mechanisms: radiation, convection, and conduction. Radiation involves the transfer of heat via electromagnetic waves and does not require a medium for propagation. Convection occurs in fluids, where heat is transported by the movement of the fluid itself, while conduction takes place in solids through direct molecular interactions. In the context of a fire, radiation plays a significant role, as a substantial amount of heat is lost to the surroundings through the air especially in non-compartmental fires [29, 30].

Ignition can happen in 2 ways: piloted ignition, wherein the fuel undergoes physical ignition induced by an external source, and spontaneous ignition, which ensues when an adequate thermal environment allows for the self-ignition of the pyrolysis gases produced, eliminating the need for a pilot flame [31].

2.5 Fundamentals Fire Safety

Fire safety is about the safety of the inhabitant, fire fighters as well as the preservation of the property. FSE makes use of performance-based engineering, meaning that the design needs to meet certain criteria in different categories to be seen as a successful design. This type of designing means that the project specifications differ per site and that the fire safety concepts are tailor-made to fit that specific building. There are many building codes and standards which also differ per function and building size to create a guideline of how to design in a fire safe manner [3].

Performance-based fire safety engineering encompasses 3 main categories: fire characteristics, building characteristics and human characteristics, with environment characteristics and intervention characteristics also playing a role as seen in Figure 6. When adding a VGS the building characteristics change, meaning that this will also have an impact on the fire characteristics and that the human characteristics may need to be changed in situations.

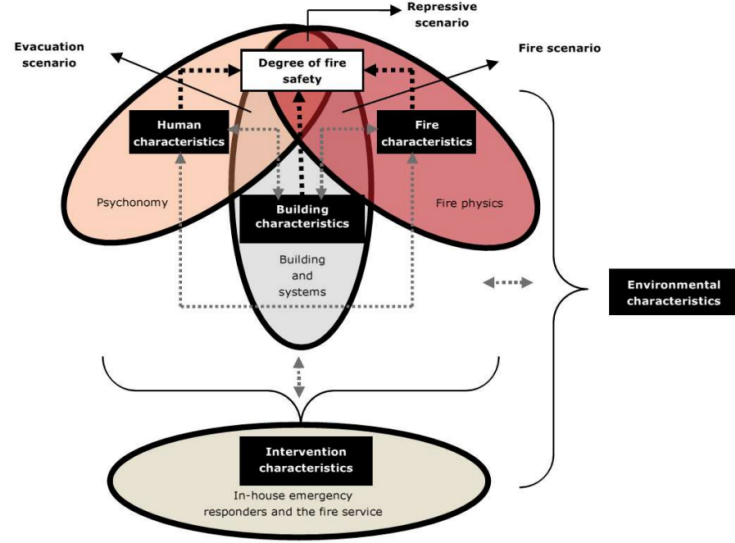


Figure 6: Performance Based Fire Safety Engineering [3]

During this research the aim is to see how the fire characteristics change and what should be adapted, whether it is building characteristics or human characteristics, to come to a successful and safe final design when using VGS. This is also known as a performance-based approach to fire safety engineering.

2.6 Types of VGS

There are different types of VGS. They can differ in either way that they are connected to the building or the types of plants. The distinction should be made between outdoor and indoor VGS. For this research, only outdoor systems will be taken into consideration which is why the indoor VGS will not be discussed.

The plants of the VGS may or may not be attached to the facade of the building which lies behind the greenery. One of the big distinctions is whether the greenery is ground-bound or not. Ground bound is when all the vegetation is rooted in the ground and climbs up the facade as opposed to some type of substrate module in which the plants can grow [23, 32, 33]. Ground-bound VGS have a limit on how high they can grow as the plants can not grow endlessly and can thus only be used for a maximum of around 3 floors.

The facade-bound VGS are commonly made up of the following components: the vegetation, a mounting system, the substrate and an irrigation system [34]. Some VGS also have a substrate holder which keeps the substrate in place. The different types can be seen in Figure 7. Facade bound VGS are more complex, as they introduce an extra cavity to the facade as well as a layer of combustible material. There are more mechanism combined in this type of VGS and there is more chance of complex behaviour taking place, like the chimney effect which occurred during the Grenfell fire and is very dangerous [35, 36].

The substrate can be either organic or inorganic. Organic substrate is mostly made up of peat soil to which certain materials and minerals have been added to create the optimal soil for the growth of the chosen greenery. These organic substrates are commonly used in combination with a pot system. An inorganic substrate is often created of insulation materials, like rock wool, in which small spaces have been made in

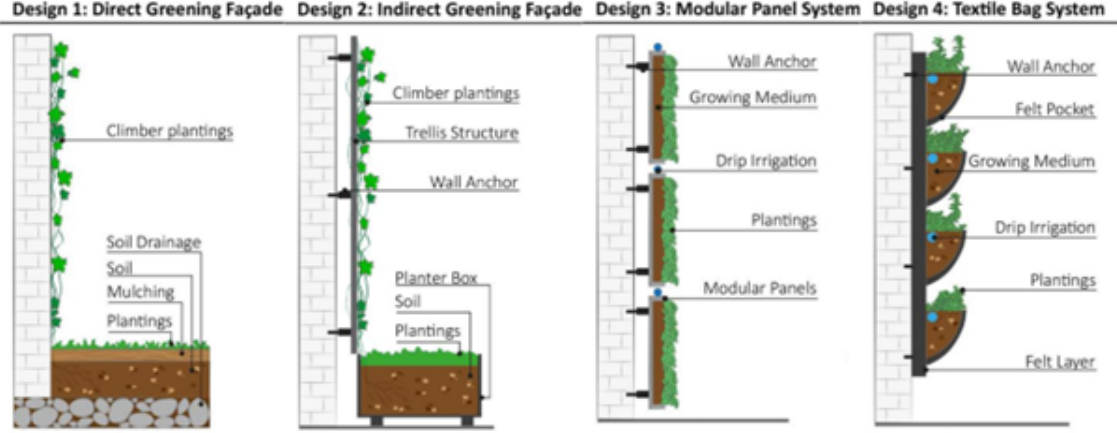


Figure 7: VGS types [4]

which the vegetation can grow. The irrigation system also has to supply the vegetation with nutrients due to the inorganic substrate not having any as the organic substrate does [34].

The types of plants differ per type of VGS. Commonly used plant species include *Hedera helix* (Common Ivy), *Peperomia obtusifolia*, and *Aglaonema commutatum* [37], as shown in Figure 8. In this study *Hedera helix* plants were studied which are most often used in combination with an indirect greening facade or a direct greening facade, see figure Figure 7.

Different plant species possess distinct characteristics that can influence fire behaviour in various ways. Therefore, understanding these characteristics during a fire is crucial for assessing fire performance and identifying plant species that enhance fire safety.



(a) *Helix Hedera* [38]

(b) *Peperomia obtusifolia* [39]

(c) *Aglaonema commutatum* [40]

Figure 8: Most Common VGS plant types

When considering fire resilience in VGS, moisture content is a critical factor influencing combustibility and ignitability. Dry vegetation ignites more readily, burns faster, and generates greater heat output compared to wet vegetation, as demonstrated in experiments conducted by C.L. Chow et al. [41]. The presence of greenery can serve as an additional fuel source, posing a significant fire hazard if it comes into contact with a window plume, potentially leading to rapid fire spread and severe consequences.

When considering the moisture content of the vegetation not just the initial plant type moisture content needs to be regarded, but the moisture content due to maintenance is also of great importance. When vegetation is not maintained correctly the plants will dry out and the moisture content will dwindle leaving dry fuel which is easily ignited [42]. As was the case in Sydney with a VGS which was lit by a burning candle or cigarette due to an improper irrigation system and thus a lack of maintenance of the plants [41].

The leaf and stem structure of the VGS can also influence the burning behaviour. Broad and thick leaves tend to be less flammable compared to thin and spread-out leaves. This is due to their contact area with the fire being smaller for these leaf types. This notion is also supported by Equation (1) which shows that a larger area will lead to more mass loss of the vegetation during a fire[8].

$$m'' = \frac{hA(\Delta T)}{LH_c} \quad (1)$$

where: [8]

m'' = mass loss rate [kg/m^2s]

h = heat transfer coefficient [W/m^2K]

A = Area of contact between flame and plant [m^2]

ΔT = temperature difference between the flame and plant ignition temperature [K]

L = Latent heat of vaporization of water in plant tissue [J/kg]

H_c = heat of combustion [J/kg]

2.7 Method

In this study, various plant characteristics will be analysed. However, due to the limited availability of physical specimens for experimental testing, simulation software was chosen to investigate the effects of these characteristics. The selected simulated software must be sufficiently detailed and accurate to capture the nuances of these characteristics and their influence on the burning behaviour. Which is why computational fluid dynamics (CFD) software was chosen.

To ensure accurate simulations and identify areas where the model either underestimates or overestimates its results, experiments were conducted to establish a validation baseline study. These validation input values were then used to develop application studies, incorporating different plant characteristics to assess their influence on the results. Additionally, the validation study provides insights into how CFD results may deviate from real-world conditions.

Fire dynamics simulator (FDS) was chosen as the simulation software for this research due to its detailed calculation method. This is a CFD software regarding fire conditions and has been designed to simulate for this purpose. Unlike simplified fire models (for example zone models) FDS uses the Navier Stokes equation on a fine grid which can capture the detailed fluid flow, heat transfer and combustion process [43, 44]. FDS is often used to capture more complex fire scenarios whilst CFAST (a zonal model) is used to offer quick approximations [43, 45]. Furthermore, zonal models were primarily designed for compartment fires as opposed to external fires and thus do not simulate very accurately for outdoor situations [46].

CFD software using LES was chosen as LES resolves the large turbulent eddies directly and only models the small-scale eddies. This allows for more detailed turbulence compared to Reynolds-Average Navier Stokes (RANS) CFD software. RANS mostly solves for the average flow and the turbulence model is user defined. Making it unacceptable for unrealistic simulation due to much the numbers on which the entire output is based being an input for the user. LES solves in detail the vortices and the turbulence behaviour over time [47, 48].

3 Experiments

To ensure that the simulations performed during the application study can be considered useful for real-world application, the simulations need to be validated. This is done by performing experiments and then recreating these experiments in the simulation software to evaluate whether the results given by the simulations are realistic. Additionally, it helps to see what restrictions the simulation software has and thus what behaviour one can expect to be different if the application study was performed in real life. For this reason, experiments are conducted using a VGS specimen. The experiments were conducted in the Peutz firelab, using materials provided by Mobilane.

3.1 The Aim

The primary objective of these experiments is to generate data for validating the FDS before utilizing it for the application study. To ensure accurate validation, the experimental setup must be identical to the conditions used in the simulations. This allows for a direct comparison between the experimental data and the simulated results, which will ensure consistency. Once validated, the same setup can be employed for the application study. Without this validation process, the reliability of the application study's results would remain very uncertain.

In addition, these experiments aim to isolate and analyse the influence of vegetation on fire behaviour. By eliminating all other elements of the facade, the results will demonstrate the effect of vegetation.

3.2 Peutz

Peutz is a building physics, acoustics and fire safety advisory group with multiple different laboratory. Peutz has 12 offices located in the Netherlands, France and Germany. With their mission being: With research and advice, they contribute to a safe, sustainable and comfortable living environment.

Peutz currently has an acoustic, building physics, windtechnology, firesafety, pyrotechnical, windturbinenoise laboratory. They are also currently building a heat pump laboratory. They are able to perform standardized tests in these locations with the help of their trained personnel and offer high-quality and reliable consulting services.

Peutz provided access to their fire safety laboratory for this research. The experiments were carried out with the support of experienced professionals working in the laboratory, who offered valuable insight and expertise throughout the research process.



Figure 9: Peutz Firesafety Lab [5]

3.3 Mobilane

Mobilane was able to provide me the samples for the experiments. Mobilane is a company which specializes in sustainable ready-to-use green systems which can be added to roofs, facades or walls. Their goal is to create a green, healthy and sustainable future for all. Special thanks to Mobilane for gifting the samples.

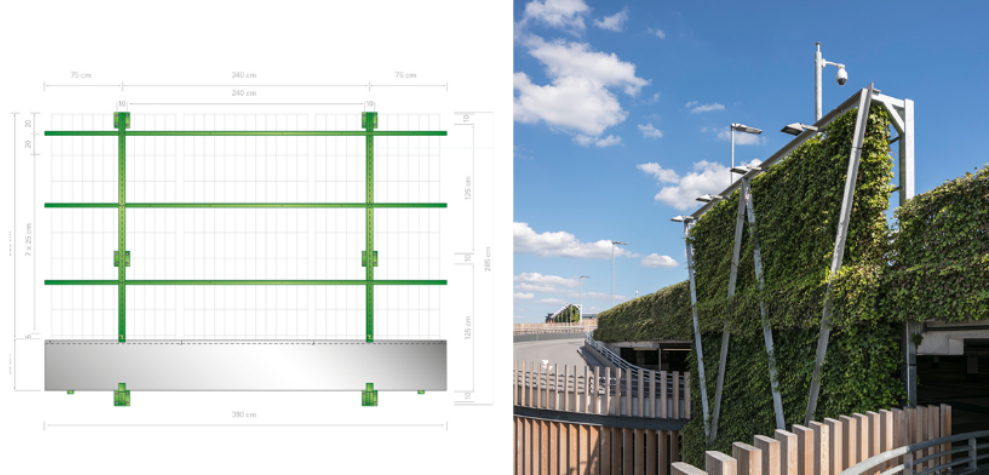


Figure 10: MobiGreenFence Wall Planter VGS [6]

3.3.1 samples

Mobilane was able to provide/gift 4 samples for this research. The 4 samples were cut out of 2 different MobiGreenFence which are also used for their wall planters, these are shown in Figure 11a.

Delivered samples MobiGreenfence

- 2 pc. **Hedera helix Woerner** (klimop/common ivy) 120x180cm

The samples used in the experiments were extracted from the delivered hedges. Prior to testing, the roots at the base of the hedge, as depicted in Figure 11a, were removed. Additionally, the samples were trimmed to the required dimensions for the experiments. To minimize dehydration and potential alterations to the results, the cutting process was conducted on the same day as the experiments. An angle grinder was employed for this procedure, as its use was necessary due to the metal grate within the hedge structure, as well as the substantial thickness of the hedge's wooden components.

All samples were cut the same size, 0.5m wide by 1.5m high (0.5mx1.5m), the hedge was higher than 1.5 so the top of the hedge was cut off as opposed to the lower half. This approach was chosen as the lower part of the hedge is more mature, and will thus provide a more realistic result of how a fully grown hedge mounted to a facade would perform.



(a) MobiGreenfence sample



(b) Cut sample

Figure 11: VGS Samples

3.4 Method

3.4.1 intermediate fire test ISO 13785

The experimental setup closely resembles that of the ISO 13785 intermediate-scale test; however, certain differences exist in both the setup and specimen preparation.

First of all, the specimen of an ISO 13785 test have to be conditioned to a constant mass of 23 ± 2 °C and a relative humidity of $50 \pm 5\%$. However, due to the necessity of testing live vegetation immediately upon delivery to prevent dehydration, these conditions were not strictly adhered to. Nor was the specimen weighed 24 hours before testing to verify that their mass variation remained within the prescribed limit of 0.1%. In an ISO 13785 test, if a specimen's weight fluctuates by more than 0.1%, the test must be postponed for at least another 24 hours to allow for proper stabilization. Despite these deviations, the ambient temperature of the test environment adhered to the ISO 13785 requirement of 20 ± 10 °C during the conducted experiments [7].

Figure 12 shows the precise setup an ISO 13785 must adhere to. As depicted in Figure 12, multiple thermocouples are placed in an even spacing on both sides of the specimen sides monitoring the temperature distribution. In addition, a heat flux meter at the top of the specimen to measures the radiant heat exposure at one side.

The specimens of an ISO 13785 test are created in a corner setup with a width of 1.2m on the wide part of the specimen and the other width being 0.6 and a height of 2.4m. The lineburner is placed under the wider side of the specimen and also has a width of 1.2m. There is a 0.25m space between the line burner and the sample. The specimen is mounted on an adiabatic back wall, which in turn will not affect the results.

The ISO 13785 tests last for a total of 30 minutes during which the line burner needs to be ignited within the first 10 seconds. The line burner has a total output of 100 kW, this output also needs to be reached within the first 10 seconds. The sampling period for the data logger must not exceed 10 seconds. Furthermore, it is important that the horizontal wind speed in the vicinity of the test does not exceed 0.5 m/s, as this will influence the final results.

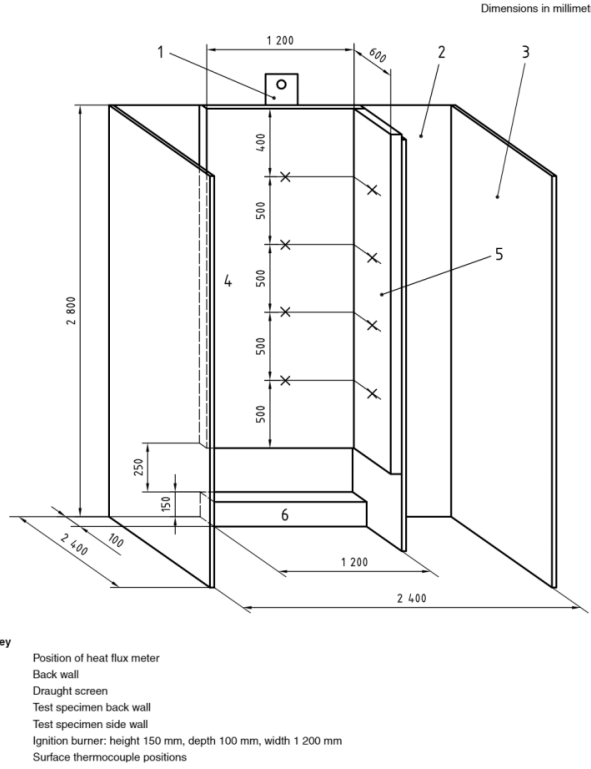


Figure 12: Setup ISO 13785 (intermediate facade test) [7]

3.4.2 Experimental setup

The experiments were completed with the help of Peutz BV. Multiple experimental setups were evaluated due to the initial configurations yielding limited results. Specifically, the first two setups did not provide significant variations in the recorded temperatures, necessitating modifications to the experimental design. This adjustment was essential, as minimal temperature variation makes it challenging to assess whether the simulations accurately represent real-world conditions. Without sufficient data variation, it becomes difficult to analyse fire behaviour and validate the accuracy of the simulation results [49].

Setup - 1

The initial experimental setup is shown in Figure 13. The samples were mounted on an adiabatic wall, with a calcium silicate board (Promatect) serving as the backplate for stability. To prevent the thermal heat absorption properties of Promatect from affecting the measurements, a layer of Rockwool was placed on top of the heated side of the board. Additionally, rockwool was placed along the sides of the specimen. Minimizing the heat loss due to convection and preventing potential influence as a result of airflow within the testing environment blowing the flames in a certain direction. This arrangement ensured that the fire remained focused on the specimen. Furthermore, Rockwool was placed on the ground around the gas pipe to enhance safety and maintain a controlled environment in the event of flaming sample debris falling during the experiment.

The specimen was suspended using metal rods that hooked into the metal grate located within the hedge, as illustrated in Figure 56 in Appendix A. This setup allowed the specimen to be positioned at a controlled distance from the Rockwool backing, creating a cavity, as shown in Figure 57. The first sample was positioned 25 cm directly above the line burner (measured from the top of the burner) with a 20 cm cavity between the specimen and the Rockwool backing. The adiabatic back wall was secured to a metal support system, which provided structural stability. The metal hooks attached to the specimen were also inserted through the metal backing system to enhance the overall stability of the setup. The entire assembly was placed on a Pro-

mactect plate, which was positioned on a scale to enable precise measurement of mass loss during the experiment.

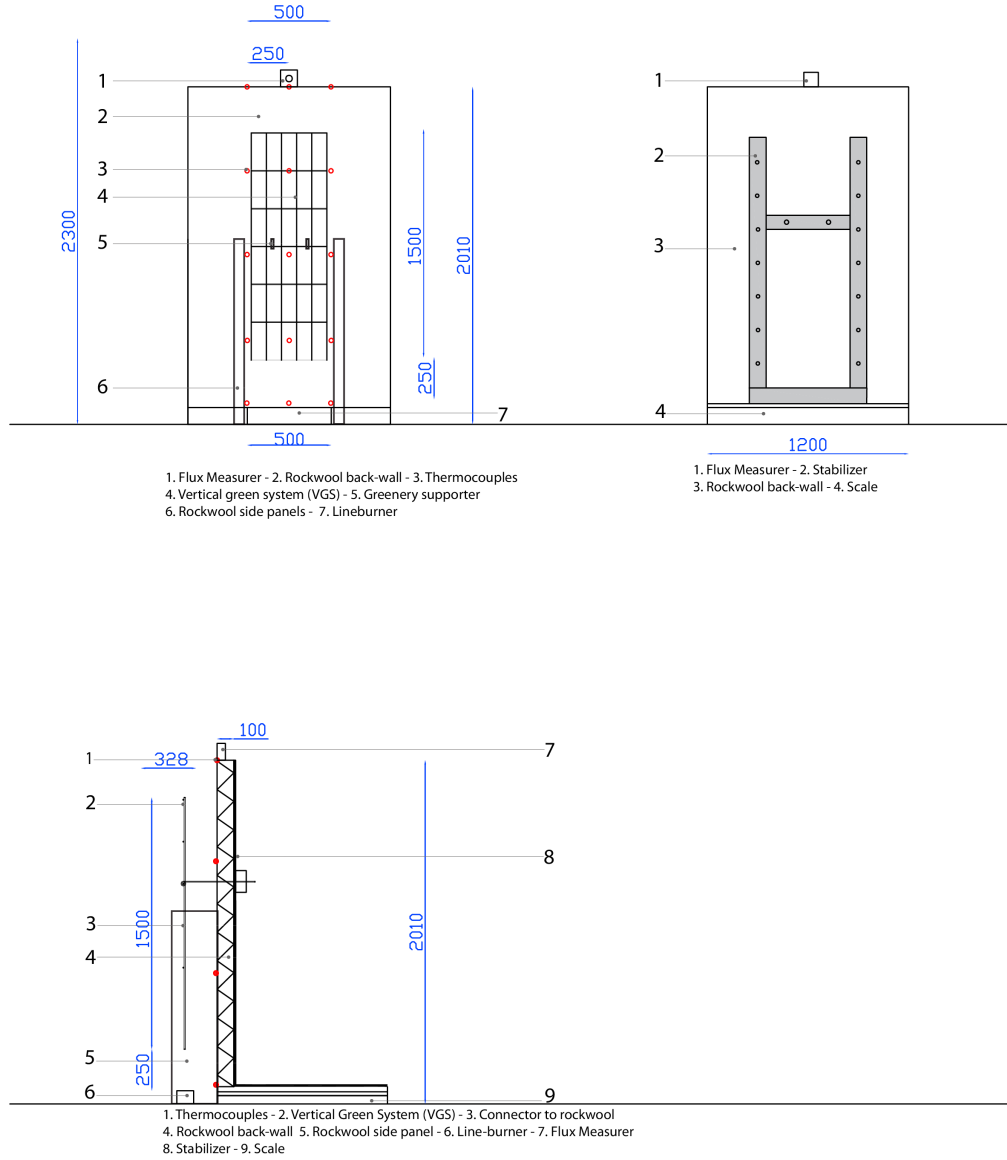


Figure 13: Setup 1

In addition to the scale, the setup incorporated a flux meter and 15 thermocouples for data collection. The flux meter was placed atop the set-up, shown in Figure 13 and 14, in a manner similar to its placement in the Intermediate-Scale Fire Test. However, due to the extended height of the adiabatic back wall, which accommodated thermocouple placement, the flux meter was not positioned directly above the specimen but was instead slightly offset. A total of 15 thermocouples were placed in the setup, distributed across three columns with uniform spacing between them, following a setup similar to that outlined in ISO 13785 as discussed in Section 3.4.1. These thermocouples were pushed through the backplate Promatect plate as well as the Rockwool and just poked out so the temperatures that were measured were the temperatures upon the back wall, were the facade would normally be located, this way the full effect of the vegetation upon a potential facade could be measured.



Figure 14: Setup back view

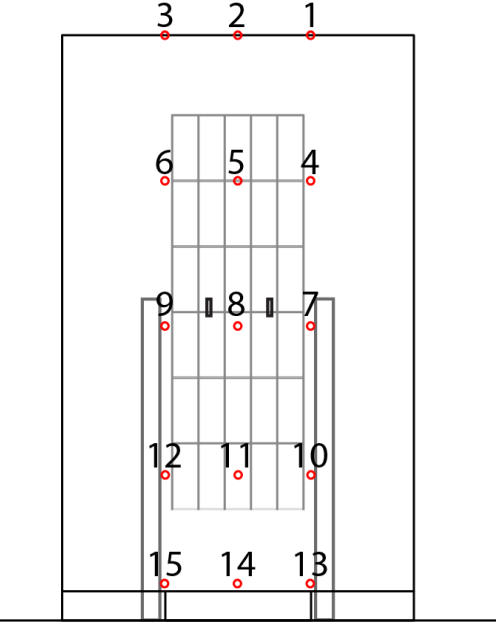


Figure 15: Numbering of thermocouples front view

The thermocouples numbering stayed the same throughout all experiments. They were plugged into a data logger which recorded every 0.01 sec, setup seen in Figure 16. This was not changed throughout all of the tests. Before the tests were conducted the lineburner was adjusted to ensure that the heat released was 30kW. This was done by using the following formula:

$$RHR = \frac{Q_{total}}{t} \quad (2)$$

where:

RHR = rate of heat release of fuel burner [kW]

Q_{total} = total energy released [MJ]

t = time the fuel burned [s]

To ensure that the output was 30kW the weight change of the burning fuel was used to calculate the overall output and the gas valve was adjusted until the right output was achieved. The precise calculations can be found in Appendix A.2.1.



Figure 16: Data logger setup



Figure 17: Specimen in setup 1



Figure 18: Final Setup 1 with Specimen

All experiments were recorded with a GoPro which was positioned directly in front of the specimen. All experiments lasted a total of 30 minutes, during which the lineburned maintained a constant output of 30 kW. Measurements were taken at intervals of 0.01 seconds and all peculiarities during the experiments were noted down by hand. Markers were taped to the rockwool back wall at 0.5m intervals to serve as height references, allowing for real-time observation of flame height during the experiments. These are the silver tape markings observed in Figure 17

Setup - 2

During the first experiment, minimal changes in temperatures or burning behaviour were observed. As discussed in Section 3.4.2, a broader range of results is preferable to ensure the simulations can be accurately

tested for reliability. As a result, it was decided, in consultation with Peutz workers and the supervisor, that the second sample would be lowered closer to the lineburner to increase the variability in the results. This adjustment was made in hopes of enhancing the burning behaviour, thereby creating a more varied dataset for the FDS modelling. The cavity size remained unchanged, the only modification made was the reduction of the gap between the specimen and the flames from 25cm to 5 cm. Apart from this adjustment, all other experimental conditions remained the same. The setup is shown in Figure 68 in Appendix A.

Setup - 3

Whilst the results were observed to be more diverse with setup 2 compared to setup 1, a third setup was introduced to further enhance result variation. Setup 3, shown in Figure 78 in Appendix A, was based on setup 2, however, the width of the cavity was reduced from 20cm to 7 cm, with the lineburner still placed directly under the specimen. This adjustment led to significantly more variation in the result temperatures. This setup was used for test 3 and 4.

3.5 Results

Setup - 1, test 1

As mentioned above the tests were filmed. In Appendix A images at different time intervals document the burning behaviour of the samples. The sample remained largely unburned throughout the experiment. Within the first minute following the ignition of the line burner, slight smoke emissions were observed, as shown in Figure 59 in Appendix A.2.1. This subsided after the first minute. At approximately 3 minutes and 45 seconds (Figure 19a), the specimen ignited, with flames spreading rapidly along the stem of the ignited plant. However, the rest of the plant did not ignite, and once the single burning stem was consumed, the flames diminished.

Over time, the leaves gradually dehydrated as they lost moisture. Nevertheless, the specimen did not reignite until 13 minutes and 45 seconds (Figure 19b). Similar to the previous ignition, only a single stem burned, after which the flames subsided, leaving the rest of the specimen unaffected. No further ignition was observed for the remainder of the experiment.

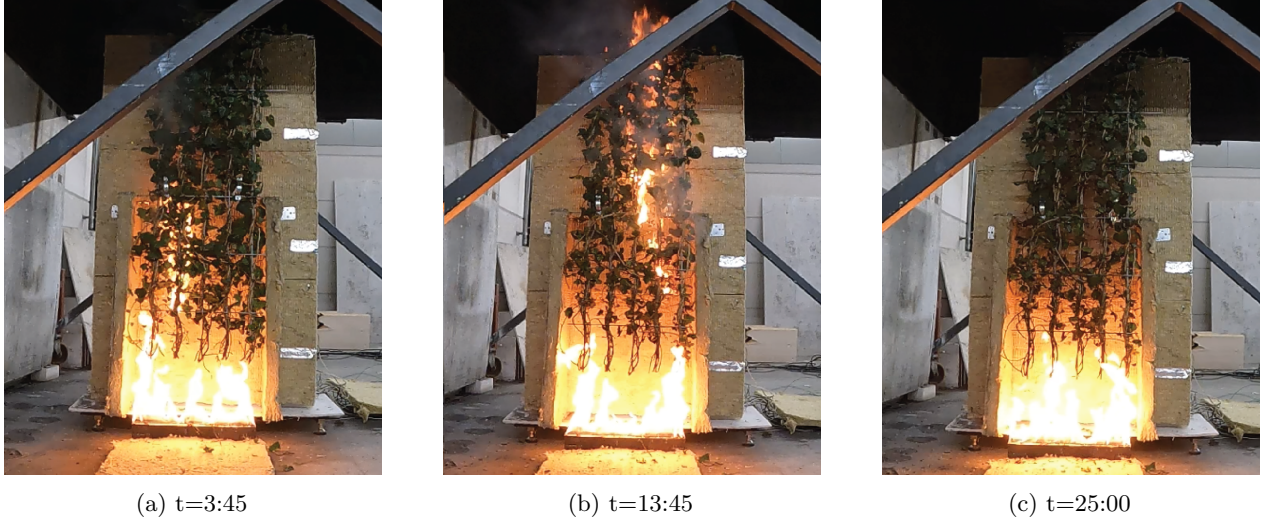


Figure 19: Test 1

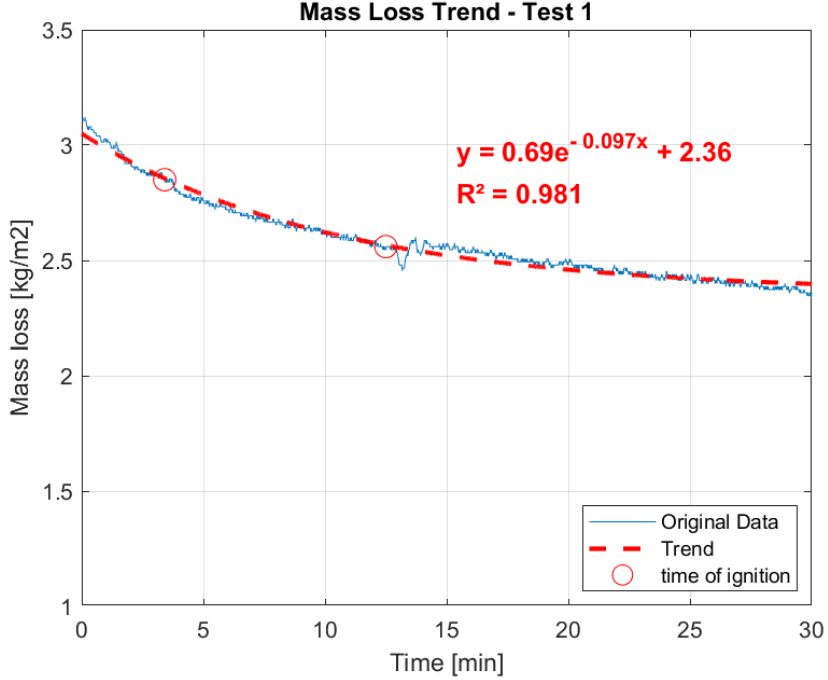


Figure 20: Mass loss regression trend test 1

These ignitions are also reflected in the mass changes shown in Figure 20. Drops in the mass are shown around the points of ignition indicating a quick change in the mass composition of the sample. The trend line which was fitted to the mass loss is an exponential decay function. This means that initially, the mass loss decreases exponentially, however over time the mass loss rate slows down. The coefficient of determination is shown to be 0.98 in figure 20. This indicates an excellent fit as the closer R^2 is to 1 the better the fit is.

As mentioned in Section 2.4, when vegetation burns pyrolysis takes place. The general combustion of biomass is shown below [50]:



The chemical formula for complete combustion represents an idealized scenario. In reality, combustion also produces carbon monoxide (CO), char (C), and other hydrocarbons. However, for the purpose of quantifying pyrolysis in relation to moisture evaporation, this simplified model is employed.

A piece of the specimen was dried out with Peutz equipment to measure the moisture content of the specimen, which returned a moisture content of 22.51%, the precise numbers are shown in Appendix A.2.1.

Setup - 2, test 2



Figure 21: Test 2

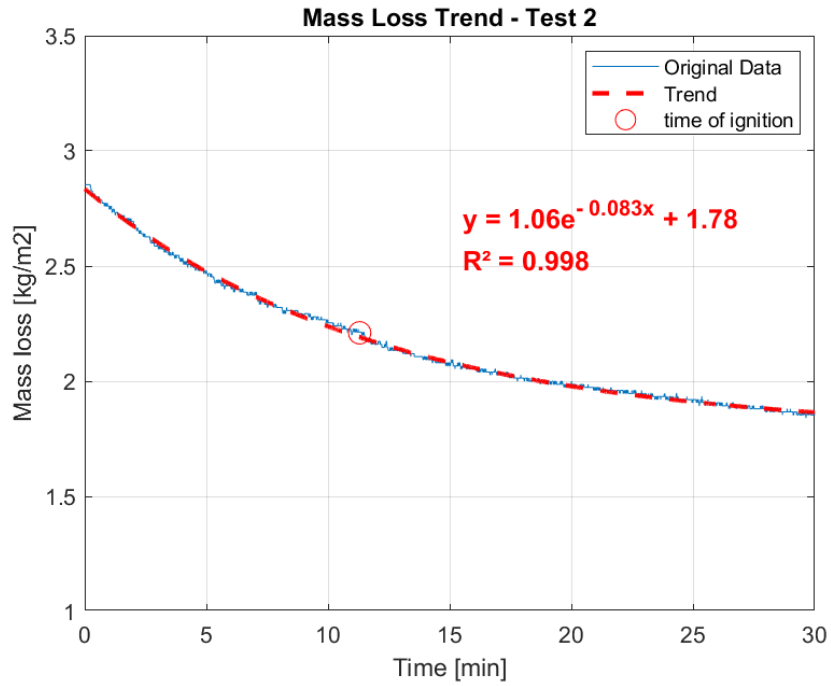


Figure 22: Mass loss trend test 2

Test 2 was done using the second setup described in Section 3.4.2. During the test, the specimen only ignited once at 11:20. Apart from that there were some loose leaves which happened to ignite sometimes but the ignition would die out after the 1 to 2 leaves burned.

The lower vegetation in contact with the flames burned away during the first 10 minutes of the experiment, without a very clear overwhelming ignition of the vegetation. When this fuel was burned the flames did not

ignite another part of the sample. The only part of the sample that was burned was the part of the sample that came into contact with the flames.

The overall temperature reached during the test was higher and more uniform compared to test 1. The heating of the specimen was much more consistent compared to test 1. Like test 1, the most uniform temperatures were in the middle of the specimen compared to the two sides. The overall heat distribution seemed more balanced in test 2 compared to test 1. Just like test 1 the left side of the specimen was hotter than the right side, this is also clearly shown in Figure 27 and 28, as well as Figure 77 in Appendix A.

Setup - 3, test 3

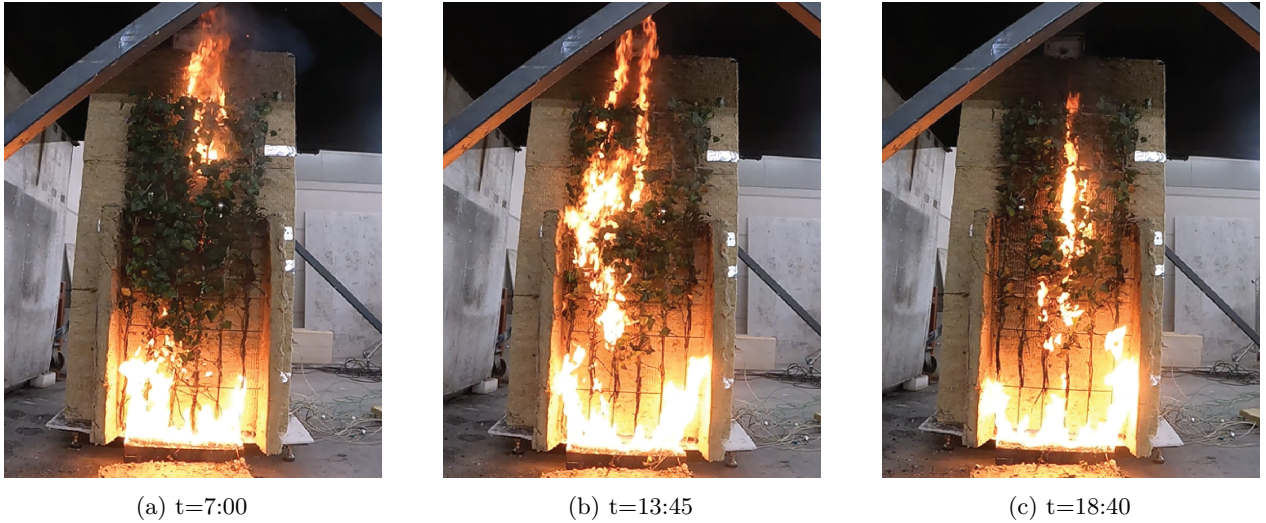


Figure 23: Test 3

Test 3 had a modified setup compared to test 2 and 1 as described in Section 3.4.2, shown in Figure 78, the cavity was reduced, and the specimen was held low to the lineburner as in setup 2.

Shortly after the ignition of the line burner, small firebrands from burning leaves were observed. However, these were quickly extinguished due to their lack of fuel load. Similar to test 2 the fire initially propagated along the sides of the specimen whilst the centre remained relatively unburned. This is corroborated by Figure 23a and 23b, which show that a greater number of leaves remained intact in the central portion of the specimen compared to the sides.

No significant ignition took place until the 7-minute mark when the first ignition took place. This ignition propagates both vertically along the middle and the left side of the specimen. The associated temperature spike is shown in Figure 86 and 87, with the latter also showing a pronounced temperature increase in both the centre and the left side of the specimen.

A second major ignition took place at 13:45 and lasted for about 5-7 seconds. This was significantly longer compared to those of tests 1 and 2. The final ignition took place at t=18:40.

In total, three ignitions occurred during test 3, a significant increase compared to tests 1 and 2. Additionally, the ignitions which occurred also lasted longer. Figure 86, 87, 27 and 28 show that the overall temperatures recorded with setup three were higher overall compared to test 1 and 2, further indicating a more intense burning process.

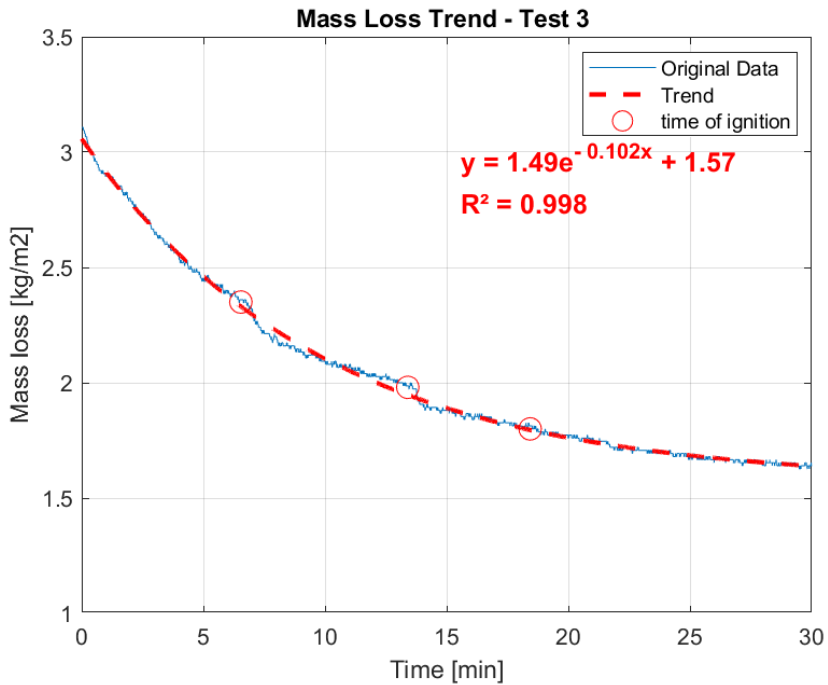


Figure 24: Mass loss trend test 3

Setup - 3, test 4

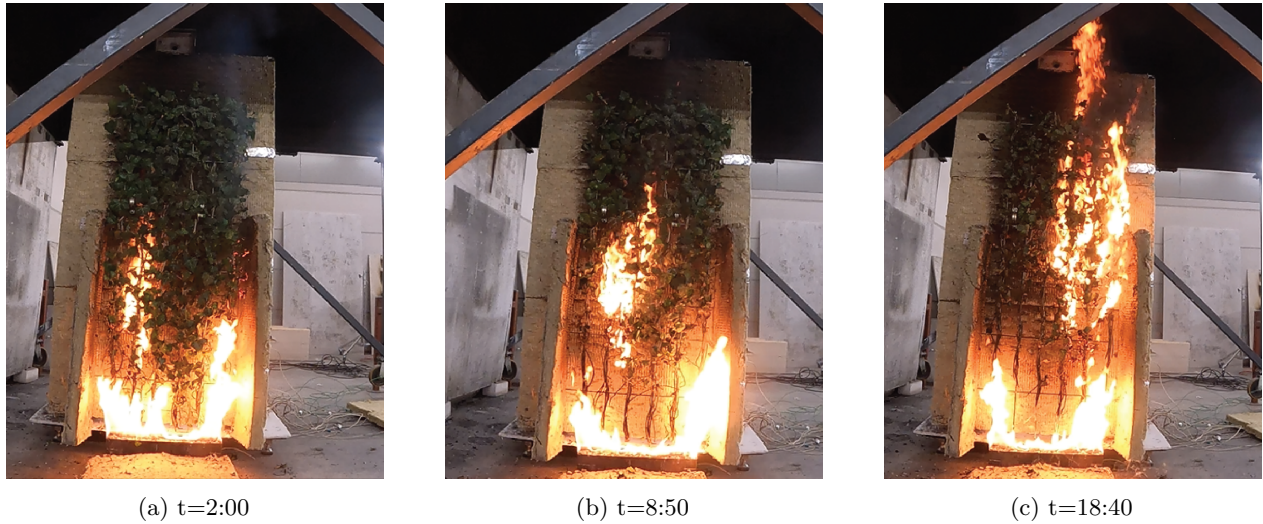


Figure 25: Test 4

Test 4 was conducted using setup 3. As with test 3 there were firebrands shortly after ignition. Similarly to test 3 as well, the sides of the specimen burned before the centre, which has leaves intact for a longer period. The first ignition happened quite quickly at $t=2:00$ with the second taking place at 8:50.

At $t = 14:00$ a window in the lab was opened which caused a significant airflow to occur which blew the flames towards the adiabatic back wall, this is shown in Figure 91. Causing a big increase in the temperatures recorded by the lower thermocouples, shown in Figure 95 and 96. This also explains why the maximum

temperatures recorded by the thermocouples is about 200 °C higher compared to test 3, see Figure 28. The mass loss rate is also much steeper when the window was open compared to before the window was opened, shown in Figure 26. The window was quickly closed after seeing the flames blowing back and the experiment was able to resume as before.

The last ignition of the specimen took place at 18:40, however, this temperature spike is more difficult to observe due to the high temperatures around the lower thermocouples due to the window that was opened. All thermocouple temperature curves can be found in Appendix A. The window being opened and corrupting the data also explains why the mass loss curve does not fit as well as the previous mass loss curves. It is also why the formula suggests a more gradual decline as opposed to an exponential curve decay which test 3 strongly suggests.

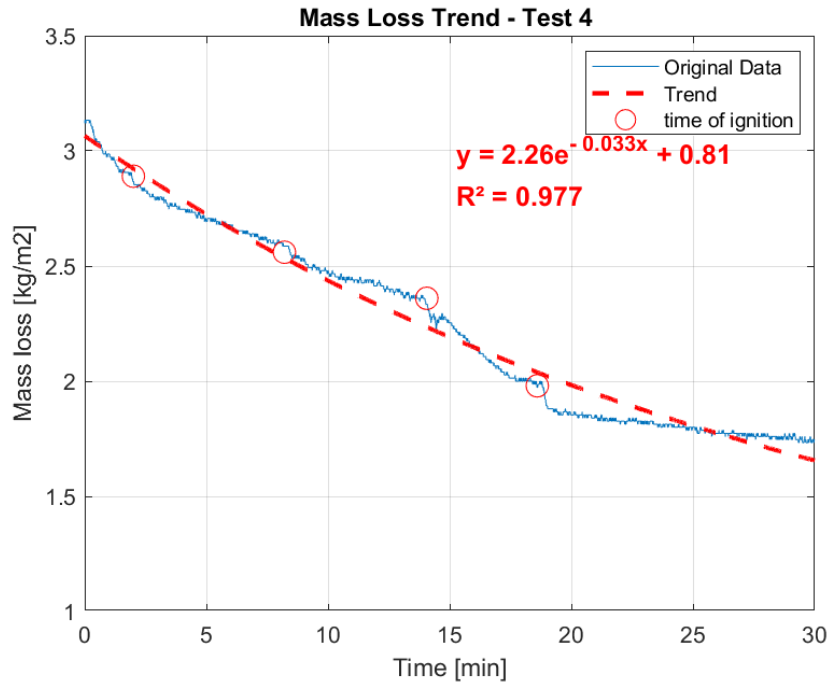


Figure 26: Mass loss trend test 4

3.6 Conclusion

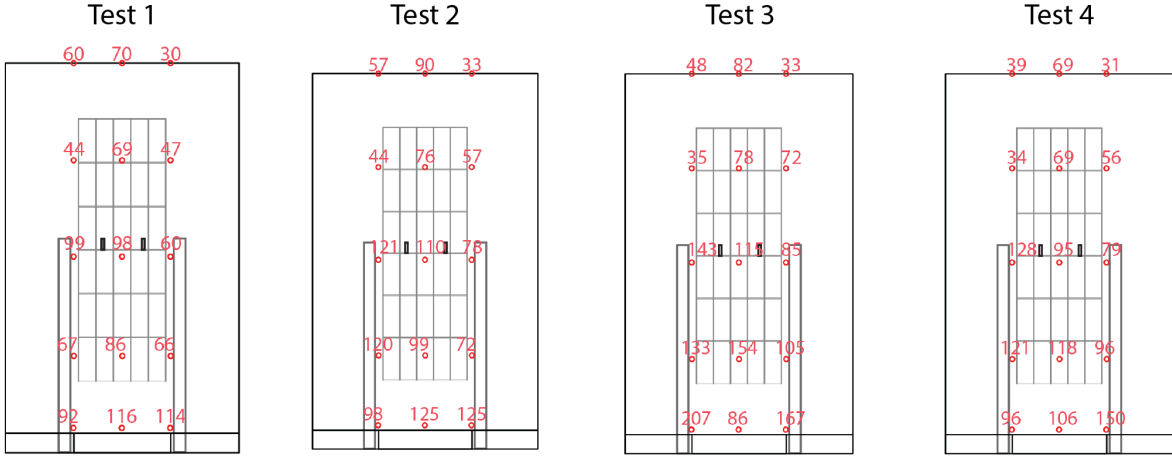


Figure 27: Median Temperatures of each Thermocouple per Test

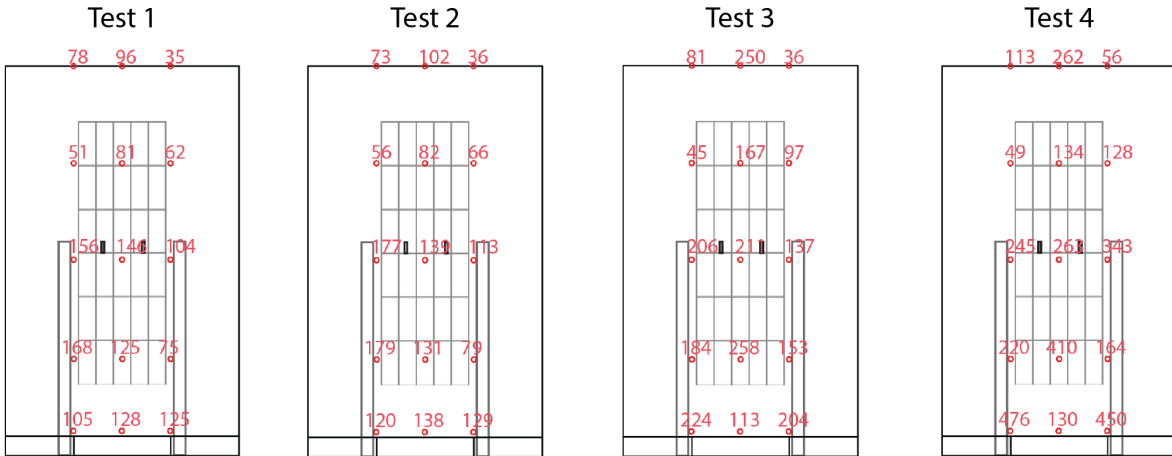


Figure 28: Maximum Temperatures of each Thermocouple per Test

Based on the experimental results, the following conclusions can be drawn. The reduction of the cavity width and the lowering of the specimen contributed to higher surface temperatures on the adiabatic back wall. This effect is clearly illustrated in Figure 27 and 28.

This phenomenon can be explained by the principles of heat balance and energy conservation ($q_{in} = q_{out}$). By reducing the cavity width, heat loss due to convection is minimized, forcing a greater portion of the heat to move upward within the cavity. Consequently, this leads to higher temperatures at elevated points within the cavity [51].

Equation (4) further supports this notion. As the cavity would be reduced, h_c would also be reduced which would trap more heat. Effectively raising T_f . Additionally, the reduction in heat loss due to thermal radiation further contributes to the observed temperature rise which attributes much more to the rise in temperature compared to convection.

When surfaces are positioned closer together, the view factor between the heated surfaces (i.e., the vegetation and the back wall) increases. This increased view factor enhances radiative heat transfer within

Test	Mass loss Formula	R^2	Total mass loss	Calculated released Pyrolysis
Test 1	$y = 0.69e^{-0.097x} + 2.36$	0.981	0.57kg	7.67 MJ
Test 2	$y = 1.06e^{-0.083x} + 1.78$	0.998	0.76 kg	10.23 MJ
Test 3	$y = 1.49e^{-0.102x} + 1.57$	0.998	1.12 kg	15.08 MJ
Test 4	$y = 2.26e^{-0.033x} + 0.81$	0.977	1.05 kg	14.133 MJ

Table 1: Overview mass loss and heat production

the cavity, effectively trapping more radiation and further raising temperatures, as described by the radiative heat transfer equation (Equation (5)) [51, 52].

$$q_{conv} = h_c(T_f - T_{air}) \quad (4)$$

with:

q_{conv} = heat loss due to convection

h_c = heat transfer coefficient convection
[W/m²K]

T_f = temperature facade surface [K]

T_{air} = ambient air temperature [K]

$$q_{rad} = \epsilon\sigma AF_{ij}(T_f^4 - T_{sky}^4) \quad (5)$$

with:

q_{rad} = heat loss due to radiation

ϵ = emissivity of the surface

σ = Stefan-Boltzmann constant

A = Surface area

F_{ij} = view factor

T_f = temperature facade surface [K]

T_{air} = the effective sky temperature [K]

The thermocouples placed on the left side of the specimen consistently recorded higher temperatures compared to those on the right side of the sample. This difference is likely attributed to airflow dynamics within the testing environment. On the left side of the specimen, a wall was present, whereas the right side was open to the testing room which also had a partially open door on the right side which led to a large hall in which other operations were conducted. This opening on the right side most likely generated airflow from the right, leading to the flames being pushed to the left side of the specimen. Resulting in higher localized temperatures compared to the right side.

Notably, in all 4 tests, the sides of the specimen experienced more turbulent fire behaviour compared to the centre of the specimen. This is most likely due to the airflow within the testing environment. As a result, the flames get pushed around more and the specimen will thus not always be in the flames compared to the centre which always experiences the heat from the flames. This turbulent nature is shown in the recorded temperatures of the thermocouples, the graphs are placed in Appendix A.

Test	Overall median temperature
Test 1	75.86 °C
Test 2	87.0 °C
Test 3	102.9°C
Test 4	94.5 °C

Table 2: The median temperature recorded all thermocouples over the whole test time

Furthermore, post-experimental observations revealed that combustion was less pronounced at the exact center of the samples compared to areas slightly offset from the center. The burned samples, as illustrated in Figure 29, indicate that this phenomenon is likely attributed to the presence of a recirculation zone in the slightly offset regions. In these areas, the turbulent nature of the flames causes hot air to be redirected downward, leading to enhanced localized burning and increased material degradation.

Table 1 presents the regression trend formula for each test, providing a clear comparison of mass loss rates. Among the tests, Test 3 has the highest decay rate, meaning it burns fastest. While test 4 has the most complete burning which is indicated by the number after the + sign in the formula. However, due

to the window being opened for part of the experiment the data is partially corrupted and the result may not be entirely representative of the general trend. This table also shows the total mass loss and the total heat produced due to the burning of the specimen, this produced heat was calculated using the molar mass equation, the equations are shown in Appendix A.

A reduction in cavity size led to an overall increase in recorded temperatures, mass loss as well as heat produced, as shown in Table 2. The produced heat was calculated using complete combustion of cellulose, which is not wholly realistic but allows for a representative estimation of the produced heat to be made.

A clear increase in recorded temperatures is observed from test 1 and 2 to 3 and 4, as illustrated in Figure 30. This figure represents the temperature distribution across thermocouples, highlighting the range within which 80% of the recorded temperatures fall. The median temperatures in Tests 3 and 4 are significantly higher compared to those in Tests 1 and 2.

To generate this plot, corrupted data from Test 4 (minute mark 14–19) was removed and replaced with corresponding temperatures from Test 3 as these tests had the same setup. The 80% range was chosen for representation, as this is a commonly used threshold in fire safety research [53].

Table 5 presents the standard deviation of temperature readings per thermocouple over the entire test duration. The results indicate that Tests 1 and 2 exhibit lower standard deviations, suggesting a narrower temperature range, whereas Tests 3 and 4 display greater variability. Additionally, lower thermocouples, positioned closer to the sample, record higher standard deviations. This outcome is expected, as these thermocouples are exposed to greater temperature fluctuations due to their proximity to the line burner and the increased occurrence of vegetation ignition at lower levels.



Figure 29: Samples after testing

Thermocouple	1	2	3	4	5	6	7	8	9	10	11	12	13	14	15
Test 1	4	10	8	7	9	7	11	17	19	12	13	18	17	23	11
Test 2	3	8	7	5	6	4	11	11	18	10	14	20	15	17	12
Test 3	4	21	12	10	15	5	13	24	23	16	32	19	30	27	44
Test 4	4	23	9	13	15	5	18	25	23	13	26	21	28	21	52

Table 3: Standard Deviation per Thermocouple all Simulations

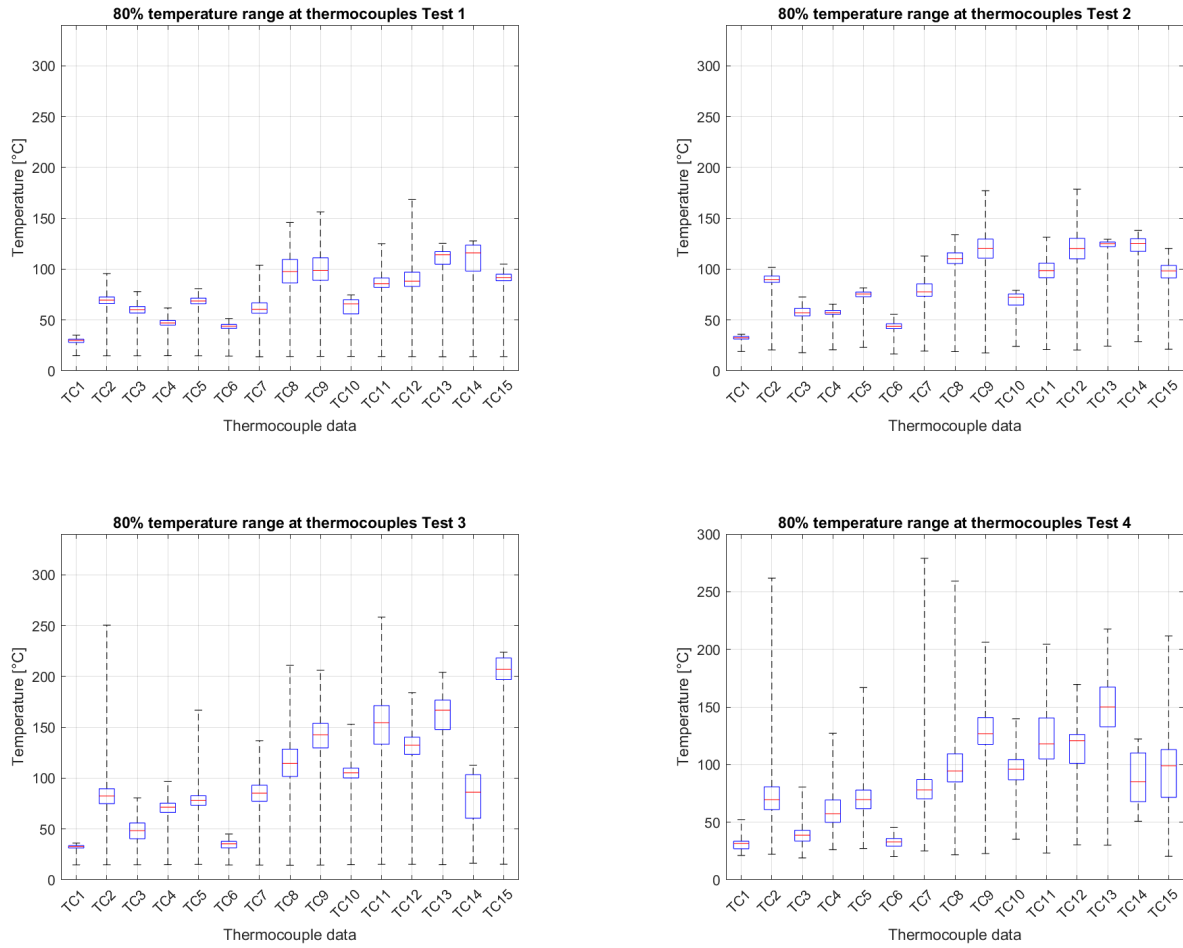


Figure 30: Temperature ranges 80% datapoints per test per thermocouple

4 Validation Study

4.1 Computational Domain and Geometry

The geometry of the validation study must be as close to the real-life experiments as possible. This way uncertainties can be eliminated, which should allow for a realistic simulation. The simulated setup can be seen in Figure 31a. As shown this setup closely resembles testing setup 3, which was the setup that gave the most diverse results in terms of temperatures which is why these results were the easiest to use when modelling in FDS as mentioned in Section 3.4.2.

In this case, the field of interest is the size of the specimen, which has a height (h) of 1.5m as it also was in the experiments. So the field of interest for this particular simulation has an h of 1.5m. It is critical that the computational domain does not influence the final results of the simulation. This is why the domain has to be large enough as to not influence the calculations.

For CFD simulations the ideal simulation has a space of 3-5 h of the field of interest along the line of flow, h being the height of the field of interest. Around 2 h upstream of the field of interest and about 2 times the body width around the field of interest [54, 55]. This is however the case for CFD simulations which deal with airflow calculations. So the domain might affect fire simulations differently seeing as these do not deal with airflow velocity specifically. In this instance, the line of flow has been chosen to be vertically seeing as heat rises. However, to cut down on computational time it was chosen to use 2.5 h instead of 3 h above the field of interest.

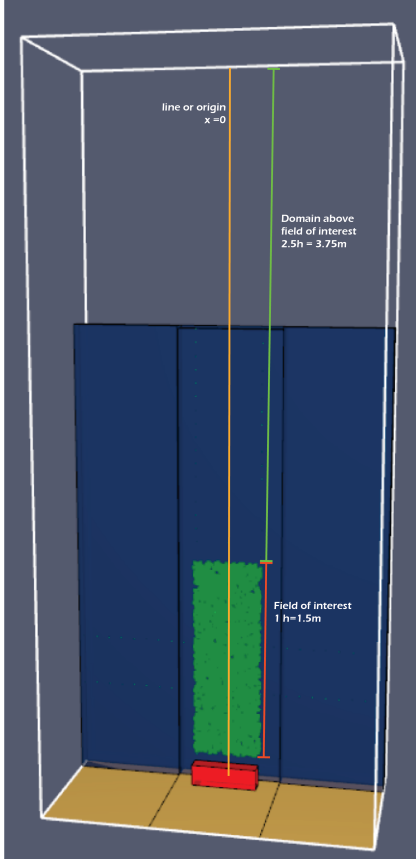
To cut down on computational time different meshes were created, using different meshes allows for more cores to run the calculations at the same time. Meaning that one uses more computer power simultaneously compared to when one mesh would be used [8]. In this scenario, the computers which were used to run the simulations had 4 cores which thus allowed for 4 meshes, shown in Figure 31b. Mesh 1 is located behind mesh 2, 3 and 4 and spans the whole width of the domain. This mesh is very slim and is located behind the adiabatic back wall.

A finer computational grid increases computational time; however, it enhances the detail and accuracy of the calculations by providing a more precise representation of turbulent flow dynamics [56]. To optimize computational efficiency while maintaining the necessary grid refinement in regions of high turbulence, a non-uniform (dynamic) grid was implemented. This approach ensures accurate results by employing smaller grid cells near the primary driving force of the flow—the fire—where turbulent interactions are most significant [56]. In this study, the central mesh (Mesh 3) was designated as the primary region of interest, as illustrated in Figure 31b.

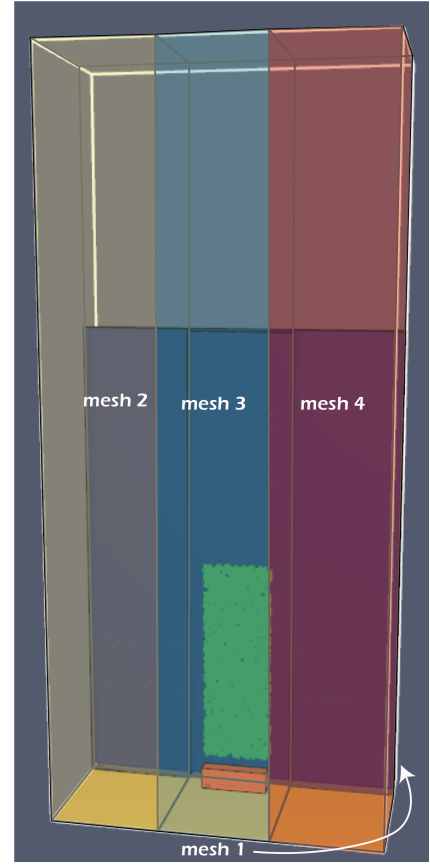
4.2 CFD Software Type

There are different ways that CFD software can solve its calculations. CFD simulations which analyze the windflow most often use CFD which solves based on RANS. RANS solves for a steady flow. Meaning that it solves for a time-averaged flow and thus takes out a lot of the turbulences experience in real life [48]. The turbulences it experiences in the flows are modeled by $k - \epsilon$ or $k - \omega$. The k in these models stands for turbulent kinetic energy, with the ϵ being good in simulating free shear flows and more so for large-scale flows far from walls [57]. Whilst the ω is more suitable for near wall modelling and is able to model the boundary layer flows, including the laminar-turbulent transition quite well [58].

As mentioned in Section 2.7 RANS, which stands for Reynolds-Averaged Navier-Stokes, models all turbulences using statistical averaging. Whilst Large Eddy Simulations (LES) resolves all large eddies and only models the small scale turbulences [47]. This does mean that LES models come at a computationally higher cost, but they are able to capture much more detailed flows and structures over time. Whilst RANS



(a) Domain in field of interest, Validation study



(b) Meshes for validation study

Figure 31: Validation study test domain

more so provides the mean flow characteristics. Due to the very turbulent nature of fire and smoke LES captures reality much more closely compared to RANS which smooths out the behaviour and gives more so the average behaviour, missing its critical fire dynamic characteristics [59, 60].

4.3 Grid discretization

4.3.1 Grid levels

To ensure that the grid sizing does not influence the results, multiple grids have been run which can be used to calculate the Grid Convergency Index (GCI). While the GCI can be computed using just two grids, previous research has shown that using three grids improves accuracy [61]. Therefore, three different grids: coarse, medium, and fine—were created. Their exact dimensions are provided in Table 4.

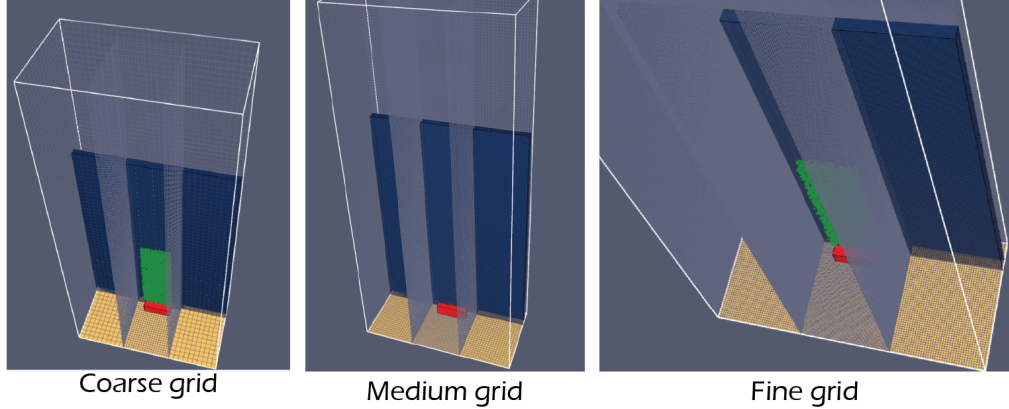


Figure 33: Grid levels

	coarse	Medium	Fine
Mesh 1	30, 3, 68	60, 4, 135	120, 8, 270
Mesh 2	10, 13, 68	20, 25, 135	40, 50, 270
Mesh 3	20, 26, 136	40, 50, 270	80, 100, 540
Mesh 4	10, 13, 68	20, 25, 135	40, 50, 270
Cell size	Mesh 3 = 4 cm Mesh 1, 2 and 4 = 8 cm	Mesh 3 = 2cm Mesh 1, 2 and 4 = 4 cm	Mesh 3 = 1cm Mesh 1, 2 and 4 = 2 cm

Table 4: Mesh sizing, number of cells [x, y, z] direction

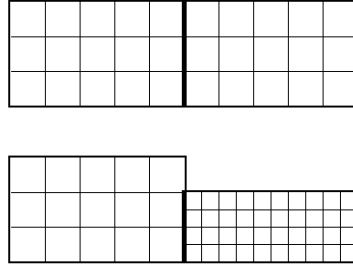


Figure 32: Allowed meshes in FDS from [8]

The grids which are formed in FDS are always rectangular and evenly spaced [56]. The user guide states that for the most optimal results, the cells should be as cubic as possible [8]. Finer grids generally lead to more accurate simulations. Table 4 shows the number of cells in each direction of the overall computational domain.

As mentioned above a dynamic grid was created to save on computational time. The field of interest, represented by Mesh 3, always maintained the finest resolution among the implemented meshes. Within this region, the coarse grid had a resolution of 4 cm per cell, the medium grid 2 cm per cell, and the fine grid 1 cm per cell. Outside this region, cell sizes were twice as large, resulting in coarse, medium, and fine grid sizes of 8 cm, 4 cm, and 2 cm, respectively.

When creating multiple grids in FDS it is imperative to ensure that the grids line up with one another. Otherwise, no heat transfer will occur between the grids and the simulation will not reflect reality. When choosing a dynamic grid the smaller cells must be a multiple of the larger cells to ensure correct mapping of the mesh, see Figure 32 for the correct type of meshing.

4.3.2 Calculation Lines

To conduct a comparative analysis of the different meshes as well as comparing them to the experimental results calculation lines were created. These lines were carefully chosen to match the points to match the thermocouple placement in the experiment. Three lines were created from the bottom to the top of the adiabatic back wall at spacing; $x=0.3$, $x=0$ and $x=-0.3$. With the origin taken in the middle of the adiabatic back wall as seen in Section 4.3.2. As well as, two horizontal lines along the back wall at height 0.7m and 1.1m.

4.3.3 Grid Convergence Index (GCI)

The mesh or grid size plays a critical role in the accuracy of CFD simulations. A coarse grid can result in inaccurate results that deviate from reality, while an overly refined grid demands incredible computing power making them very expensive and time-intensive. Therefore, grid refinement studies are an essential part of CFD simulations. A common way to study grid refinement is to perform a grid convergency index (GCI). "The GCI calculates a percentage error between the numerical solution and the asymptotic value, offering insight into how the solution will change with further grid refinement" [62] (Nguyen, 2021, p. 213). Although the GCI can be computed for only two grid levels, it is recommended to compute for three grid levels for an accurate GCI estimation [62]. Three grid levels (coarse, medium and fine) are computed which means that two GCIs can be computed; one GCI which calculates the deviation between the coarse and medium grid and one GCI between the medium and fine grid

It shows the change in solution with further refinement of the grid. If the GCI is smaller than 5%, it means that the deviation between the two grids is small enough and that the finer grid out of the two compared grids can be chosen [61]. The medium grid was the chosen grid for the validation and application studies. The GCI can be computed by:

$$GCI = \frac{F_s \cdot |\epsilon|}{(r^p - 1)}, \quad (6)$$

$$\epsilon = \frac{u_1 - u_2}{u_2}, \quad (7)$$

$$p = \frac{\ln(\frac{\epsilon_{32}}{\epsilon_{21}})}{\ln(r)} \quad (8)$$

where:

F_s = the safety factor

ϵ = the relative error

r^p = the refinement factor

p = the apparent order of accuracy

u_1 = the chosen metric, in this case temperature of grid 1

u_2 = the chosen metric, in this case temperature of grid 2

F_s is 1.25 when three grids are compared [54] and r^p is $\sqrt{2}$, since there is a difference of $\sqrt{2}$ between the amount of cells between every grid. The velocity magnitudes are obtained from the simulation results of the calculation lines determined in Section 4.3.2. In this case the temperature was chosen to compare the different grids with one another.

The code used to calculate the GCI for the 3 grids is found in Appendix B.2. The GCI which was found between the coarse and medium grid was 2.84%. Which is smaller than the before mentioned 5%. As a result,

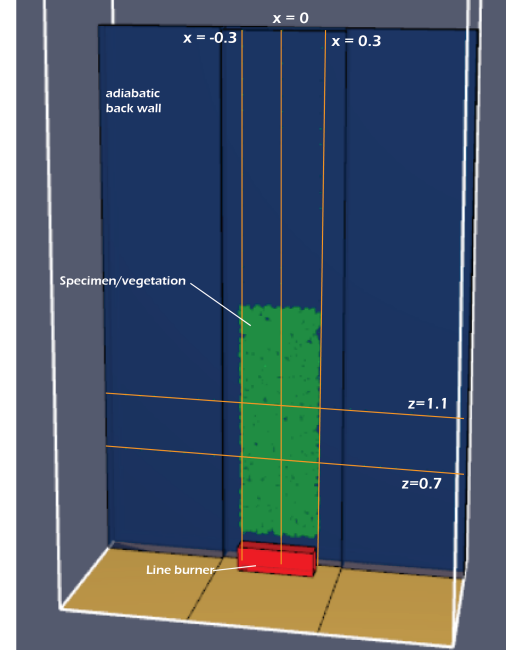


Figure 34: Calculations Lines Validation Study

it can be stated that the mesh does not impact the results significantly so of these 2 meshes the finest can be chosen and this mesh can be used for the following application studies.

4.4 Combustion model

The current FDS input file creates a solid-phase pyrolysis model with a moisture evaporation burning model. This burning model consists of 2 main stages; the evaporation stage and the solid phase pyrolysis stage.

To start off the vegetation which is modeled is wet vegetation having a moisture fraction which needs to be input by the modeller. In this case that is 22.5% which was the exact moisture content found during the experiments in Section 3.5. This model first evaporates the moisture of the object before it can ignite. The water is modelled to start evaporating at 100 °C. The enthalpy of vaporization is the amount of energy required to transform a quantity of water into water vapour. This energy is required to change the molecular connections and change the phase from liquid to gas [63].

The specific latent heat of water vaporizations is also defined in the code, as 2260 kJ/kg which was taken from literature [63]. The total heat needed is calculated by the model by Equation (9) which is then implemented in the model for overall accuracy.

$$Q = m * h_{evap} \quad (9)$$

with:

Q = Total heat required [J]

m = mass of liquid [kg]

h_{evap} = latent heat of evaporation [J/kg]

Once the water vapour is released into the domain, the vegetation is considered dry plant material, at which point it becomes susceptible to pyrolysis. The initiation of pyrolysis is governed by the reference temperature defined in the computational model. In this study, a threshold temperature of 270°C was selected, representing the onset of the next chemical reaction phase, during which pyrolysis gases are generated. This choice was based on literature which established ignition temperatures for cellulose-based materials, which typically range between 250°C and 350°C [64, 65]. As well as, trying different ignition temperatures and seeing which results more closely resembled the experimental data.

Unlike most FDS models this model will have to incorporate a VGS which has a different burning behaviour compared to a standard exterior wall. It is important to know the physical properties of the added greenery. It is difficult to measure thermal properties of thin biological specimen like plant leaves [66]. What needs to be modeled in the FDS simulations is the dry vegetation and the char and ash when the vegetation is burned. To model this the following thermal properties are needed: the density ($\frac{kg}{m^3}$), conductivity ($\frac{W}{mk}$) and specific heat ($\frac{kJ}{kgk}$). The density as well as the conductivity can be assumed to be constant over all temperatures. However, the specific heat of all three materials is dependent on the temperature [37]. To calculate the specific heat of the materials the following formula's were defined by Karunaratne et al. [37, p. 2]:

$$C_v = 0.1031 + 0.003867T \quad (10)$$

$$C_c = 0.42 + 0.002T + 6.85 * 10^{-7}T^2 \quad (11)$$

$$C_a = 1.244\left(\frac{T}{300}\right)^{0.315} \quad (12)$$

With:

C_v = Specific heat dry vegetation

C_c = specific heat char

C_a = specific heat ash

T = Temperature.

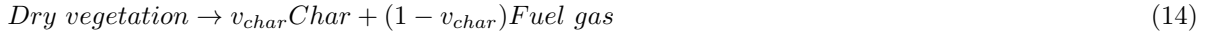
With the help of the RAMP function in FDS the user can specify a function with one independent variable, which in this case is the temperature, and one dependent variable, the specific heat [37]. Using this RAMP function allows for more accurate fire modelling rather than using a single specific heat value.

To correctly model the fire behaviour a pyrolysis model needs to be implemented. FDS has their own pyrolysis model to "study the upward fire spread along the VGS which simulates the solid-phase thermal degradation process using three reactions: the endothermic moisture evaporation, endothermic pyrolysis of dry vegetation and exothermic char oxidation." [37, p. 3] equations are from [8]. Below are shown the chemical reactions which take place during the burning process of vegetation.

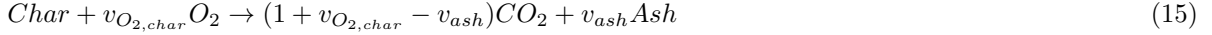
Endothermic moisture evaporation



Endothermic pyrolysis of dry vegetation



Exothermic char oxidation



v_{H_2O} = the mass fraction of water within the solid or the moisture fraction (MF)

v_{char} = the mass fraction of dry vegetation that is converted to char during pyrolysis

$v_{O_{2,char}}$ = the mass of oxygen required per unit mass of char consumed

Equation (13) shows how the initial moisture in the plant would evaporate which results in dry vegetation and water vapour. Equation (14) shows the reaction taking place afterwards, in which the dry vegetation undergoes volatile pyrolyzation by further decomposing and emitting gasses. Finally, Equation (15) shows the last step which is the oxidation of the remaining char by omitting CO_2 and leaving just ash [37]. The rates of these reactions are based on the initial density (ρ_s) of the combination of the following: dry vegetation ($\rho_{s,dry}$), moisture (ρ_{s,H_2O}), char ($\rho_{s,char}$) and ash ($\rho_{s,ash}$). As well as the vegetation kinetic constants which exist of the pre-exponential factor (A) and the activation energy (E). These formulas are also defined by the FDS pyrolysis model and shown below [8].

$$r_{H_2O} = \left(\frac{\rho_{s,H_2O}}{\rho_s(0)} \right) A_{H_2O} T^{-\frac{1}{2}} \exp\left(-\frac{E_{H_2O}}{RT}\right) \quad (16)$$

$$r_{pyr} = \left(\frac{\rho_{s,dry}}{\rho_s(0)} \right) A_{pyr} \exp\left(-\frac{E_{pyr}}{RT}\right) \quad (17)$$

$$r_{char} = \left(\frac{\rho_{s,char}}{\rho_s(0)} \right) A_{char} \exp\left(-\frac{E_{char}}{RT}\right) \frac{O_2 \sigma (1 + \beta_{char} \sqrt{Re})}{v_{O_{2,char}} \rho_s(0)} \quad (18)$$

$$Re = \frac{\rho U D_v}{\mu} \quad (19)$$

Re is the Reynolds number which defines the speed of the airflow close to the charred surface. where ρ is the gas density, U the gas velocity, and $D_v = \frac{4}{\sigma}$ for a cylinder in which σ is the surface to volume ratio [37].

4.4.1 Lagrangian particle model

The lagrangian particle model was created to specifically represent vegetation in FDS. The model allows for the representation of vegetation like leaves, grass and so on. It does this by creating different particles in a chosen volume and placing them inside the chosen volume. It allows for the tracking of individual particles as they move through fluid or in this case air. It allows for individual creation of the leaves instead of simulating them like a solid block of material which is more realistic to the real scenario [8, 67]. The model has been validated by NIST itself. They have created multiple validation studies on which they have based their models to ensure realistic modelling. The validation study which was used as an example for the model of this particle study was the pine needle validation study. During this validation study, 1 kg of wet pine needles in $1m^3$ was burned. The vegetation was heated until all the water and fuel were evaporated. Note that the fuel gas was not allowed to burn due to them setting the ambient oxygen concentration to 1%. The results of this simulation can be seen in Figure 35 [8].

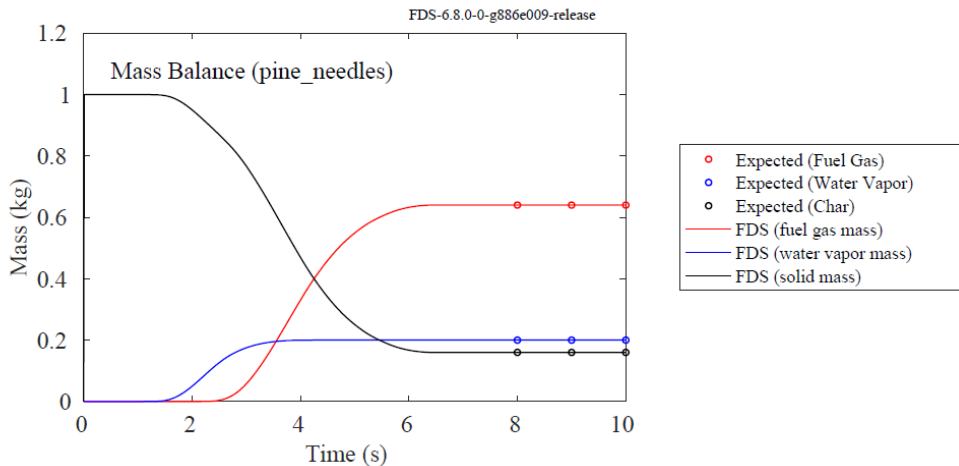


Figure 35: Pine Needle Validation Study FDS [8]

It should however be noted that whilst this model does accurately represent the leaves it does not model the twigs. The choice was made to use the lagrangian particle model because the vegetation had a much higher rate of leaves compared to the twigs this is clear when reviewing the specimen shown in Section 3 [8, 37, 68].

Due to the modelling of individual particles, airflow can take place in between the leaves. The drag force per unit area (f_b) is shown in Equation (20) below.

$$f_b = \frac{\rho}{2} C_d C_s \beta \sigma u \|u\| \quad (20)$$

With: [8]

f_b = force per unit volume exerted by the vegetation

ρ = air density

C_d = the drag coefficient

C_s = the shape factor (shape of the leaves)

β = packing ratio (the mass per unit volume divided by the material density)

σ = surface area to volume ratio

u = air velocity

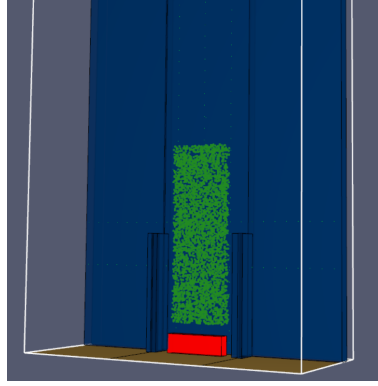


Figure 36: Validation study setup

4.5 Result Validation Study

The chosen grid was the median grid as the GCI was low enough as mentioned in Section 4.3.3 and had acceptable computational times. The validation study was then performed with the input being as close as possible to the real-life experiment to ensure uncertainties will not influence the results, see Figure 36.

The experimental results used for comparison were obtained from Tests 3 and 4. However, due to the window opening during Test 4, the data recorded between 13 and 19 minutes was deemed corrupted and subsequently removed from the dataset. Aside from this excluded data, the median values of the remaining results from both tests were calculated to represent the overall experimental dataset.

The simulation was conducted for a total of 30 minutes and was modelled based upon setup 3 discussed in Section 3.4.2. Figure 37a and Figure 37b show the median temperatures recorded at each thermocouple position for both the simulation and the experimental tests.

A significant deviation is observed between the simulated and experimental results. The exact difference is presented in Figure 37c. Notably, the middle and top thermocouples in the simulation recorded substantially higher temperatures than those in the experiment. In contrast, the exterior thermocouples measured a considerably higher temperature in the experiments than the simulations, with differences exceeding 100 °C.

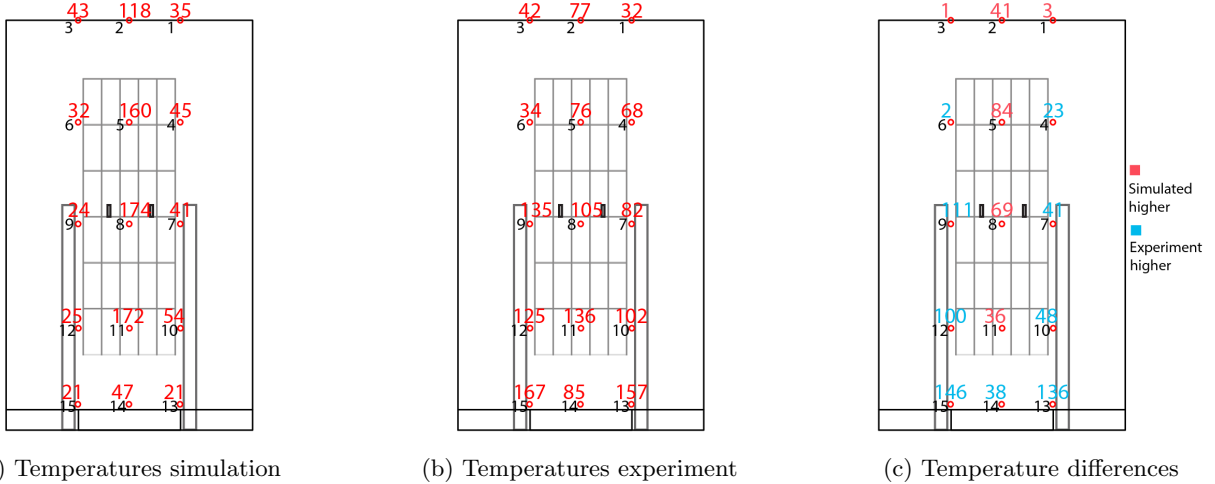


Figure 37: Median temperatures per thermocouple

One key observation that becomes abundantly clear from this is that the temperatures on the sides of the

simulation are much lower compared to the experimental data. when reviewing the temperatures close to the measurement points on the sides, the temperatures are very clearly low. However, moving slightly inward from these points, the temperature rises sharply, suggesting a strong spatial gradient in the simulation.

This trend is also supported by Figure 38a and Figure 38b. At $x = -0.3$, the simulated temperatures remain notably low and fail to follow the trend observed in the thermocouple data. In contrast, Figure 38b demonstrates a better agreement in trend. The simulation captures the temperature peak at lower values, followed by a rapid cooling phase, before experiencing a minor increase again. This data is extracted from the $x = -0.18$ line, indicating that while the overall trend aligns more closely with experimental results. The thermocouples placed at $x=-0.3$ and $x=0.3$ are placed on the sides of the sample as shown in Figure 34

When analysing the temperatures at the $x=0$ line, the centre of the specimen see Figure 34, the simulated temperatures are consistently higher, resulting in a higher median temperature compared to experimental results. Despite this difference in magnitude, the overall temperature trend in the simulation aligns with that observed in the experimental results. However, a notable discrepancy is that the cooling rate in the experimental data is significantly faster than in the simulation, suggesting that heat dissipation mechanisms may not be fully captured or accurately represented in the numerical model.

Figure 39b shows the mass loss both experimental and simulated. The trend is very similar, with a steep initial loss and then following a gradual decline. The experimental data shows an even more rapid decrease and also a faster decline rate compared to the simulated data. This could be due to the ignition temperature of the plants which is input by the user being too high being input too high compared to real life. This range is known to be quite wide based on literature and could thus vary from the input temperature.

However, the overall trend remains consistent between the datasets. This is further supported by the calculated correlation coefficient. A correlation coefficient of 1 indicates a highly similar trend, while 0 signifies no relationship, and a negative value suggests an inverse correlation [69]. For these two datasets, the correlation coefficient is 0.7, indicating a strong similarity in their trends.

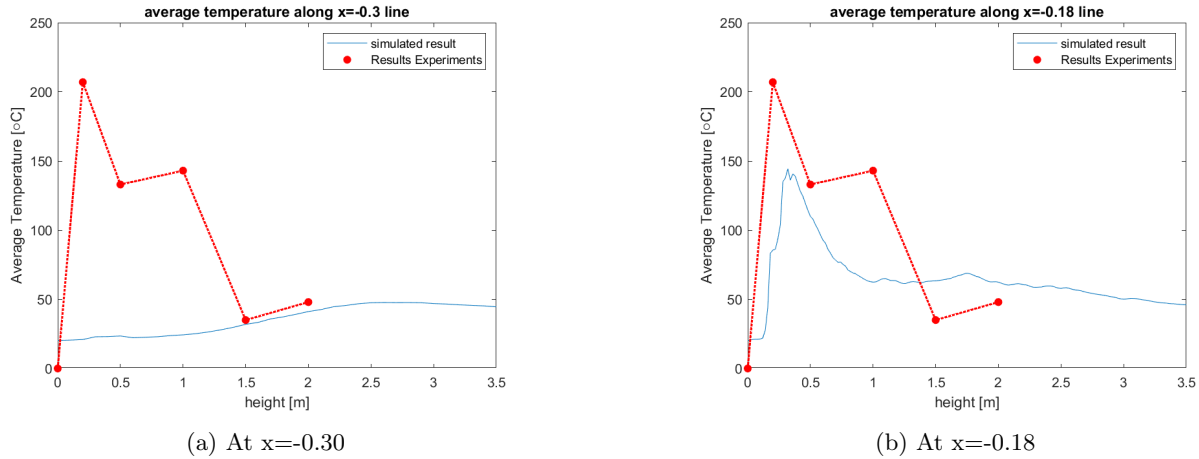
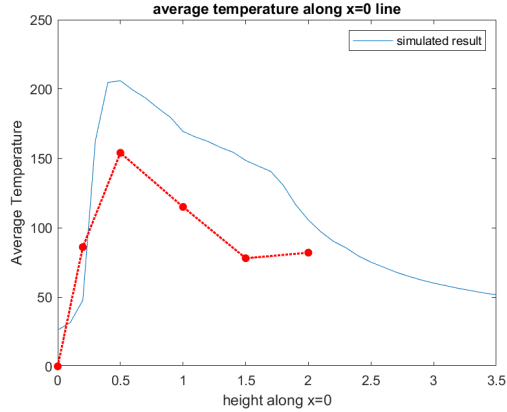
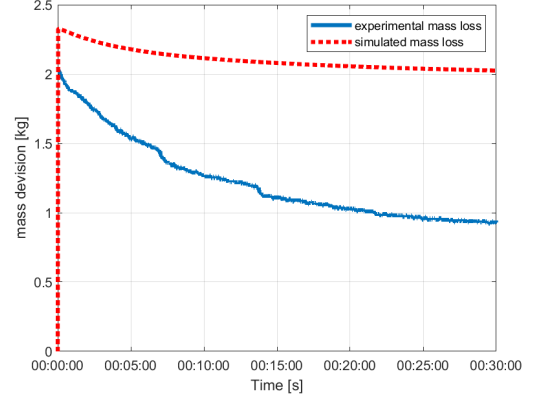


Figure 38: Simulated and experimental temperatures



(a) Simulated and experimental temperatures At $x=0$



(b) Mass loss simulated and experimental

Figure 40 illustrates the overall average temperature recorded throughout the experiment. This was achieved by analyzing each pixel individually and determining its RGB color code for every frame in the recorded data. The process involved extracting the RGB values of each pixel across all frames, summing these values, and subsequently dividing by the total number of analysed frames. This approach results in an average pixel colour representation, providing a visual indication of the temperature distribution over the entire duration of the experiment. This was done with matlab the precise code for this process can be found in Appendix B.2.

This figure clearly shows that the sides of the sample exhibit higher temperatures compared to the centre. This trend was also evident in the experimental samples, where the sides of the sample experienced more extensive burning compared to the centre as shown in Figure 29 in Section 3.5. This result corresponds with the findings discussed in Section 3.5. So one can conclude that this burning behaviour is true to life.

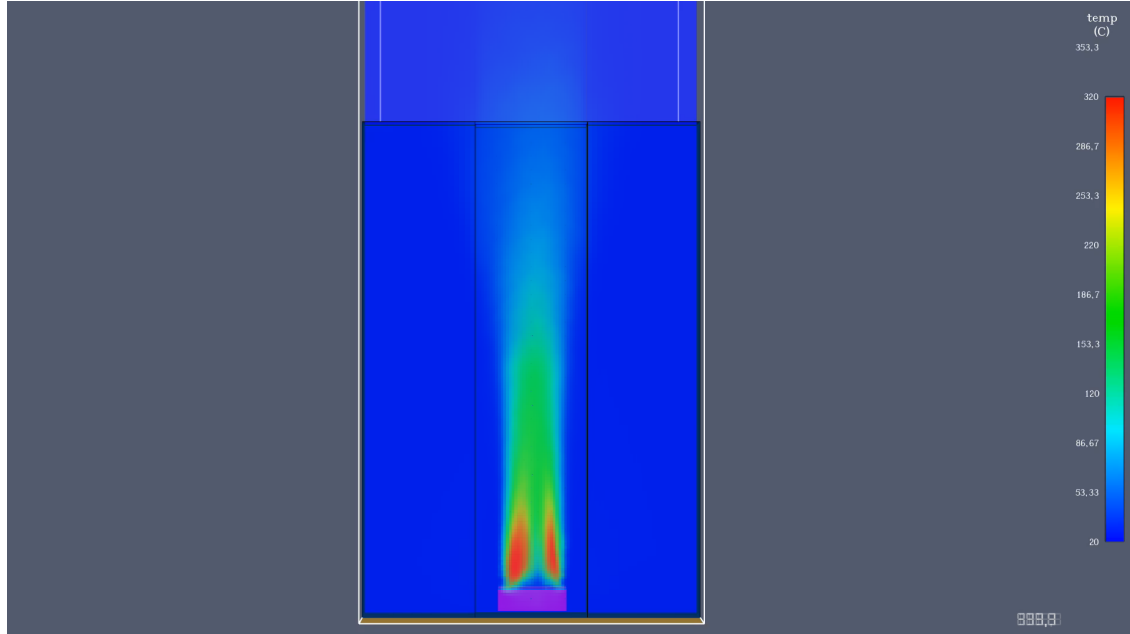


Figure 40: Average temperature recorded image

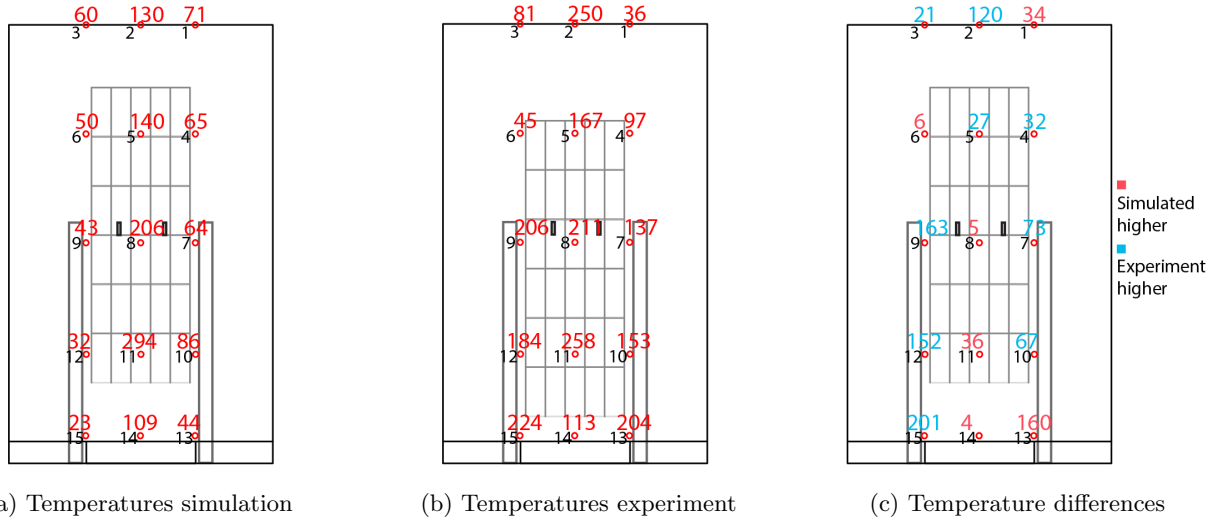


Figure 41: Maximum temperatures recorded per thermocouple

charts of Temperatures at Thermocouples for Different Moisture Contents (80% I)

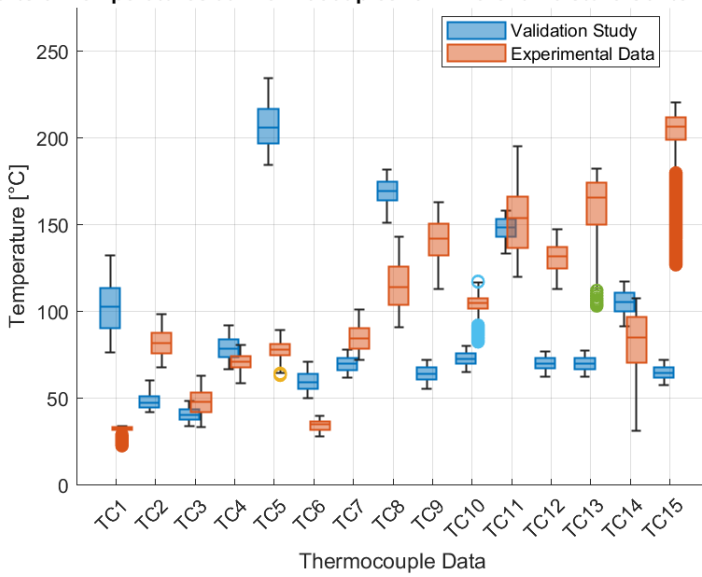


Figure 42: Boxplots Experiments and Validation Study

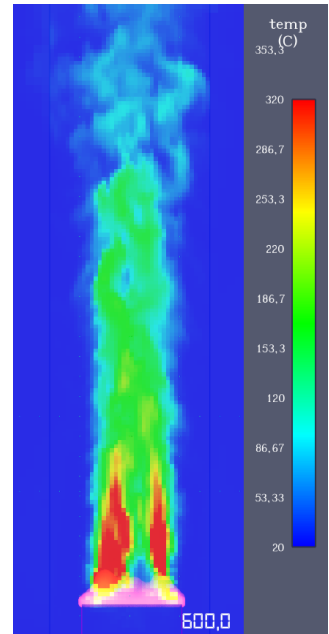


Figure 43: Temperatures at t=600

4.6 Conclusion

The validation study demonstrates that however the Fire Dynamics Simulator (FDS) effectively captures the overall fire dynamics and trends observed in experiments, certain discrepancies exist. The simulations correctly replicate general burning behaviour. The following should however be kept in mind when reviewing the application study results.

- The turbulence in FDS is not as turbulent as in real life. This is why the sides of the sample have a much lower temperature in the simulations compared to the experiments.
- The mass loss is not as great as the experimental data, this could be because the chosen ignition temperature input in the FDS code is too high. This value was chosen based on the literature found but it could be lower for this particular specimen. Conclusion I also influence the mass loss rate.
- The combustion model used is not complete combustion however it is a stochastic combustion model where the modeller defines how much % of the vegetation will turn into char and how much will burn. In this case, 20% was chosen as was recommended by the FDS user guide [8]. This however is not totally true to life and can create human error in the simulation.

5 Application Studies

With the completion of the validation study, the application studies can be conducted, with the validation study as a baseline. This way the limitations of FDS have been mapped out for the following simulations.

Multiple studies were conducted to assess the overall impact of varying specific vegetation parameters on the simulation outcomes. In each study, only a single parameter is modified, while all other aspects of the simulation setup remain unchanged. As a result, the effects that the changed parameter has on the burning behaviour can be precisely analysed.

Due to the computational limitation and the amount of studies which were performed, the time of the study was shortened significantly. This allowed for more studies to be conducted this way more characteristics could be studied. The time of the original simulations were the same as the experiments which were 30 minutes or 1800 seconds. For the application studies the time was changed to 350 seconds total, or 5 minutes and 50 seconds. The validation study that was used as baseline was also shortened to 350 seconds which is why some of the output differs from the Section 4.

With the help of the elementary effects method the exact impact of each parameter can be analysed. This method also allows for a ranking of the influence which the changed parameter has compared to the other parameters.

5.1 Different Application Studies Conducted

The different studies which were conducted were as follows:

1. Different moisture fracture in the plants

- (a) lower moisture fracture (10%)
- (b) higher moisture fracture (50%)

Two simulations were conducted to examine the impact of vegetation moisture content on burning behaviour. The vegetation in the validation study had a moisture content of 22.51%. To assess the effect of varying moisture levels, one simulation was performed with a reduced moisture content of 10%, and another with an increased moisture content of 50%.

A lower moisture content is expected to result in a faster mass loss, as less water needs to evaporate before the vegetation dries out and becomes combustible. Conversely, vegetation with a higher moisture content is expected to exhibit a slower mass loss.

These simulations emphasize the importance of proper vegetation maintenance and preventing vegetation from drying out and becoming more susceptible to combustion. Additionally, it also shows the importance of choosing the right plants for vertical systems, as different plant types have a different moisture content.

2. Different plant density

- (a) lower density (20 kg/m^3)
- (b) higher density (80 kg/m^3)

This simulation examines the packing rate/density of the vegetation. As the vegetation ages, it typically grows and becomes denser unless it undergoes regular maintenance. In these studies, the vegetation is lower and higher compared to the baseline study. However, the calculation pc's on which the higher density simulation was running crashed which is why there is only partial data for this particular study. Moreover, for the lower density part of the data was lost, the data between 80.5-160 sec.

3. Different leaf area

- (a) smaller leaf area (2.5 cm)
- (b) larger leaf area (10 cm)

To investigate the effect of leaf area on burning behaviour, two simulations were conducted. The first simulation examined a smaller leaf size of 2.5 cm, compared to the 5 cm leaves used in the validation study. The second simulation analysed the impact of a larger leaf size, increasing it to 10 cm. This study is conducted to show the importance of choosing the right plant specimens which have different leaf sizes. To see how this influences the burning behaviour.

4. Removing the lineburner after 150 seconds

During the experiments, an interesting observation was that only the vegetation in direct contact with the flames burned. Which is why this simulation was conducted to analyse if the vegetation will stop burning or smouldering combustion will occur.

5.2 Assessment Criteria/Method

In this case, the sensitivity analysis will be performed with the help of the elementary effects method, which is a screening method with global characteristics [70]. With this method, the input factors can be ranked in case of importance by how much influence they hold over the results exploring which input parameters influence the FDS model in a systematic way [71]. To correctly rank the importance of the parameters it is important to normalize input parameters [71].

The Elementary Effects method determines the so-called elementary effect (EE) of a model $y = y(x_1, \dots, x_k)$ with input factors x_i . The Elementary Effect for the i^{th} input factor at a point \mathbf{x} is: [70]

$$EE(x_i, \dots, x_k) = \frac{y(x_1, x_2, \dots, x_{i-1}, x_i + \Delta, x_{i+1}, \dots, x_k) - y(x_1, \dots, x_k)}{\Delta} \quad (21)$$

The model sensitivity for each factor is evaluated by the mean value and the standard deviation of the elementary effects

$$\mu = \sum_{i=1}^r \frac{EE_i}{r} \quad (22)$$

$$\sigma = \sqrt{\sum_{i=1}^r \frac{(EE_i - \mu)^2}{r}} \quad (23)$$

μ = mean value of the absolute values of EE determining if the factor is important

σ = standard deviation of the elementary effects measure of the sum of all interactions with x_i with other factors and of all its nonlinear effects

r = number of elementary effects investigated for each factor [70]

Through analysis of these findings alongside the outcomes derived from various simulations, a comparative assessment can be conducted with the experimental results. This facilitates the selection of inputs for the application study that closely mirror real-life scenarios.

5.3 Results

5.3.1 Different Moisture Content

Two different simulations were run with different moisture contents, one lower (5%) and one higher (50%) than the validation study. The average temperatures recorded, see Figure 98, in the lower moisture content simulation were higher compared to the one with the higher moisture content. This is due to the moisture first having to evaporate before the vegetation can be ignited which uses up a lot of energy.

Figure 44d illustrates that lower moisture content results in significantly higher pyrolysis gas production within the first few minutes. This occurs because vegetation with lower moisture content combusts rapidly in the flames of the line burner. In contrast, vegetation with higher moisture content must first undergo moisture evaporation before pyrolysis gas can be generated.

Regarding the mass loss, normalized shown in figure Figure 44b, the vegetation with 50% moisture content seems to exhibit greater overall mass loss. This observation may seem counter-intuitive, given that vegetation with lower moisture contents burns quicker. However, the mass loss also accounts for moisture evaporation. Consequently, the 50% moisture content sample experiences additional mass loss due to more moisture evaporation taking place compared to the other simulations, leading to a steeper mass loss curve. This is also shown in the moisture production curve Figure 44c.

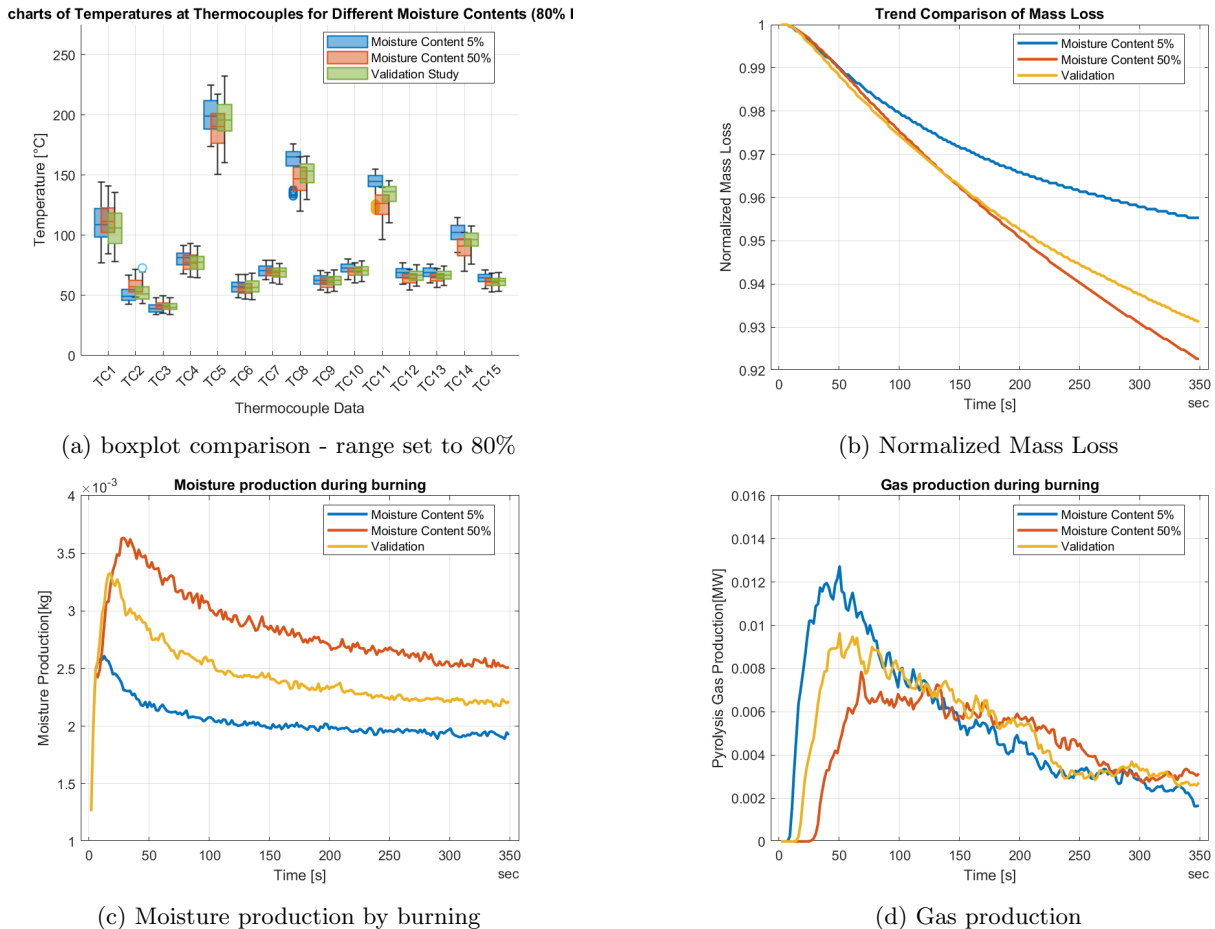


Figure 44: Different moisture Content Results

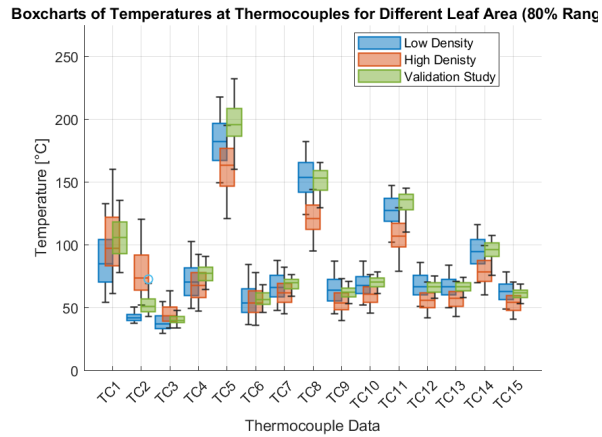
5.3.2 Different plant density

The different plant density simulations look at the different overall densities of the plants. This analysis is crucial, as plant density naturally increases over time in the absence of active maintenance. In the Fire Dynamics Simulator (FDS) model, the key parameter used to explore this effect is mass per unit volume, initially set at 40 kg/m^3 . To assess the influence of varying plant densities, two additional simulations were conducted: one with a higher density of 80 kg/m^3 and another with a lower density of 20 kg/m^3 .

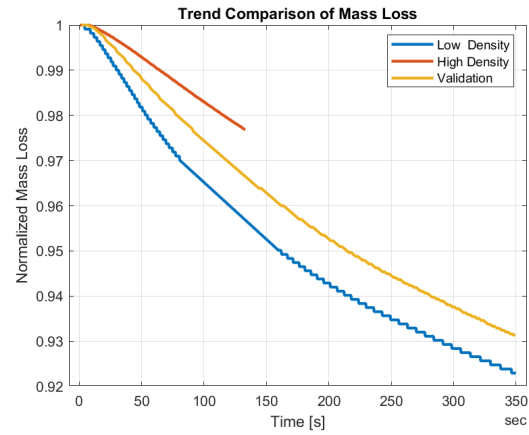
The mass per volume encapsulates both the packing factor of the simulation, the dry density of the leaves and the dry density of the stems. The original value was based on literature which suggested that the stems of *helix hedera* had a biomass density of approximately $600\text{--}900 \text{ kg/m}^3$, and the leaves $400\text{--}600 \text{ kg/m}^3$ which gives a combined density of approximately $500\text{--}800 \text{ kg/m}^3$ [72, 73]. This results in an estimated combined biomass density of $500\text{--}800 \text{ kg/m}^3$ [72, 73]. However, since the mass per unit volume parameter accounts for both dry biomass, which already accounts for a lot of the density. As well as the packing ratio of the hedge, it must reflect the porosity of the vegetation which is how the above-mentioned values came to be.

The simulation results indicate that the mass loss rate of the less dense hedge declines significantly more steeply (Figure 45b). This behaviour is attributed to faster ignition and lower overall biomass, which facilitate a more rapid combustion process. In contrast, the denser hedge produces substantially more pyrolysis gases due to the greater availability of combustible material.

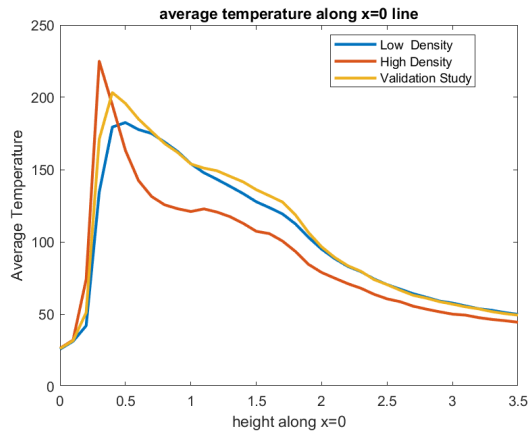
Analysis of the median temperatures recorded by thermocouples (Figure 45c) reveals that the lower-density hedge exhibits overall lower temperatures compared to the validation study. This occurs because the vegetation burns more rapidly and intensely. In contrast, the higher-density hedge undergoes a slower combustion process with a prolonged duration and lower peak intensity. However, over time, it ultimately reaches a higher median temperature than the low-density hedge due to the greater fuel availability, which sustains heat release over an extended period. This is the expected behaviour of higher-density vegetation, as the lower density has a lower median temperature as shown in Figure 45c so the higher median temperature is expected to lie on the other side of the validation curve.



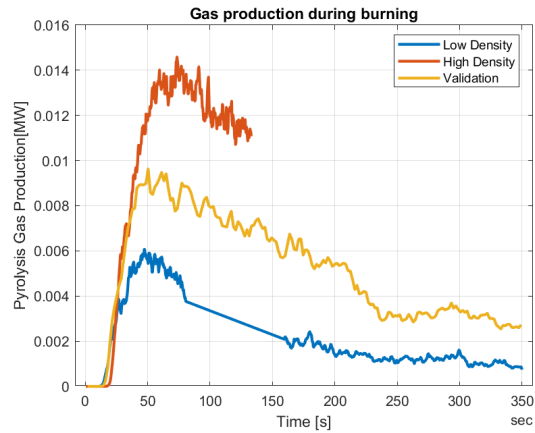
(a) boxplot comparison - range set to 80%



(b) Normalized Mass loss Plant Density



(c) Average recorded temperature at $x=0$



(d) Pyrolysis gas formation Density

Figure 45: Average temperature image different moisture levels

5.3.3 Different leaf area

Another physical plant attribute which was tested was the leaf area. This change went from an original leaf thin leaf which had a size of 5cm wide and 2mm thick to a larger one of 10cm and a smaller one of 2.5cm, all were 2mm thick. This changes the surface area which the flames can heat. The median temperatures over the whole sample area were however still very close together as shown in Figure 46a.

The results shown in Figure 47 show that there was a slight influence of changing the leaf area. The larger leaf area seemed to burn hotter, see Figure 46a and Figure 46d. However, the mass loss of the smaller leaf area was steeper indicating more of the vegetation was burned with the smaller leaf area. This was also shown in the pyrolysis gas production where the smaller leaf produced more gas, see Figure 46c.

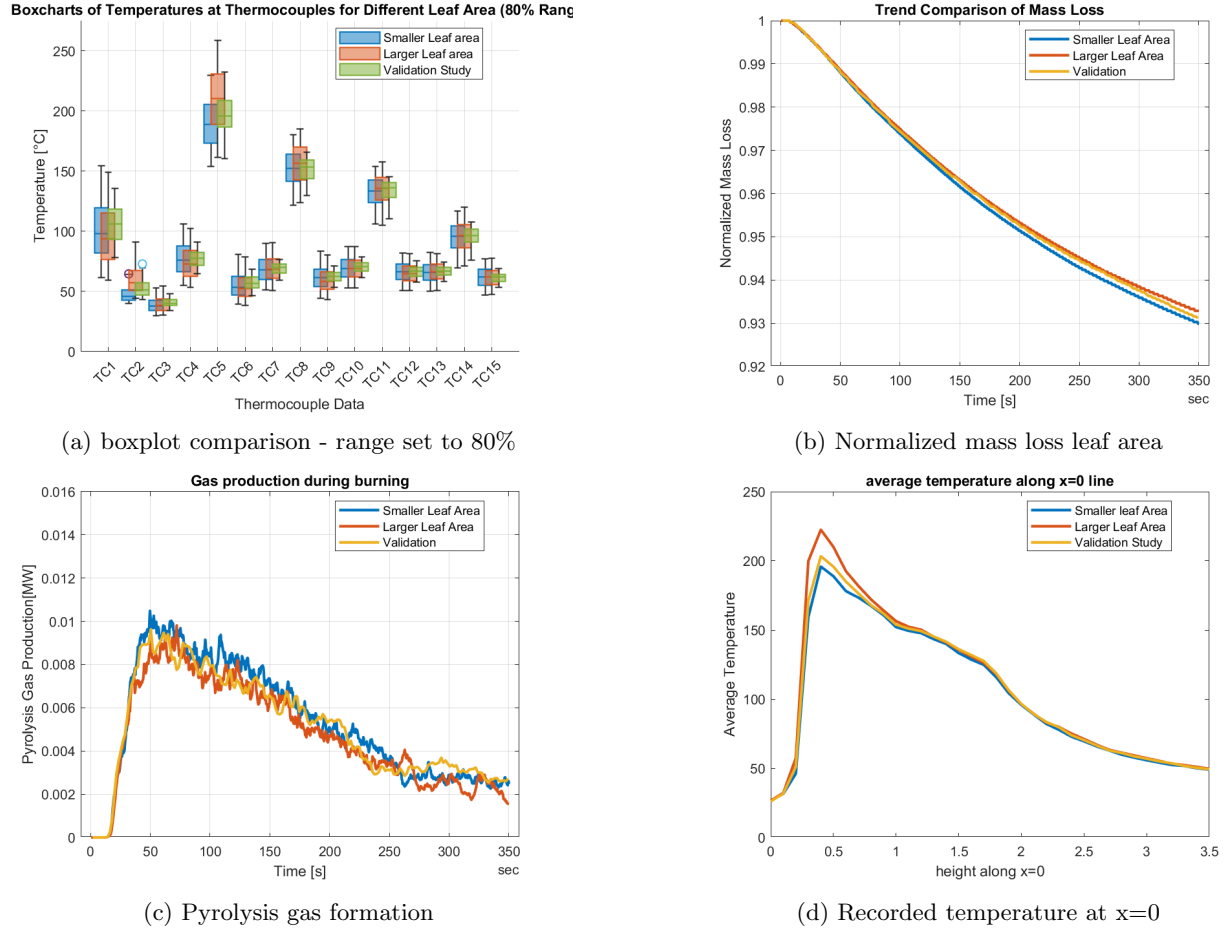


Figure 46: Results different leaf area simulation

5.3.4 Lower Ignition Temperature

The lower ignition temperature of the vegetation looks at the temperature of ignition of the vegetation. This is an attribute of the vegetation which is linked to the vegetation type and its chemical properties. The original burning temperature was 270 °C based on found literature as mentioned in Section 4.4. The lower burning temperature that was chosen was 200 °C.

The lower ignition temperature resulted in a significantly steeper mass loss curve (Equation (1)) and substantially higher pyrolysis gas production (Figure 47c). However, the median temperature during combustion was lower than that observed in the validation study, as shown in Figure 47a and ???. Despite this, the temperature range was broader and included higher values compared to the validation study. This can be attributed to the greater heat release associated with the combustion of vegetation at a lower ignition temperature.

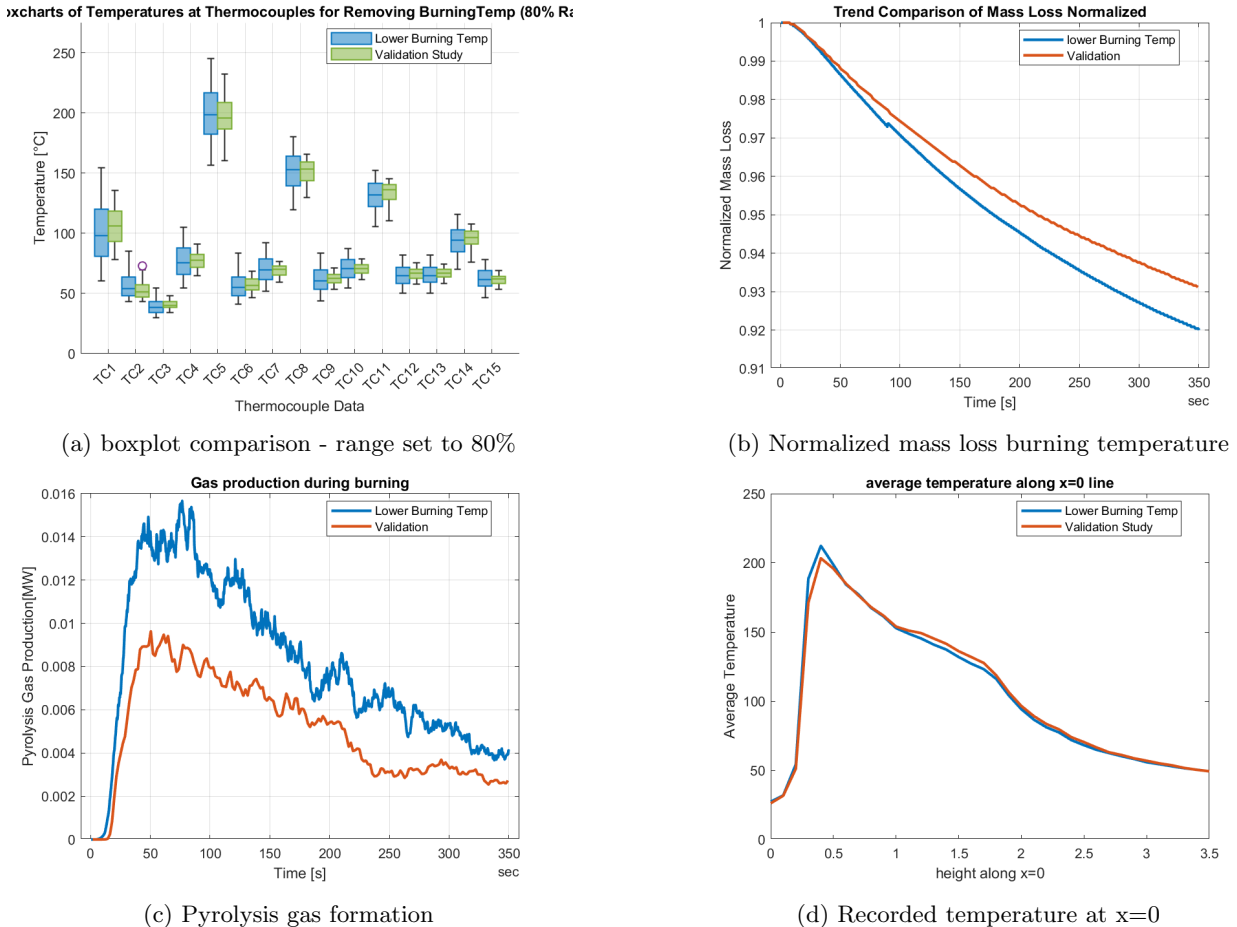


Figure 47: Results different leaf area simulation

5.3.5 Removing lineburner

An important observation made during the experiments was that vegetation only ignited when in direct contact with the flames (Section 3.5). Which is why this application study was created in which the line burner was turned off after 150 seconds to assess whether this phenomenon was also reflected in the simulations or if smouldering combustion would occur.

As shown in Figure 48b, the mass loss rate declines rapidly after 150 seconds, though a slight decrease persists, indicating that the vegetation continues to smoulder to some extent after the line burner is extinguished.

This observation is further supported by the recorded temperature data presented in Figure 48a, which demonstrates a sharp and significant drop in temperature. However, complete cooling requires additional time.

The pyrolysis gas production, however, very quickly drops to 0 after the lineburner has been turned off. At 160 seconds the formation of pyrolysis gasses is at 0, Figure 49a which seems contradictory to the mass loss. This means that all the mass loss that happens after 160 seconds occurs due to the evaporation of moisture which was present in the vegetation. This is supported by Section 5.3.5 which shows the moisture production in the air. It shows that it takes longer to level out which is what is also shown in the overall mass loss.

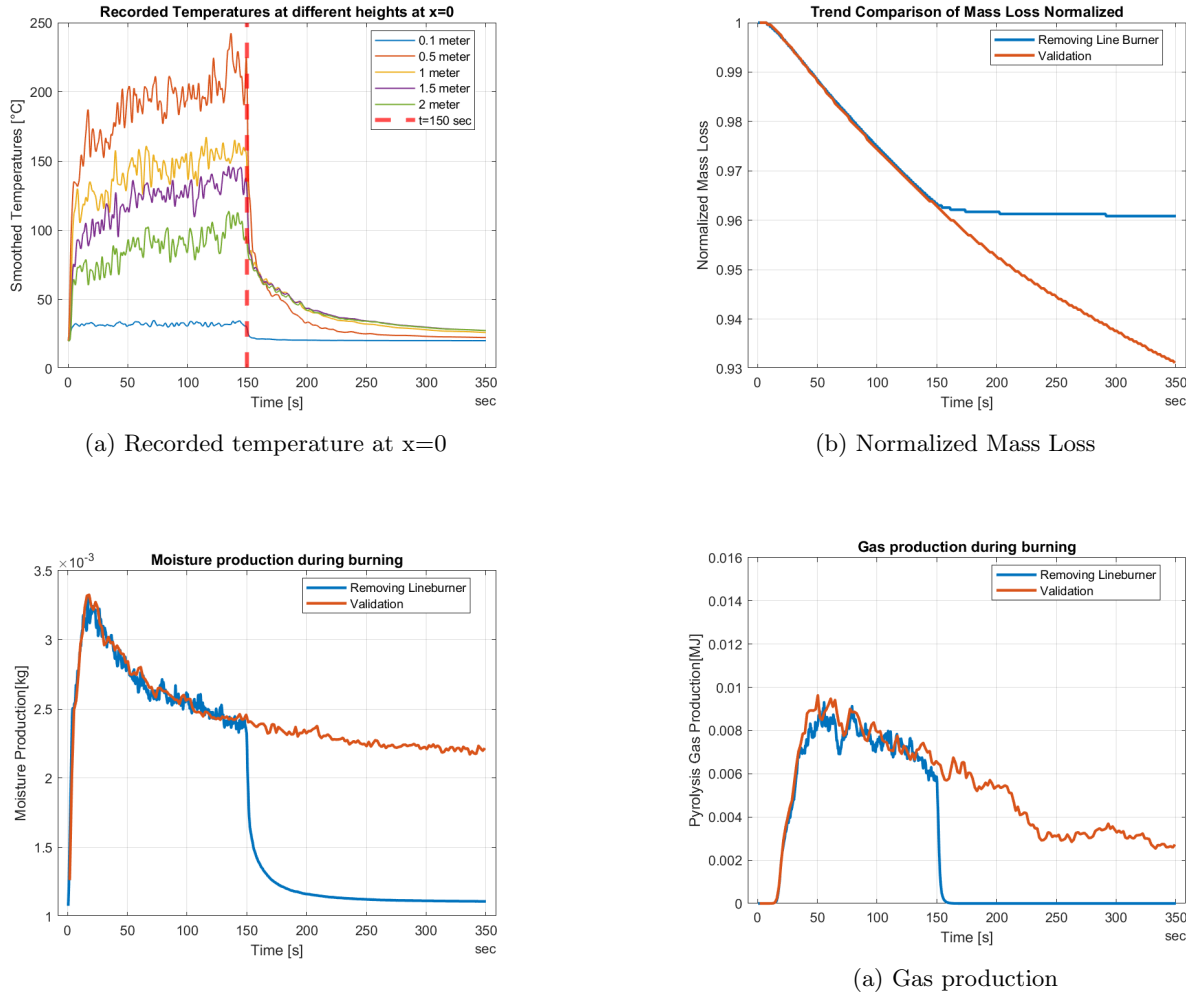


Figure 49: Different moisture Content Results

5.3.6 All Simulations

The simulation results reveal that changes in key vegetation parameters significantly influence fire behaviour, with some factors having a greater impact than others. Figure 53 illustrates mass loss trends, showing that low-density vegetation burned the fastest, while the high-density scenario retained the most mass. The latter deviated most from the validation study in terms of mass loss, whereas other simulations remained relatively close, shown in Figure 53. This is however based only on the first bit of data which is all that was simulated for the high density. The 5% moisture content case also deviated quite a bit from the validation study. The reduced initial mass resulted in lower total mass loss due to the absence of moisture evaporation.

Thermocouple	1	2	3	4	5	6	7	8	9	10	11	12	13	14	15
Validation Study	8	15	8	8	19	8	8	21	8	9	30	11	9	12	25
Moisture Content 5%	8	16	8	8	21	9	8	21	8	9	27	11	6	10	26
Moisture Content 50%	8	15	8	8	20	8	8	21	8	9	29	12	6	10	22
Smaller Leaf Area	12	19	13	12	21	14	15	25	15	17	32	21	10	13	39
Larger Leaf Area	12	20	13	13	22	14	15	26	16	17	40	20	12	20	35
Lower Plant Density	12	19	14	14	21	14	17	26	16	20	30	22	11	10	33
Higher Plant Density	12	27	12	12	21	13	14	22	15	18	31	19	13	27	39
Lower Burning Temperature	13	18	13	13	21	14	16	25	16	17	36	21	11	19	38

Table 5: Standard Deviation per Thermocouple

Pyrolysis gas production, see Figure 50, was highest in simulations with lower burning temperature, and increased plant density, while the lowest values were observed in their respective counterparts. The low moisture content also had quite the pyrolysis peak at the start of the simulation however, it quickly decreased after the initial peak.

The temperature profiles, however, followed a different trend. The large leaf area scenario exhibited high combustion intensity close to the ignition source, but temperatures dropped more quickly at higher elevations. In contrast, low-moisture vegetation burned hotter than the validation case and maintained elevated temperatures throughout the entire simulation, as shown in Figure 52 and 51.

The high-density simulation crashed, limiting the available data. Consequently, its median temperature appeared lower than in other cases, but a more refined evaluation would require a proportional comparison within the recorded time frame.

An important insight came from the simulation where the line burner was turned off after 150 seconds, mimicking the real-life experimental observations. The results confirmed that vegetation alone was unable to sustain combustion, as pyrolysis gas production ceased almost immediately after flame removal. This suggests that self-sustaining smouldering ignition is unlikely under these conditions, emphasizing the dependence of vertical green systems (VGS) on external heat sources for sustained fire propagation.

Overall, these findings highlight that moisture content, plant density, leaf area, and ignition temperature are key determinants of fire behaviour in VGS. Lower moisture and smaller leaves enhance flammability, whereas higher-density configurations slow but prolong combustion. Additionally, VGS fire risk is largely dependent on external ignition sources, as vegetation does not sustain combustion independently. These insights provide a valuable foundation for further investigations into large-scale fire behaviour and fire safety measures in green façades.

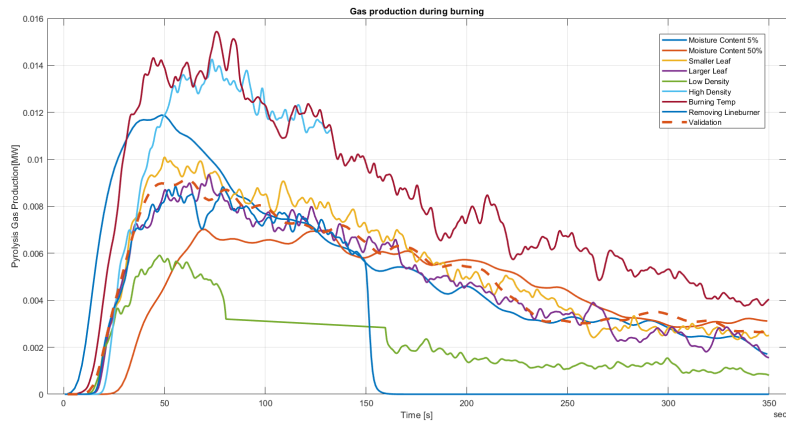


Figure 50: Pyrolysis Gas Production All Simulations, With Gaussian Smoothing

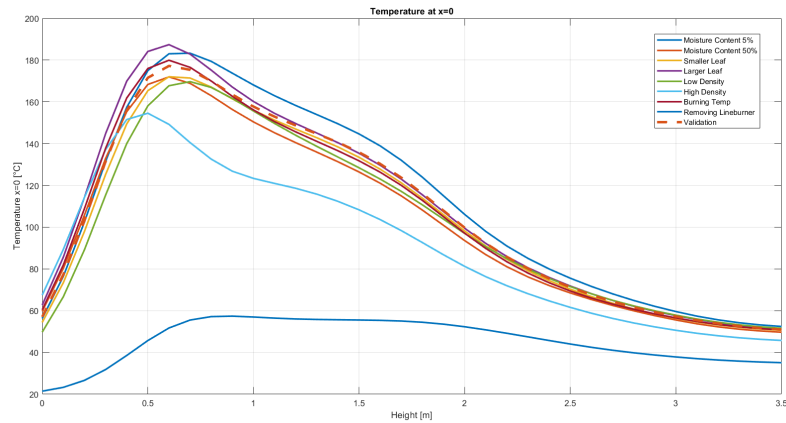


Figure 51: Median Temperature at $x=0$ all simulations, With Gaussian Smoothing

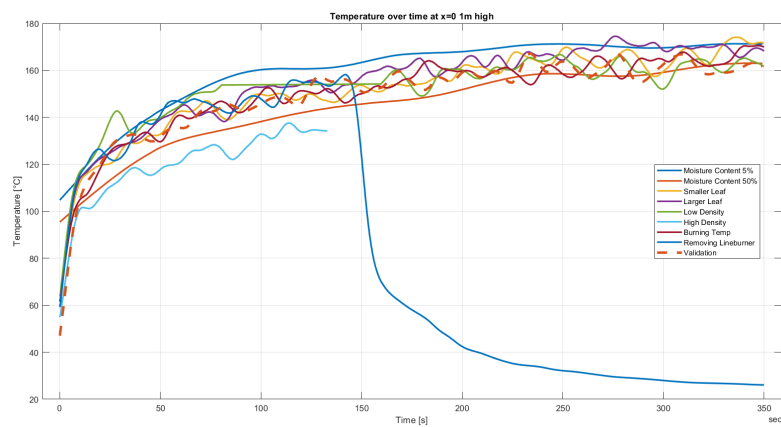


Figure 52: Temperature over time of $x=0$ 1m high

Simulation	Total Pyrolysis Gas Produced [MJ]
Validation	1.789
Moisture 5%	1.9024
Moisture 50%	1.5694
Energy Small Leaf	1.8577
Energy Large Leaf	1.6743
Lower Plant Density	0.7772
Higher Plant Density	1.2597
Lower Burning Temperature	2.8394
Removing Lineburner	0.9437

Table 6: the total formed pyrolysis gas during the simulation

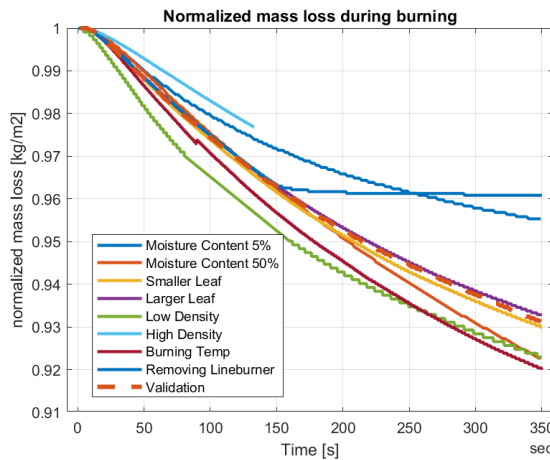


Figure 53: Normalized mass loss all Application Simulations

5.4 Elementary Effects Analysis

Section 5.5 shows the outcome of the Morris elementary effect analysis which was performed. The precise code which was created to perform this analysis can be seen in Appendix C.6. The Elementary Effects (EE) method gives two outputs, μ which shows the average impact of an input on the output differences [70]. A high μ indicates that changing that input value has a large effect on changing the output value. The standard deviation, σ , is how much the input's impact changes in different situations. A high σ indicates that the input impact is inconsistent or non-linear and changes depending on interactions with other parameters. Meaning if it is low the parameter is more consistent and predictable [70].

A low σ indicates that the effect of the input variable remains relatively consistent across the tested range. When coupled with a high μ , it suggests a consistent strong and predictable influence. On the contrary, a low σ combined with a low μ implies that the input variable has little to no impact on the output [74]. Overall, μ is seen as the more important result of the EE method as it shows the influence magnitude of the input variable [70].

The heat flux which is measured over different heights at the surface of the back wall is strongly influenced by the parameters that control the fire's energy release and the vegetation (fuel) geometry. When reviewing the μ of the EE analysis for the heat flux outputs it shows that the vegetation density as well as the leaf area influence the output a lot. This is mostly the case for the heat flux which is measured at lower points, as shown in Section 5.5. The raising of the plant density has a lot of impact, as more fuel will lead to greater heat release, thus a higher radiative flux.

When considering the leaf size the output is dependent on the size of the leaf. The radiative heat output is different for the leaf size as small fuel particles (small leaves) ignite quicker and burn more intensely which increases the heat flux. Compared to large fuel which burns slower and longer which leads to a lower heat flux peak. The leaf size influences the burning rate as the mass loss rate is related to the surface area-to-volume ratio.

The median temperature is also more strongly influenced by parameters which influence the fire's intensity and the burning rate. This shows that the leaf size and the moisture content are the biggest influences.

When reviewing the pyrolysis gas formation the strongest influences are the vegetation density and the vegetation burning temp. So the most important influences for pyrolysis gas production are related to the fuel structure and burning conditions, as these control how much fuel is available for pyrolysis as well as the ignition threshold. The moisture content has the lowest effect.

The water vapour release is very much so controlled by the amount of water available for evaporation. This is shown by the two most influential inputs being the moisture content as well as the plant density. The moisture content controls the precise amount of moisture in the plant and a higher density means more plants are present and thus more water will be available for evaporation.

The mass loss is controlled by how much fuel is available and how quickly it burns. Which is why the plant density has a very high impact. After the plant density, the moisture content is the most important. This is because having more moisture in the plant slows down the ignition time, due to the moisture first having to evaporate before the plant is dried out and ignition can take place.

Another aspect to examine is whether an input variable consistently exerts a significant influence on all outcomes or primarily affects a specific one. For instance, when reviewing the moisture content as an input parameter it dominates in mass loss and water vapour production. However, its influence on thermal output—measured by heat flux and median temperature—is relatively limited. This suggests that vegetation with higher moisture content requires more energy for moisture evaporation. However, once the moisture has been removed, the subsequent combustion process and the resulting peak heat flux or temperature output remain largely unaffected, with other input parameters exerting a more significant influence.

The vegetation density, however, has a large influence on all parameter outputs, except the median temperature. It could however be that the median temperature influence is skewed due to there not being a lot of data available for high density. An increase in vegetation density provides more fuel for combustion, which should result in higher median temperatures and elevated heat fluxes. Furthermore, greater vegetation density contributes to increased moisture content and vegetation mass, which affects both the mass loss and water vapour production. The vegetation density, thus the fuel load, is the primary determinant for heat flux, temperature and mass loss as well as the production of pyrolysis gases, which are released during biomass combustion.

The physical attributes of the leaves which are defined by the leaf size as well as the surface-to-volume area, and the vegetation density, have a big impact on the heat flux as well as the temperature output. fine fuels, like small leaves and high surface areas, promote rapid combustion. As shown in Section 5.5 this yields a high μ for these outputs. However, the leaf area has almost no input on the pyrolysis gas and water vapour formation nor the mass loss. From this can be concluded that it primarily changes how the fuel burns (fast and hot vs. slow and cool) rather than how much fuel is burned or vapour produced.

In contrast, the chemical parameter which is examined (the burning temperature) of the vegetation consistently affects all outputs dependent on combustion completeness. A lower ignition temperature will make it easier for the fire to consume the fuel, thereby raising the heat flux, and median temperature. It also raises pyrolysis gas production, as more fuel is burned.

The inputs which have a consistent effect on all outputs are the vegetation density and the leaf area. This

makes them fundamental drivers of a fire's size and duration, changes in these inputs will be felt in the outputs.

5.5 Conclusion

The findings from the elementary effects analysis and simulation results lead to several key conclusions regarding the fire behavior of vertical green systems (VGS).

- **Fuel Load and Vegetation Density:** The most significant factor influencing fire behaviour is the fuel load, which is directly related to vegetation density. A higher density results in a prolonged combustion process, leading to greater mass loss and higher temperature and heat flux outputs.
- **Leaf Geometry and Combustion Characteristics:** The impact of leaf size on fire behaviour, though consistent, remains relatively minor. Smaller leaves burn more intensely and rapidly, whereas larger leaves sustain combustion for a longer period, producing higher overall temperatures over time. This aligns with the observed trends in median temperature and pyrolysis gas production.
- **Chemical Composition and Ignition Temperature:** The ignition temperature of vegetation plays a critical role in fire propagation. A lower ignition temperature leads to faster combustion, increasing mass loss rate, and heat flux. Thus, selecting vegetation with higher ignition temperatures can help mitigate fire risks.
- **Moisture Content and Fire Resistance:** Moisture content primarily affects ignition time, acting as a natural barrier by delaying combustion. Lower moisture levels accelerate the ignition and result in higher median temperatures, shown in Figure 52. However, once the moisture has evaporated, the combustion process proceeds with little additional influence from the initial water content.
- **Self-Sustaining Combustion and External Ignition Sources:** The simulations confirm that vegetation alone does not sustain prolonged combustion. When external flames are removed, smouldering continues for only a short duration before self-extinguishing. This suggests that external ignition sources, such as adjacent burning materials, play a crucial role in sustaining fire propagation in VGS.

These conclusions highlight the importance of carefully selecting vegetation types based on their characteristics as well as showing the importance of correct maintenance of these systems.

Parameter	Heat Flux at 0.25m	Heat Flux at 1m	Heat Flux at 1.5m	Heat flux at 2m	Temperature	Median Gas	Pyrolysis Gas	Water Vapour	Mass Loss
Moisture Content	7.5062 μ 11.0523 σ	2.6711 μ 3.7183 σ	3.3834 μ 4.1946 σ	1.6674 μ 2.2564 σ	48.0021 μ 66.3326 σ	0.0016 μ 0.0015 σ	0.0055 μ 0.0065 σ	6.4509 μ 6.7712 σ	
Leaf Area	61.0637 μ 10.1158 σ	3.5441 μ 3.5921 σ	2.7016 μ 3.5835 σ	3.2522 μ 3.0968 σ	53.6633 μ 54.5002 σ	0.0019 μ 0.0015 σ	0.0042 μ 0.0029 σ	0.7125 μ 0.9583 σ	
Vegetation Density	27.4896 μ 36.1848 σ	2.4148 μ 3.3663 σ	2.4620 μ 3.2913 σ	2.3021 μ 2.6926 σ	41.6230 μ 63.6230 σ	0.0049 μ 0.0048 σ	0.0075 μ 0.0084 σ	31.1382 μ 28.9299 σ	
Vegetation Burning Temp	16.5777 μ 25.9369 σ	3.1708 μ 4.1370 σ	2.7672 μ 3.1560 σ	2.0476 μ 2.5512 σ	46.8655 μ 63.7299 σ	0.0029 μ 0.0023 σ	0.0027 μ 0.0030 σ	0.6973 μ 1.0694 σ	

6 Discussion

This study aimed analyse the burning behaviour of VGS, solely focussing on the vegetation and analysing how different parameters of the vegetation would influence the burning behaviour.

The experimental results provided a foundation for developing and validating Fire Dynamics Simulator (FDS) models. The validated models allowed for a controlled exploration of various vegetation parameters, enabling a deeper understanding of their effects. By combining experimental data and simulation outputs, key limitations, potential overestimations, and underestimations were identified. This awareness helped refine subsequent application studies.

Both the experimental and simulated data found that the vegetation does not burn easily. Furthermore, upon removal of the flames the vegetation seemed to extinguish very quickly.

The usable data from the experiments for the validation study was however quite limited due to the first 2 setups being too limited in their result range, and during the fourth experiment part of the data was corrupted due to the window being opened. So while the rest of the fourth experiment did give data similar to that of experiment three this cannot be fully confirmed as accurate data, due to there only being one dataset.

FDS is a highly detailed fire behaviour simulation program, which was a key factor in its selection for this study. However, it has several limitations. As discussed in Section 4, the final simulation results exhibit lower turbulence compared to real-life burning. This leads to an underestimation of temperatures at the edges of the specimen and an overestimation at the centre. Additionally, while the simulated mass loss follows the same trend as the experimental results, it experiences significantly less mass loss. These discrepancies in mass loss were the biggest differences found between the simulation and the experimental results. In contrast, the simulated temperature behaviour closely aligned with experimental trends, and the average thermal image (Figure 99c) confirms that the highest temperatures are concentrated in two distinct peaks—one at the bottom of the specimen and another at the sides.

A major limitation of FDS is that it only supports square or cubic geometry, making it challenging to model organic forms accurately. Furthermore, the Lagrangian particle model was used in this study, which represents only the leaves of the vegetation while excluding the stems. This limitation may partially explain the observed discrepancies in mass loss, as stems constitute a significant portion of the vegetation and exhibit different combustion behaviour compared to leaves. Additionally, some discrepancies could stem from inaccuracies in the input parameters used for validation. While most plant characteristics were sourced from literature, there is limited available research on the specific properties of *Hedera helix* hedges, which may have contributed to deviations between the simulated and experimental results.

The EE method while effectively showing which input parameters are more influential than others is also not safe from human bias. For each parameter a chosen range should be made which spans the whole possible range. Whilst the different input parameter values were chosen based on literature studies, the input range per parameter does not span the whole range of the parameter. This is why σ returns results based on human bias and does not accurately reflect the true variability of the parameters effect [70].

As mentioned the calculation pc which held the simulation for high density timed out which is why this simulation result is not complete which makes it difficult to successfully compare the data for the plant density with other simulation results. This is why the found pyrolysis is much lower than it should be and also why the median temperature plotted over time is much lower compared to the other simulations.

The produced pyrolysis gas which was created by FDS is much lower compared to the pyrolysis gas calculated in the experiments. This could be due to the calculation done with the experiment being very simplified and thus very much overestimating how much is created. Or the simulation very much underestimates the production or the measured quantities are missing a lot of the pyrolysis gasses which directly burned up. Most likely it is a combination of both seeing as the difference is quite large.

7 Conclusion

The primary objective of the study was to find out the fire behaviour of VGS vegetation. Both experimental and simulation results suggest that vegetation alone does not generate excessively high temperatures which will lead to dangerous situations. The mass loss due to combustion predominantly occurred in areas where the vegetation was either in direct contact or in close proximity with the flames. In the experiments, occasional ignitions propagated upward through the specimen, however, these quickly self-extinguished once the fuel in the affected stems was consumed. Beyond these isolated events, the vegetation did not ignite unless exposed to the flames.

The application studies highlight vegetation density and leaf geometry as the most influential characteristics affecting fire behaviour. A higher vegetation density increases the amount of fuel directly exposed to the flames, leading to greater combustion after moisture evaporation. When vegetation grows it becomes denser over time, which is why maintenance is of great importance especially now that the simulations have shown that this is a very influential parameter. The experiment was done with quite a young specimen of just one year growth time. Considering this when a vertical green system is placed it is meant to stay there for a long time and will grow over the years unless regular maintenance is performed and the vegetation is significantly pruned.

From a fire safety perspective, the primary concern associated with VGS is the potential for excessive temperatures to damage the facade and its openings, increasing the risk of fire spreading into the building. Window openings are particularly vulnerable, whereas modern facades can generally withstand significant thermal stress [75, 76]. However, since vegetation will not be placed directly in front of the windows, the thermal exposure at these locations is expected to be lower. According to Carlsson [77], a façade should be capable of withstanding a heat flux of 15 kW/m^2 for at least 30 minutes. The additional fire load introduced by the vegetation does not appear to generate temperatures or heat fluxes exceeding this threshold. Therefore, it is reasonable to conclude that the façade openings will maintain their integrity under the expected fire conditions.

Additionally, the experimental results demonstrated that the temperature recorded behind the VGS increased when the cavity between the back wall and the vegetation decreased. The VGS vegetation effectively trapped the heat not allowing it to dissipate in the open air. This finding shows the role design has in mitigating the fire risk, as a larger cavity will return lower temperatures.

To minimize the fire risk associated with VGS, the following vegetation characteristics are most effective in reducing temperatures and heat flux:

- **Low vegetation density:** This reduces the available fuel and limits the extent of combustion.
- **High ignition temperature:** This will delay or even prevent ignition, thereby reducing the overall energy released.
- **High moisture content:** This delays ignition, due to the moisture first having to evaporate.
- **Smaller leaves:** This limits extreme median temperature, even though the initial ignition may be quicker and seem slightly more intense.

To conclude, with the proper maintenance and careful consideration of vegetation species with the recommended characteristics, the additional fire risk associated with the vegetation of VGS is acceptable. Ensuring that this is the case when considering a non-combustible facade behind the vegetation as my experiments and simulations were conducted using an adiabatic back wall. By implementing these measures, the use of VGS can be both aesthetically and environmentally beneficial without compromising building safety.

8 Future Research

For future research it would be interesting to simulate a case study on real life scale. This approach would allow for the evaluation of large-scale effects, rather than focusing solely on individual parameters and their influences. This way the effect that a VGS has on a building could be investigated.

Furthermore, it may be of interest to review the vegetation parameters with a different analysis tool than the EE method as this still has quite some human bias. For example using the Sobol method this bias could be alleviated much more effectively. However, to investigate both of these things a substantial amount of computing power is necessary.

Another critical aspect to investigate when evaluating VGS fire performance is the substrate and container in which the vegetation is housed. While the present study focuses exclusively on the vegetation, the substrate and container materials could also significantly influence fire behavior. Future research should therefore consider these factors to develop a more holistic understanding of VGS fire safety.

References

- [1] C. Y. Cheng, K. K. Cheung, and L. M. Chu, "Thermal performance of a vegetated cladding system on facade walls," *Building and Environment*, vol. 45, pp. 1779–1787, 8 2010.
- [2] E. Hartin, "Extreme Fire Behavior: Understanding the Hazards," tech. rep., 2005.
- [3] R. van Herpen, "Lecture Fire Safety Engineering - Performance Based fire safety — Course 7LY4M0 Building Services and Fire Safety - TU/e," 2023.
- [4] P. J. Irga, F. R. Torpy, D. Griffin, and S. J. Wilkinson, "Vertical Greening Systems: A Perspective on Existing Technologies and New Design Recommendation," *Sustainability 2023, Vol. 15, Page 6014*, vol. 15, p. 6014, 3 2023.
- [5] Peutz, "Nieuwbouw Laboratorium voor Brandveiligheid — Peutz," 2020.
- [6] Mobilane, "WallPlanter duurzaam & groene gevelsysteem."
- [7] ISO, "International Standard - iso13785-1, Reaction-to-fire tests for facades - Part 1 - Intermediate-scale test," tech. rep., 12 2002.
- [8] K. B. McGrattan and G. P. Forney, "Fire dynamics simulator (version 4) ;," tech. rep., National Institute of Standards and Technology, Gaithersburg, MD, 2004.
- [9] R. Mierlo and B. Sette, "The Single Burning Item (SBI) test method-a decade of development and plans for the near future," 2005.
- [10] H. Ritchie, V. Samborska, and M. Roser, "Urbanization," 2018.
- [11] The European Union, "Directive 2010/31/EU of the European Parliament and of the Council of 19 May 2010 on the energy performance of buildings," tech. rep., Official Journal of the European Union, 2010.
- [12] I. Andrić, M. Koc, and S. G. Al-Ghamdi, "A review of climate change implications for built environment: Impacts, mitigation measures and associated challenges in developed and developing countries," *Journal of Cleaner Production*, vol. 211, pp. 83–102, 2 2019.
- [13] U. Y. Ayikoe Tettey and L. Gustavsson, "Energy savings and overheating risk of deep energy renovation of a multi-storey residential building in a cold climate under climate change," *Energy*, vol. 202, p. 117578, 7 2020.
- [14] Y. Ma, D. Lauwaet, A. Kouti, and S. Verbeke, "A toolchain to evaluate the impact of urban heat island and climate change on summer overheating at district level," *Urban Climate*, vol. 51, p. 101602, 9 2023.
- [15] L. Yang, F. Qian, D. X. Song, and K. J. Zheng, "Research on Urban Heat-Island Effect," *Procedia Engineering*, vol. 169, pp. 11–18, 1 2016.
- [16] R. Wang, M. Helbich, Y. Yao, J. Zhang, P. Liu, Y. Yuan, and Y. Liu, "Urban greenery and mental wellbeing in adults: Cross-sectional mediation analyses on multiple pathways across different greenery measures," *Environmental Research*, vol. 176, p. 108535, 9 2019.
- [17] W. Passchier-Vermeer and W. F. Passchier, "Noise exposure and public health.," *Environmental Health Perspectives*, vol. 108, no. SUPPL. 1, pp. 123–131, 2000.
- [18] N. H. Wong, A. Yong, K. Tan, P. Y. Tan, K. Chiang, and C. Wong, "Acoustics evaluation of vertical greenery systems for building walls," *Building and Environment*, vol. 45, pp. 411–420, 2010.
- [19] K. Ornam, S. Wonorahardjo, and S. Triyadi, "Several façade types for mitigating urban heat island intensity," *Building and Environment*, vol. 248, p. 111031, 1 2024.
- [20] M. T. Hoelscher, T. Nehls, B. Jänicke, and G. Wessolek, "Quantifying cooling effects of facade greening: Shading, transpiration and insulation," *Energy and Buildings*, vol. 114, pp. 283–290, 2 2016.

- [21] F. Mayrand, P. Clergeau, A. Vergnes, and F. Madre, “Vertical Greening Systems as Habitat for Biodiversity,” *Nature Based Strategies for Urban and Building Sustainability*, pp. 227–237, 1 2018.
- [22] J. Zhao, Q. Rao, C. Sun, R. M. A. Ikram, C. Fan, J. Li, M. Wang, and D. Zhang, “A Systematic Review of the Vertical Green System for Balancing Ecology and Urbanity,” *Water 2024, Vol. 16, Page 1472*, vol. 16, p. 1472, 5 2024.
- [23] M. Radić, M. B. Dodig, and T. Auer, “Green facades and living walls-A review establishing the classification of construction types and mapping the benefits,” 9 2019.
- [24] R. Widiastuti, J. Zaini, W. Caesarendra, G. Kokogiannakis, and S. N. N. Binti Suhailian, “Thermal insulation effect of green façades based on calculation of heat transfer and long wave infrared radiative exchange,” *Measurement: Journal of the International Measurement Confederation*, vol. 188, 1 2022.
- [25] Urban Green-blue Grids, “Green facades.”
- [26] M. Hermy, M. Schauvliege, and Tijskens G., *Groenbeheer - een verhaal met toekomst*. Velt i.s.m. afdeling Bos & Groen, Berchem, 2005.
- [27] R. Herpen van, “Lectures Course 7LY4M0 Building Services and Fire Safety,” 2023.
- [28] A. L. Sullivan, “Inside the Inferno: Fundamental Processes of Wildland Fire Behaviour: Part 1: Combustion Chemistry and Heat Release,” 6 2017.
- [29] S. Khan, “Heat Transfer: Conduction Convection And Radiation Explained,” 6 2024.
- [30] Keisya, “Fire: Convection or Radiation? Understanding Heat Transfer,” 2025.
- [31] G. Olivier, *Fire Performance of Cross-Laminated Timber Investigating adhesives, compartment configuration and design guidelines*. PhD thesis, 2019.
- [32] D. Pearlmutter, B. Pucher, C. S. Calheiros, K. A. Hoffmann, A. Aicher, P. Pinho, A. Stracqualursi, A. Korolova, A. Pobric, A. Galvão, A. Tokuç, B. Bas, D. Theochari, D. Milosevic, E. Giancola, G. Bertino, J. A. Castellar, J. Flaszynska, M. Onur, M. C. G. Mateo, M. B. Andreucci, M. Milousi, M. Fonseca, S. Di Lonardo, V. Gezik, U. Pitha, and T. Nehls, “Closing water cycles in the built environment through nature-based solutions: The contribution of vertical greening systems and green roofs,” *Water (Switzerland)*, vol. 13, 8 2021.
- [33] H. Lin, Y. Xiao, F. Musso, and Y. Lu, “Green Façade Effects on Thermal Environment in Transitional Space: Field Measurement Studies and Computational Fluid Dynamics Simulations,” *Sustainability 2019, Vol. 11, Page 5691*, vol. 11, p. 5691, 10 2019.
- [34] F. Verbrugge and M. Diks, *Plantveilig: Brand uitbreidingsrisico van groene gevels*. PhD thesis, Hogeschool van Arnhem en Nijmegen, 2023.
- [35] BMJ, “Grenfell: a year on, here’s what we know went wrong — The Conversation - Injury Prevention: Editor’s Blog,” 2018.
- [36] A. Sharma and K. B. Mishra, “Experimental investigations on the influence of ‘chimney-effect’ on fire response of rainscreen façades in high-rise buildings,” *Journal of Building Engineering*, vol. 44, p. 103257, 12 2021.
- [37] T. L. W. Karunaratne and C. L. Chow, “Fire spread along vertical greenery systems from window ejected flame: A study based on a fire dynamic simulator model,” *Journal of Building Engineering*, vol. 62, 12 2022.
- [38] HaagEnzo, “Klimop - Hedera Helix 150/175 cm (in pot) .”
- [39] Gertens Garden Center, “Peperomia Obtusifolia, Baby Rubber Plant ‘Green’ .”
- [40] Davis Landscape Architecture, “Aglaonema commutatum ‘Silver Queen’ .”

- [41] C. Chow, S. Han, K. Dahanayake, and W. Chow, “Fire Hazards with Vertical Greenery Systems - SFPE,” *SFPE*, vol. 31, 2024.
- [42] Department for Communities and Local Government, *Fire Performance of Green Roofs and Walls*. 8 2013.
- [43] B. Waldeck, “A Comparison Between FDS and the Multi-Zone Fire Model Regarding Gas Temperature and Visibility in Enclosure Fires,” tech. rep., 2020.
- [44] S. Prescott, R. Christian, and R. Sampath, “INL/RPT-23-70843 Revision 0 Light Water Reactor Sustainability Program FRI3D Fire Simulation Options and Verification Tasks,” tech. rep., 2023.
- [45] D. D. Evans, G. W. Mulholland, H. R. Baum, W. D. Walton, and K. B. McGrattan, “Computer fire models and practical applications (1990s) — NIST,” *Journal of Research of the National Institute of Standards and Technology*, vol. 106, no. 1, pp. 231–278, 2001.
- [46] G. P. Forney and . Ilessr, “Computing Radiative Heat Transfer Occurring in a Zone Fire Model,” tech. rep.
- [47] H. Zoka, “LES vs RANS – CFD Online Discussion Forums.”
- [48] Ingrid Cloud, “LES vs RANS methods for CFD Simulations,” 2019.
- [49] U.S. Nuclear Regulatory Commission, “NUREG-1934, ”Nuclear Power Plant Fire Modeling Analysis Guidelines (NPP FIRE MAG),” Final Report.,” tech. rep., 2012.
- [50] M. Ioelovich, “Application of thermochemical methods for the study of cellulose and cellulose esters,” *World Journal Of Advanced Research and Reviews*, vol. 18, pp. 1477–1488, 6 2023.
- [51] J. E. Mendez and D. Lange, “Effect of cavity parameters on the fire dynamics of ventilated façades,”
- [52] A. Neale, d. Derome, B. Blocken, and J. Carmeliet, “CFD calculation of convective heat transfer coefficients and validation ? Part I: Laminar flow,” 1 2006.
- [53] “EN 1991-1-2: Eurocode 1: Actions on structures - Part 1-2: General actions - Actions on structures exposed to fire,” tech. rep., 1991.
- [54] IdealSimulations, “CFD computational domain .”
- [55] J. Fröhlich, C. P. Mellen, W. Rodi, L. Temmerman, and M. A. Leschziner, “Highly resolved large-eddy simulation of separated flow in a channel with streamwise periodic constrictions,” *Journal of Fluid Mechanics*, vol. 526, pp. 19–66, 3 2005.
- [56] “NISTIR (2001) Evaluation of a fast simplified CFD model - non uniform mesh,”
- [57] Simscale, “K-epsilon Turbulence Model — Global Settings — SimScale,” 2023.
- [58] SimScale, “K-Omega Turbulence Models — Global Settings — SimScale,” 2024.
- [59] R. E. Bensow, C. Fureby, M. Liefvendahl, and T. Persson, “(PDF) A Comparative Study of RANS, DES and LES,” 2006.
- [60] “FDS and Smokeview — NIST.”
- [61] J. W. Slater, “Examining Spatial (Grid) Convergence,” 2 2021.
- [62] K. H. Nguyen and K. Chang, “Large Eddy Simulation of Turbulent Heat Transfer in Pipe Using NEK5000 Based on the Spectral Element Method and Uncertainty Quantification by GCI Estimation,” *International Journal of Computational Fluid Dynamics*, vol. 35, no. 3, pp. 210–223, 2021.
- [63] P. Datt, “Latent Heat of Vaporization/Condensation,” *Encyclopedia of Earth Sciences Series*, vol. Part 3, pp. 703–703, 2011.

[64] I. T. Leventon, J. Yang, and M. C. Bruns, “Thermal decomposition of vegetative fuels and the impact of measured variations on simulations of wildfire spread,” *Fire Safety Journal*, vol. 137, p. 103762, 5 2023.

[65] K. C. Dahanayake and C. L. Chow, “Moisture Content, Ignitability, and Fire Risk of Vegetation in Vertical Greenery Systems,” *Fire Ecology*, vol. 14, pp. 125–142, 2 2018.

[66] M. S. Jayalakshmy and J. Philip, “Thermophysical properties of plant leaves and their influence on the environment temperature,” *International Journal of Thermophysics*, vol. 31, pp. 2295–2304, 12 2010.

[67] T. L. W. Karunaratne and C. L. Chow, “Fire spread along vertical greenery systems from window ejected flame: A study based on a fire dynamic simulator model,” *Journal of Building Engineering*, vol. 62, 12 2022.

[68] K. McGrattan, S. Hostikka, R. McDermott, J. Floyd, C. Weinschenk, and K. Overholt, “Fire Dynamics Simulator Technical Reference Guide Volume 3: Validation,”

[69] J. Fernando, “The Correlation Coefficient: What It Is and What It Tells Investors,” 2024.

[70] J. Sommerlund-Larsen, “Sensitivity Analysis of Fire Dynamics Simulation,” tech. rep., 2007.

[71] R. J. Rutjens, L. R. Band, M. D. Jones, and M. R. Owen, “Elementary effects for models with dimensional inputs of arbitrary type and range: Scaling and trajectory generation,” *PLOS ONE*, vol. 18, 10 2023.

[72] D. J. Metcalfe, “Hedera helix L.,” *Journal of Ecology*, vol. 93, pp. 632–648, 6 2005.

[73] b. Qian Yang, “Postemergence Control of English Ivy (Hedera helix L.) and Moisture Effects on Preemergence Weed Control with Flumioxazin,” 2012.

[74] H. M. Wainwright, S. Finsterle, Y. Jung, Q. Zhou, and J. T. Birkholzer, “Making sense of global sensitivity analyses,” *Computers and Geosciences*, vol. 65, pp. 84–94, 2014.

[75] Y. Wang, K. Li, Y. Su, W. Lu, Q. Wang, J. Sun, L. He, and K. M. Liew, “Determination of critical breakage conditions for double glazing in fire,” *Applied Thermal Engineering*, vol. 111, pp. 20–29, 1 2017.

[76] Y. Wang, “The breakage behavior of different types of glazing in a fire,”

[77] E. Carlsson, “EXTERNAL FIRE SPREAD TO ADJOINING BUILDINGS-A review of fire safety design guidance and related research,”

[78] The Engineering ToolBox, “Fuels - Higher and Lower Calorific Values,” 2003.

[79] FasterCapital, “Gaussian Smoothing: Enhancing Data Quality with Gaussian Smoothing,” 2024.

[80] R. v. d. Boomgaard, “6.1. Gaussian Smoothing and Gaussian Derivatives — Image Processing and Computer Vision 2.0 documentation,” 2017.

[81] R. v. Herpen, “PHBO Fire Safety Engineering,” tech. rep., Stichting Bouwfysica kennisoverdracht - PHBO Fire safety engineering, 2022.

[82] R. v. Herpen, “Oefeningen en antwoorden chemische verbrandings modellen,” tech. rep., Kennisoverdracht bouwfysica, 2022.

[83] T. Prohaska, J. Irrgeher, J. Benefield, J. K. Böhlke, L. A. Chesson, T. B. Coplen, T. Ding, P. J. Dunn, M. Gröning, N. E. Holden, H. A. Meijer, H. Mooszen, A. Possolo, Y. Takahashi, J. Vogl, T. Walczyk, J. Wang, M. E. Wieser, S. Yoneda, X. K. Zhu, and J. Meija, “Standard atomic weights of the elements 2021 (IUPAC Technical Report),” *Pure and Applied Chemistry*, vol. 94, pp. 573–600, 5 2022.

A Experiments

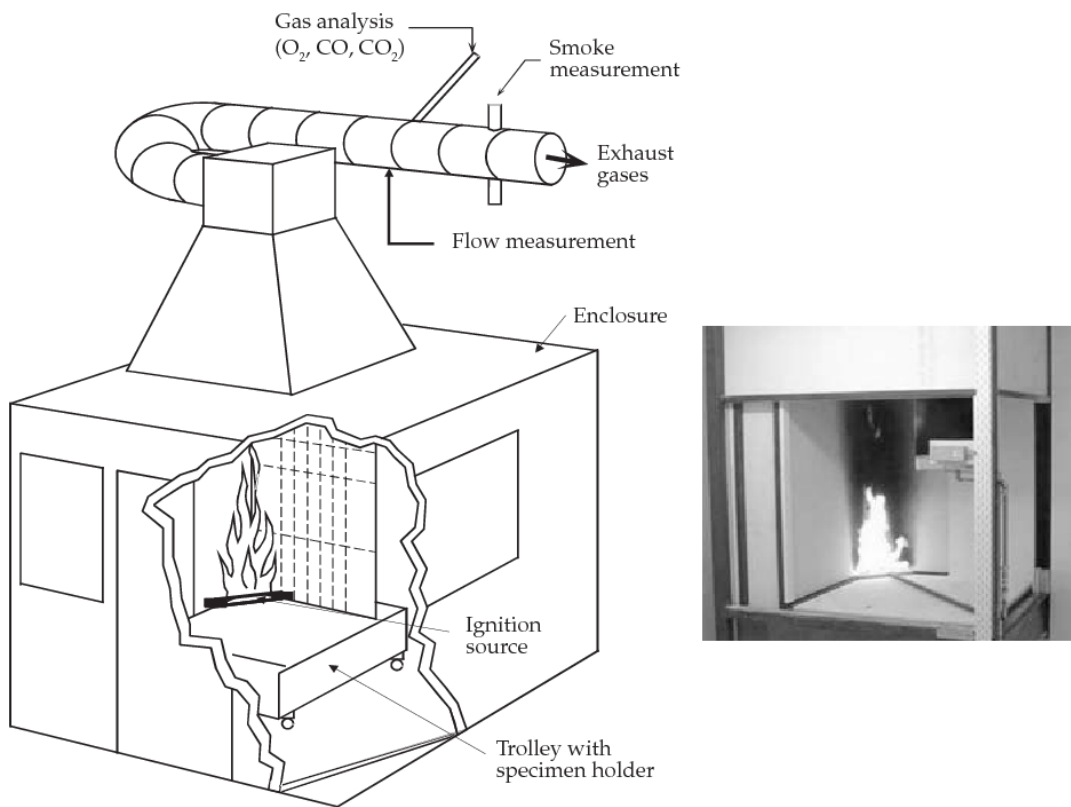


Figure 54: SBI-test Setup from [9]

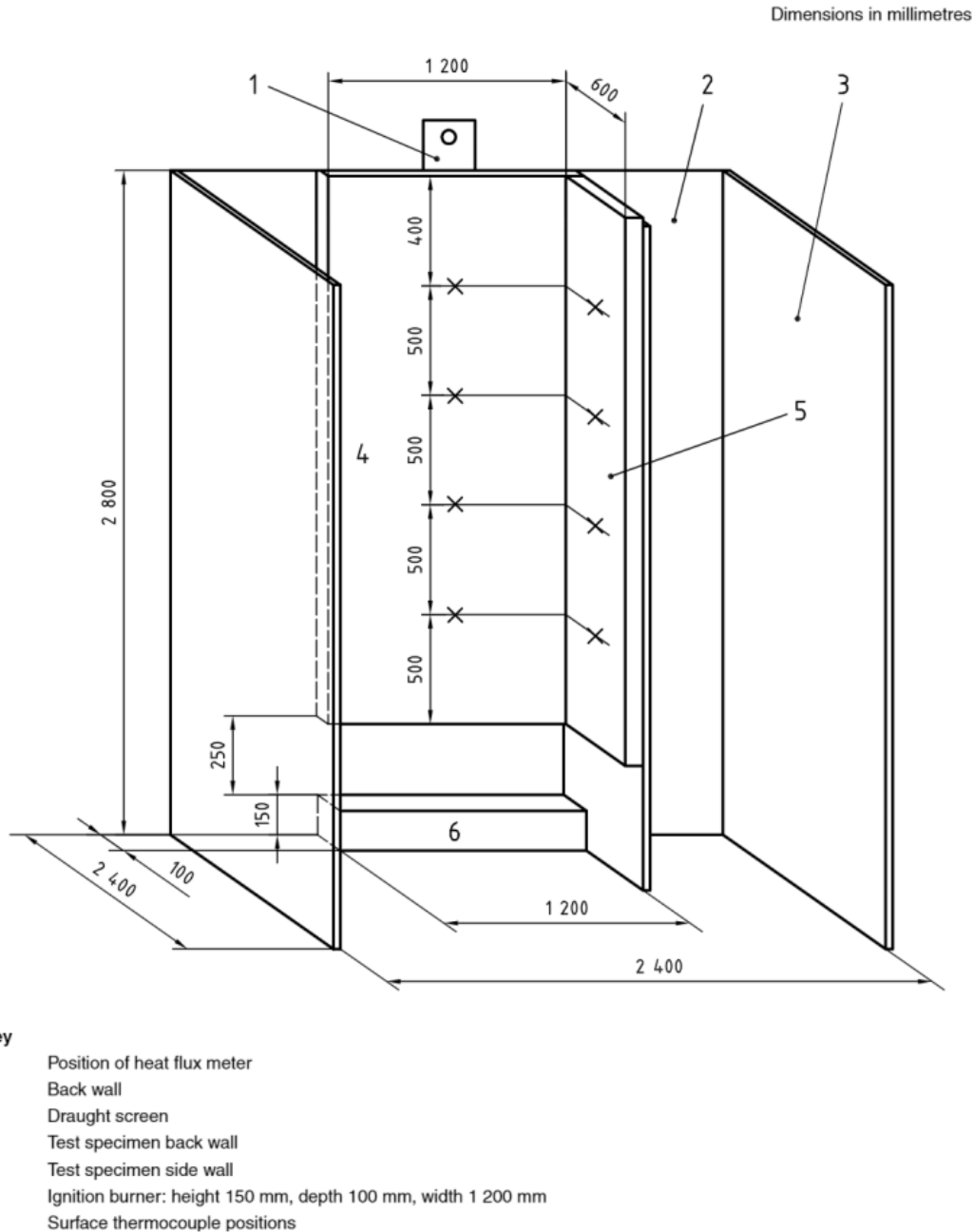


Figure 55: Intermediate-fire test setup from [7]

A.1 Experimental samples

Add all pictures of all samples

A.2 Experimental Results

A.2.1 Test 1

Below are pictures of the setup and how the samples were hooked into the setup with the use of the metal hooks/supports which they were attached to.



Figure 56: Hook Supports for the Samples



Figure 57: Sample attached and cavity shown



Figure 58: Setup Experiment no Specimen

To calculate if the lineburner had a total energy output of 30kW formula 24 was reformulated into formula 25.

The tests were conducted with propane as a fuel source, which has an energy content of ≈ 50 MJ/kg [78]. To verify that the line burner operated at 30 kW, the total mass of the burned fuel was measured. Formula 24 was reformulated into Formula 25 for this purpose. P is typically expressed in Joules per second, 30,000J/s is 30kW. To calculate the required Q for a minute in which the P is 30kW the Q is 1.8 MJ as is shown below.

$$P = \frac{Q_{total}}{t} \quad (24)$$

where:

P = power [kW]

Q_{total} = total energy released [MJ]

t = time the fuel burned [sec]

$$Q = P * t \quad (25)$$

$$Q = 30,000 * 60 = 1.8MJ \quad (26)$$

To determine the required fuel mass for this energy output, the energy content (energy per kg) of propane can be used. When ensuring the lineburner is burning at 30kW the total weight loss of the propane tank (the fuel burned) was measured. By using formula 27 it was determined that 36g of propane needed to be lost over 1 minute. The gas tank output was adjusted until this consumption rate was achieved.

$$m_{burned} = \frac{Q}{\text{Energy per kg}} \quad (27)$$

Substituting the values:

$$m_{burned} = \frac{1.8}{50} = 0.36kg = 36g$$

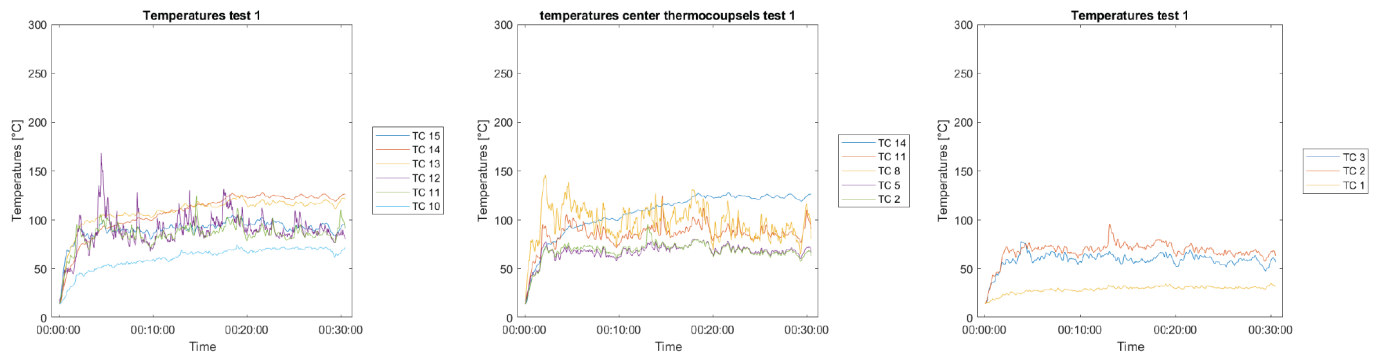


Figure 65: Temperature of thermocouples for test 1



Figure 59: Test 1 at $t=0$



Figure 60: Test 1 at $t=3:45$



Figure 61: Test 1 at $t=10:00$



Figure 62: Test 1 at $t=13:45$



Figure 63: Test 1 at $t=25:00$



Figure 64: Test 1 at $t=30:00$

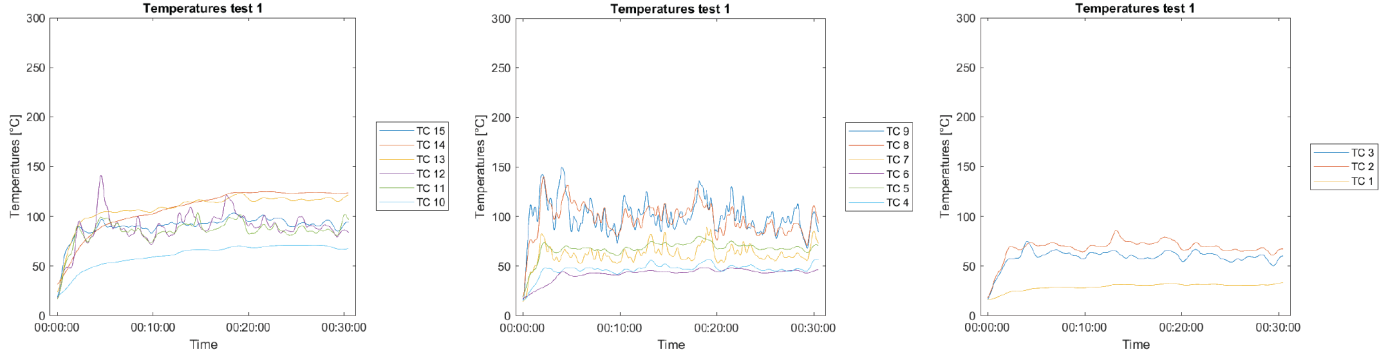


Figure 66: Temperature of thermocouples for test 1, smoothed with gaussian

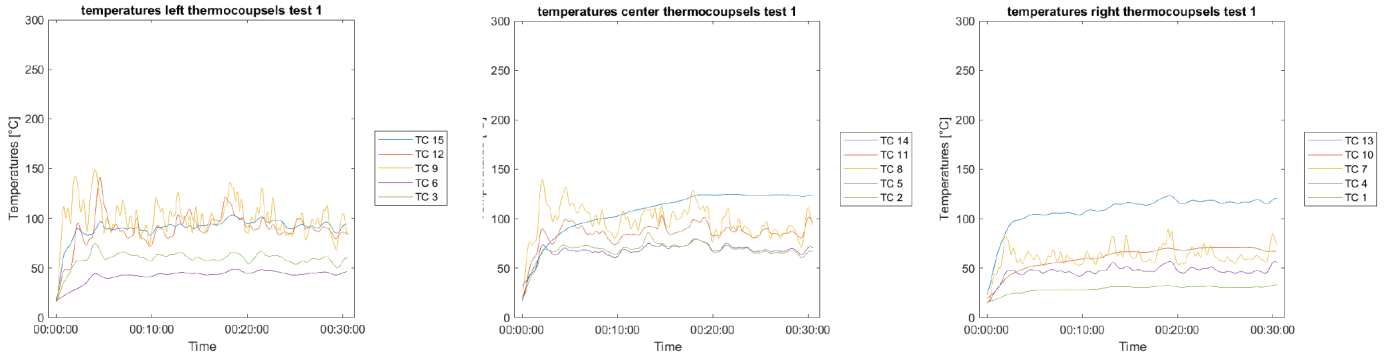


Figure 67: Temperature of thermocouples for test 1 per side, smoothed with gaussian

Figures 59-64 show the sample brning with intervals of 5 min as well as the points of ignition during the test. These images were screenshots from the GoPro recording.

The temperature data recorded by the thermocouples were smoothed using Gaussing filtering to reduce the noise and enhance the clarity, allowing for a more accurate analysis of the temperature trends. Gaussian smoothing is a widely used technique in signal processing that applies a Gaussian kernel to the dataset, effectively averaging values within a defined window while giving higher weights to data points closer to the center. This method preserves the overall trends in the data while minimizing short-term fluctuations caused by experimental noise [79, 80]. Gaussian filtering is done by the fomula's shown below. This noise reduction in the values allows for easy trent spotting.

$$G(x) = \frac{1}{\sqrt{2\pi\sigma^2}} e^{\frac{x^2}{2\sigma^2}} \quad (28)$$

with:

x = distance from the center of the filter

σ = standard deviation

e = euler's number ($e \approx 2.718$)

$$Y(i) = \sum_{j=-k}^k G(j)X(i-j) \quad (29)$$

with:

$X(i)$ = original dataset values

$Y(i)$ = filtered dataset values

$G(j)$ = gaussian kernel values

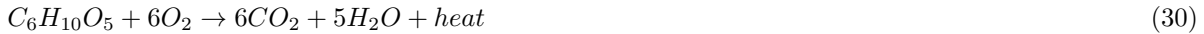
Around the 3:45 mark there is a clear spike in the temperatures recorded by the lower and middle thermocouples, seen in figures 66. This coincides with the ignition of the specimen. A second, less pronounced increase occurs around the 14-minute mark, though the fluctuations in temperature make this peak less distinct.

formation	enthalpy of formation [kJ/mol]
$C_6H_{10}O_5 + 6O_2$	975 (s)
O_2	0
CO_2	393.5 (g)
H_2O	285.8 (l)

Table 7: enthalpy of formation

The thermocouples show a rapid increase in temperature when the lineburner is ignited at the start, and do not exceed the 200 °C, the maximum temperature is also shown in figure 28. Furthermore figure 67 shows that there is a more uniform heating pattern in the thermocouples placed in the center compared to those on the left and the right. This is likely due to their constant exposure to the flames, whereas the thermocouples on the sides are subject to the turbulent nature of the flames, leading to greater variability in recorded temperatures. A similar uniform heating behaviour is also found in the lowest thermocouples on all sides, as these are positioned directly above the line burner and thus experience consistent exposure to the flames, resulting in a more stable temperature profile.

As mentioned in chapter 2, when vegetation burns pyrolysis takes place. The general combustion of biomass is shown below:



To determine the total moisture content of the specimen, a sample was dried prior to testing. The initial mass of the specimen sample was 81.43 g, and after drying, the final mass was 63.10 g. This corresponds to a mass loss of 18.33 g, resulting in a moisture content of 22.51% ($\frac{18.33}{81.43} * 100 = 22.51\%$).

The total weight of the sample used for test 1 before burning is 2.33 kg, after the test the weight was 1.76 kg which corresponds to a total mass loss of 0.57 kg, equivalent to 25% of the initial mass. This loss is attributed to both moisture evaporation and the release of volatile pyrolysis products.

$$\Delta H_{\text{combustion}} = \sum \Delta H_f(\text{products}) - \Delta H_f(\text{reactants}) \quad (31)$$

To calculate the produced heat of combustion the enthalpy of formation must be minussed the enthalpy of the reactants. in this case cellulose is the reactant as is oxygen, and water and carbon dioxide are the products. As shown below the total enthalpy of combustion is 2815 kJ/mol. To convert this to energy produced per gram the molar mass of cellulose, which is 162.14 g/mole, is used. As shown below 17.37 kJ of heat is produced per gram.

$$((6 * 393.5) + (5 * 285.8)) - (975 + (6 * 0)) = 2815 \text{ kJ/mol}$$

$$\frac{2815 \text{ kJ}}{162.14 \text{ g}} = 17.37 \text{ kJ/g}$$

Considering that of the lost sample the total moisture which was present in that piece of the sample has evaporated it would mean the total burned mass of the sample is $(0.57 * (100 - 22.5) = 0.4417 \text{ kg})$ 0.44 kg. Which would make the total produced heat $(441.7 * 17.37 = 7672.2 \text{ kJ})$ 7.67 MJ [81, 82].

Atomic weight [83]:

- Hydrogen - 1.008
- Oxygen - 16.00
- Carbon - 12.01

A.2.2 Test 2

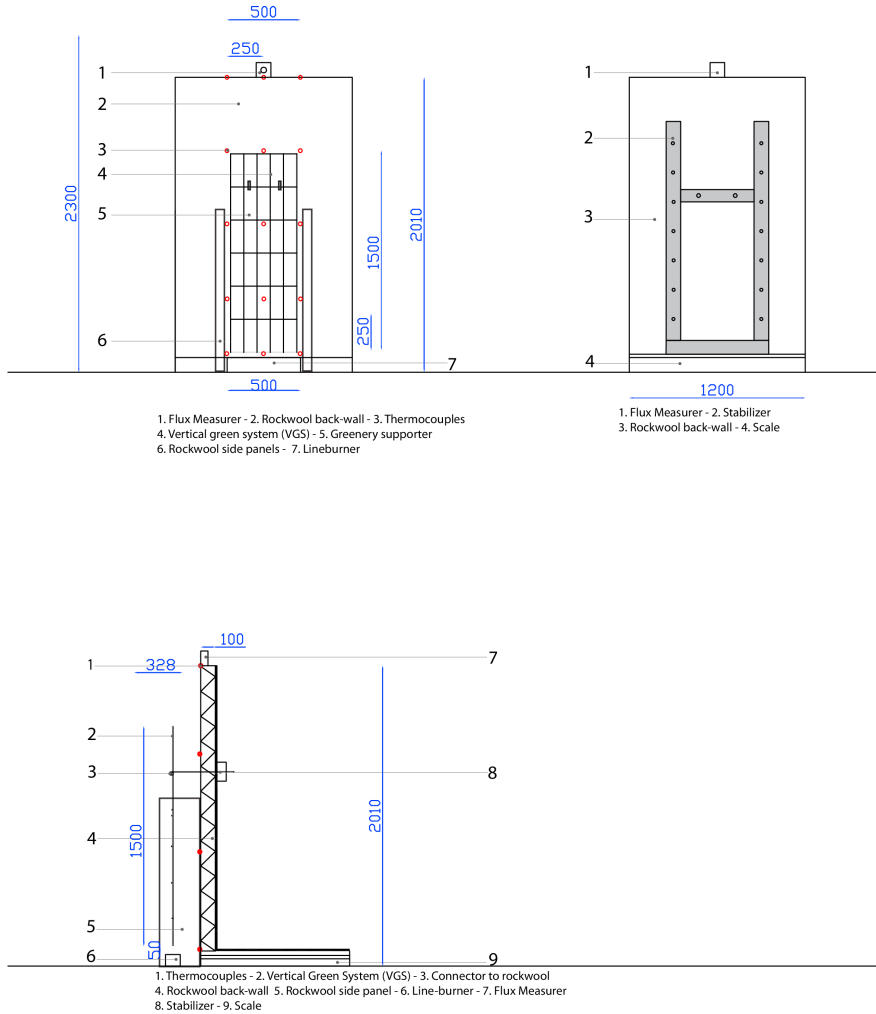


Figure 68: Setup 2

Figure 68 shows the exact setup of test 2. The only alteration being the specimen being lowered to the lineburner. Figures 69-74 show the snapshots taken from the GoPro. With figures 76 and 77 showing the temperatures recorded by the thermocouples with a Guasian filter over them.



Figure 69: Test 2 at $t=0:00$



Figure 70: Test 2 at $t=5:00$



Figure 71: Test 2 at $t=11:20$



Figure 72: Test 2 at $t=15:00$



Figure 73: Test 2 at $t=25:00$



Figure 74: Test 2 at $t=30:00$

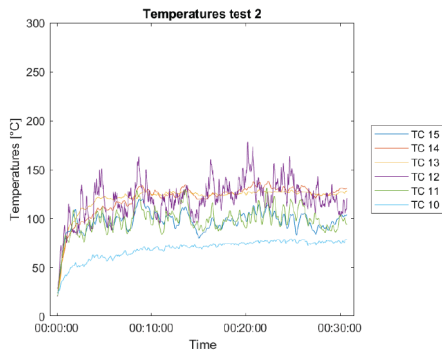
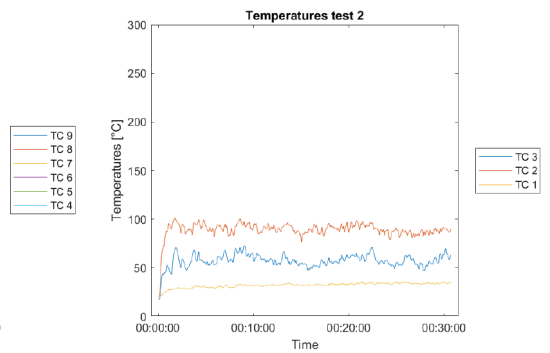
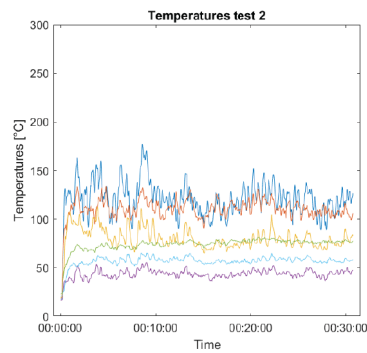


Figure 75: Temperature of thermocouples for test 2



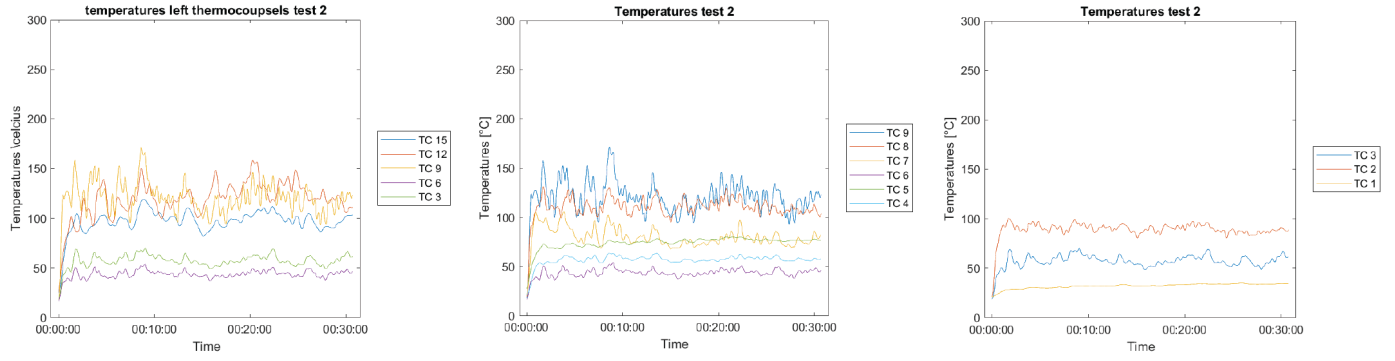


Figure 76: Temperature of thermocouples for test 2, smoothed with gaussian

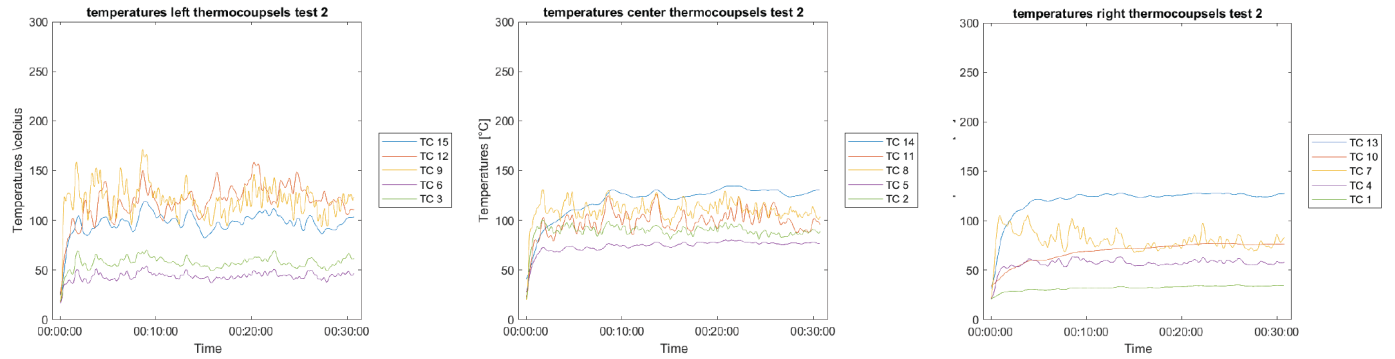


Figure 77: Temperature of thermocouples for test 2 per side, smoothed with gaussian

The initial mass of sample 2 was 2.14 kg, after the test the mass of sample 2 was 1.38. Which amounts to a total mass loss of 0.76 kg, which is means that 33% of the mass was lost. The total heat produced during the burning of the sample was $(0.76 * 0.7749 = 0.588924 \rightarrow 588.9 * 17.37 = 10229.6 \text{ kJ})$ 10.23MJ.

A.2.3 Test 3

Figure 78 shows the last setup, this setup was used for test 3 and 4. Figures 79-84 shows the snapshots at different itme intervals of test 3. With figures 86 and 87 showing the recorded temperatures of each thermocouple with guassian smoothing applied to the data.

The initial mass of the sample was 2.33 kg, the end mass was 1.21 which amounts to a mass loss of 1.12 kg, 48%. The total heat released during the burning of the cellulose was $(1.12 * 0.7749 = 0.8678 \rightarrow 867.8 * 17.374 = 15075.21 \text{ kJ})$ 15.08 MJ.

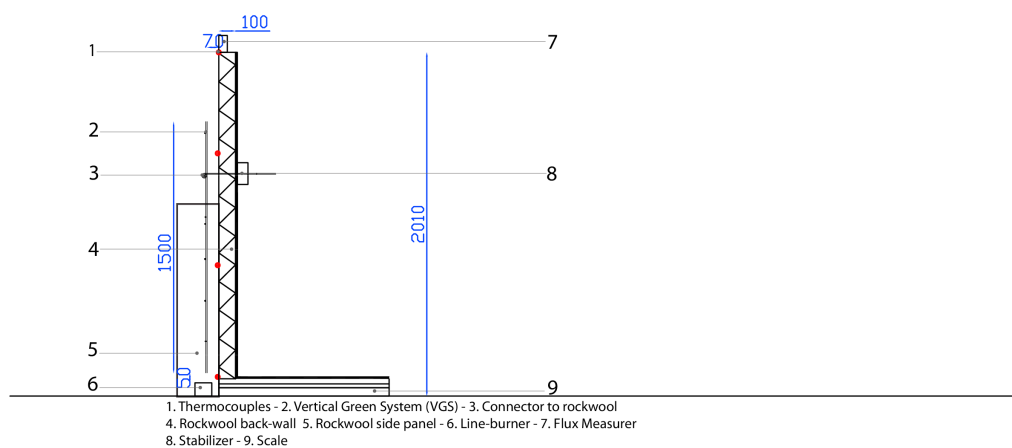
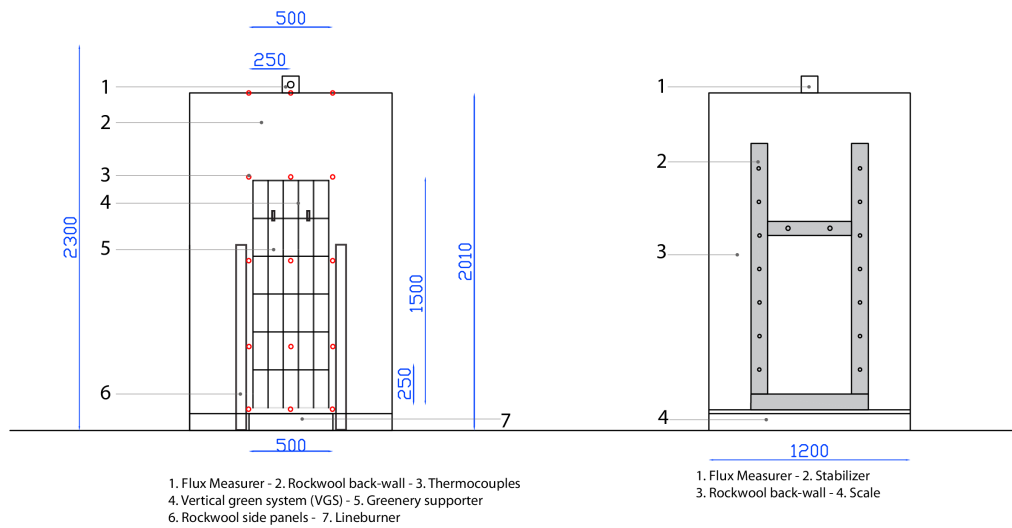


Figure 78: Setup 3



Figure 79: Test 3 at $t=0:00$



Figure 80: Test 3 at $t=7:00$



Figure 81: Test 3 at $t=13:45$



Figure 82: Test 3 at $t=18:40$



Figure 83: Test 3 at $t=20:00$



Figure 84: Test 3 at $t=30:00$

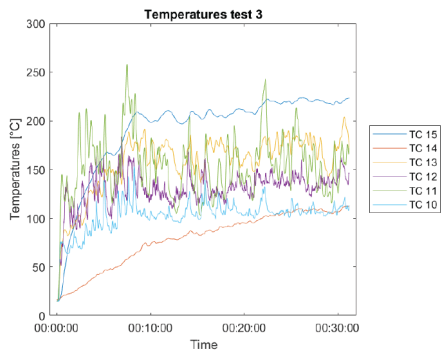
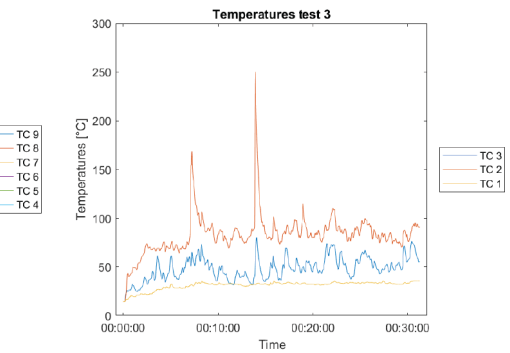
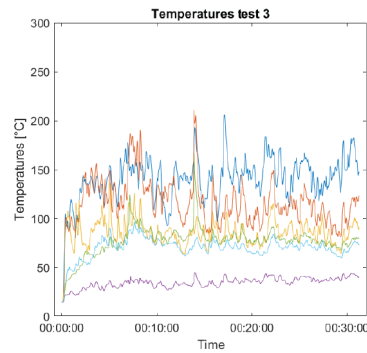


Figure 85: Temperature of thermocouples for test 3



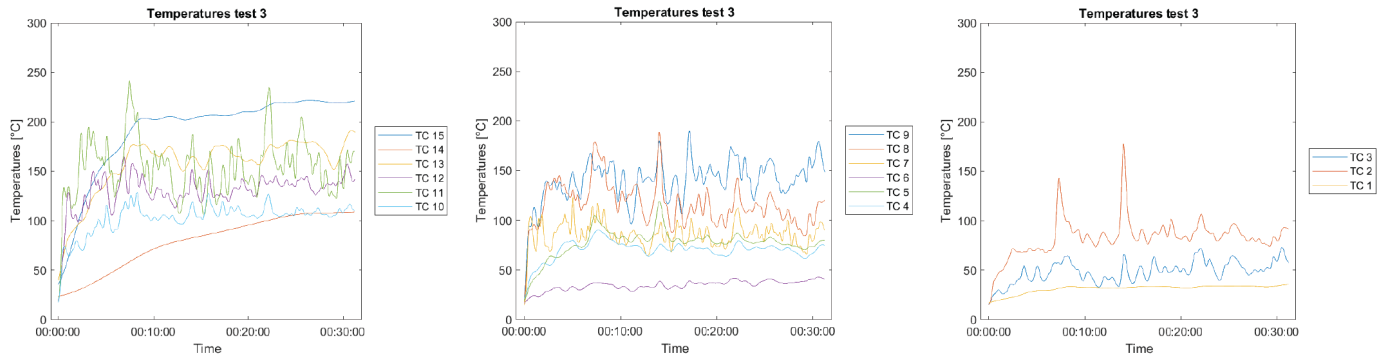


Figure 86: Temperature of thermocouples for test 3, smoothed with gaussian

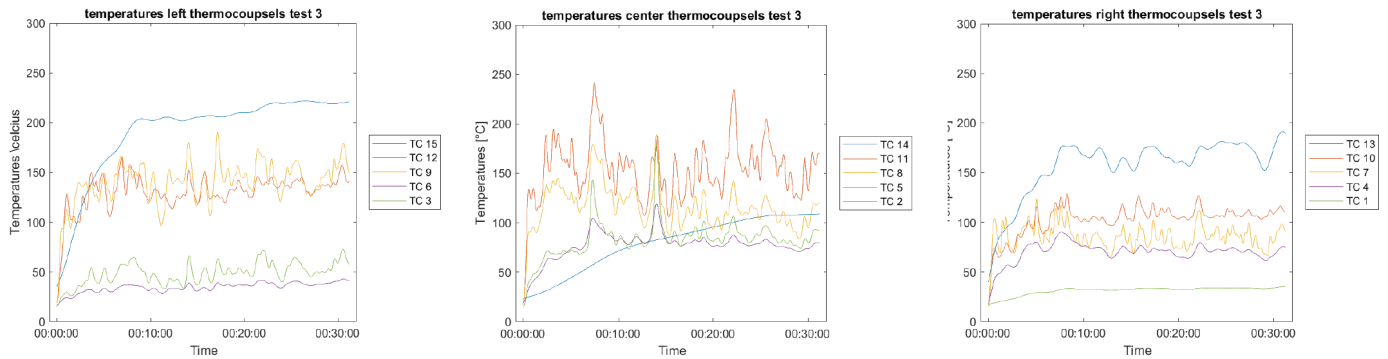


Figure 87: Temperature of thermocouples for test 3 per side, smoothed with gaussian

A.2.4 Test 4



Figure 88: Test 4 at $t=0:00$



Figure 89: Test 4 at $t=2:00$



Figure 90: Test 4 at $t=8:50$



Figure 91: Test 4 at $t=14:00$



Figure 92: Test 4 at $t=18:40$



Figure 93: Test 4 at $t=25:00$

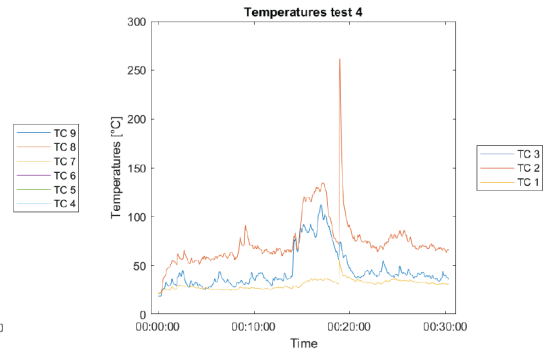
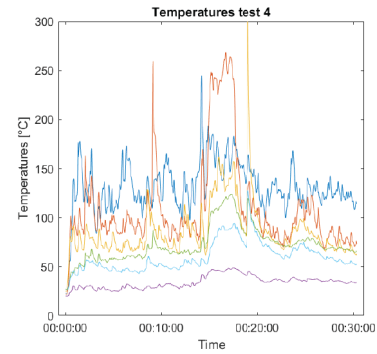
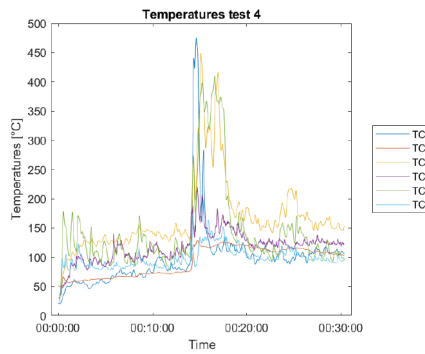


Figure 94: Temperature of thermocouples for test 4

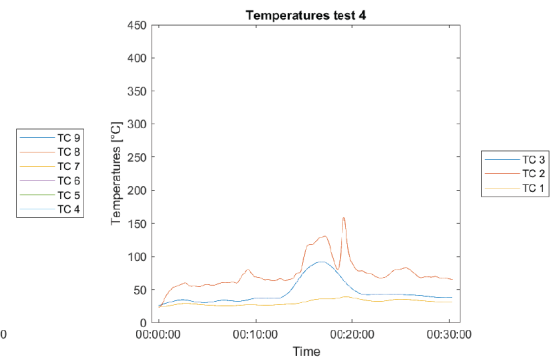
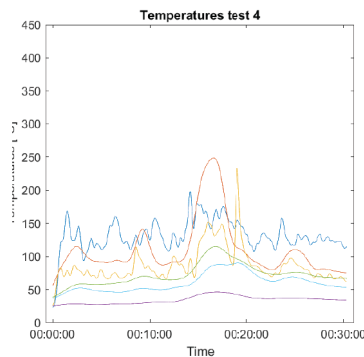
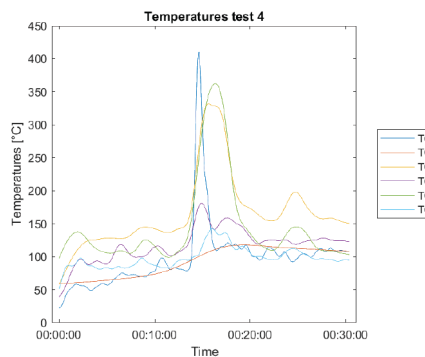


Figure 95: Temperature of thermocouples for test 4, smoothed with gaussian

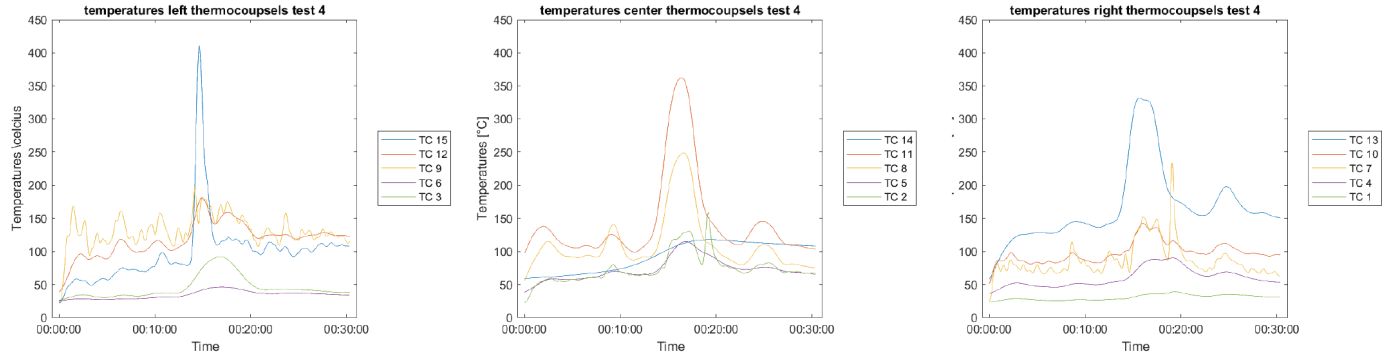


Figure 96: Temperature of thermocouples for test 4 per side, smoothed with gaussian

Figures 88-93 shows the snapshots at different itme intervals of test 4. With figures 95 and 96 showing the recorded temperatures of each thermocouple with guassian smoothing applied to the data.

The initial mass of the sample was 2.35 kg, the end mass was 1.3 which amounts to a mass loss of 1.05 kg, 45%. The total heat released during the burning of the cellulose was $(1.05 * 0.7749 = 0.8136 \rightarrow 813.6 * 17.374 = 14133.01 \text{kJ} 14.133 \text{ MJ}$.

A.2.5 Overall Results

Figure ?? shows three of the samples after the experiments. With test 3 having the most burned sample compared to the other 2. Also the sides are more burned compared to the middle in samples 2 and 3. Which indicates higher temperatures at the sides of the sample compared to the centre.

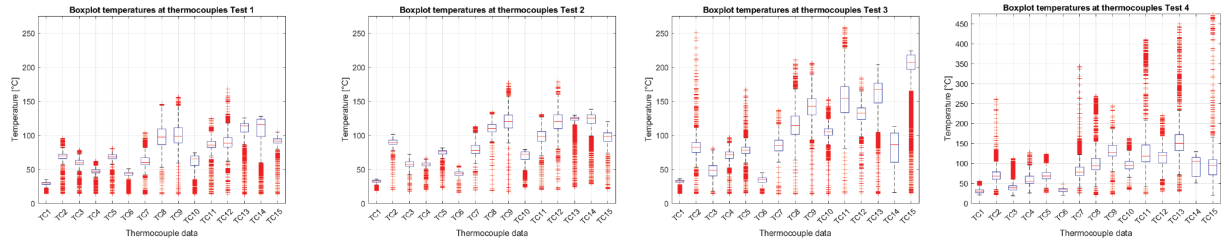


Figure 97: Boxplots of Temperatures per thermocouple per test

B Validation Study

B.1 Validation Study FDS Code

```
1  &HEAD CHID='ValidationStraling', TITLE='ValidationStraling' /
2
3 /&MESH IJK=49,23,78, XB=-1.75,1.75,-0.25,1.5,0,5.5 /coarse mesh OLD
4
5
6 &MESH ID = 'Mesh1', IJK=60,4,135, XB=-1.2, 1.2, -0.16, 0.0, 0.0, 5.4 /Mesh1
7 &MESH ID = 'Mesh2', IJK=20,25,135, XB=-1.2, -0.4, 0.0, 1, 0.0, 5.4 /Mesh2
8 &MESH ID = 'Mesh3', IJK=40,50,270, XB=-0.4, 0.4, 0.0, 1, 0.0, 5.4 /Mesh2
9 &MESH ID = 'Mesh4', IJK=20,25,135, XB=0.4, 1.2, 0.0, 1, 0.0, 5.4 /Mesh4
10
11 &TIME T_END=1800.0 DT=5/ /
12 &REAC FUEL='PROPANE', SOOT_YIELD=0.015 /
13 &DUMP SIG_FIGS=4, SIG_FIGS_EXP=2 /NFRAMES defines the total of frames per total time SIG_FIGS defines the p
14
15 &MISC HUMIDITY=0.81 /
16 &MISC RESTART=T, RESTART_CHID='ValidationStraling' /
17
18 &SURF ID='BRAND', HRRPUA=400, RAMP_Q='FLUX'/ KW per m2
19
20 &RAMP ID='FLUX', T=0, F=0.0/
21 &RAMP ID='FLUX', T=1, F=1.0/
22 &RAMP ID='FLUX', T=1799, F=1.0/
23 &RAMP ID='FLUX', T=1800, F=0.0/
24
25 &SPEC ID='WATER_VAPOR' /
26 &SPEC ID='CELLULOSE', FORMULA='C6H10O5' /
27
28 &SURF ID='WALL', ADIABATIC=.TRUE., THICKNESS=0.1 /
29
30 &SURF ID = 'wet_vegetation'
31   MATL_ID = 'dry_helix_hedera'
32   THICKNESS = 0.002
33   MOISTURE_FRACTION = 0.2251
34   SURFACE_VOLUME_RATIO = 3000.
35   LENGTH = 0.05
36   GEOMETRY = 'CYLINDRICAL' /
37
38 &MATL ID = 'dry_helix_hedera'
39   DENSITY = 250.
40   CONDUCTIVITY = 0.21
41   SPECIFIC_HEAT_RAMP= 'c_helix_hedra'
42   N_REACTIONS = 1
43   REFERENCE_TEMPERATURE = 268.
44   NU_MATL = 0.2
45   NU_SPEC = 0.8
46   SPEC_ID = 'CELLULOSE'
47   HEAT_OFREACTION= 1500
48   MATL_ID = 'CHAR' /
49
50 &MATL ID = 'MOISTURE'
51   DENSITY = 1000.
52   CONDUCTIVITY = 0.1
53   SPECIFIC_HEAT= 4.184
54   N_REACTIONS = 1
55   REFERENCE_TEMPERATURE = 100.
56   NU_SPEC = 1.0
57   SPEC_ID = 'WATER_VAPOR'
58   HEAT_OFREACTION= 2500. /
59
60 &MATL ID = 'CHAR'
61   DENSITY = 300.
62   CONDUCTIVITY = 0.05
63   SPECIFIC_HEAT_RAMP = 'c_char' /
```

```

64
65 &MATL ID = 'ASH'
66   DENSITY = 67.
67   CONDUCTIVITY = 0.1
68   SPECIFIC_HEAT_RAMP = 'c_ash'/
69
70 &RAMP ID = 'c_helix_hedra', T=293., F=1.236 /
71 &RAMP ID = 'c_helix_hedra', T=300., F=1.263 /
72 &RAMP ID = 'c_helix_hedra', T=400., F=1.650 /
73 &RAMP ID = 'c_helix_hedra', T=500., F=2.037 /
74 &RAMP ID = 'c_helix_hedra', T=600., F=2.424 /
75 &RAMP ID = 'c_helix_hedra', T=700., F=2.811 /
76 &RAMP ID = 'c_helix_hedra', T=800., F=3.197 /
77 &RAMP ID = 'c_helix_hedra', T=900., F=3.584 /
78 &RAMP ID = 'c_helix_hedra', T=1000., F=3.971 /
79 &RAMP ID = 'c_helix_hedra', T=1100., F=4.358 /
80 &RAMP ID = 'c_helix_hedra', T=1200., F=4.744 /
81
82 &RAMP ID = 'c_char', T=293., F=1.065 /
83 &RAMP ID = 'c_char', T=300., F=1.082 /
84 &RAMP ID = 'c_char', T=400., F=1.330 /
85 &RAMP ID = 'c_char', T=500., F=1.591 /
86 &RAMP ID = 'c_char', T=600., F=1.867 /
87 &RAMP ID = 'c_char', T=700., F=2.156 /
88 &RAMP ID = 'c_char', T=800., F=2.458 /
89 &RAMP ID = 'c_char', T=900., F=2.775 /
90 &RAMP ID = 'c_char', T=1000., F=3.105 /
91 &RAMP ID = 'c_char', T=1100., F=3.449 /
92 &RAMP ID = 'c_char', T=1200., F=3.806 /
93
94 &RAMP ID = 'c_ash', T=293., F=1.235 /
95 &RAMP ID = 'c_ash', T=300., F=1.244 /
96 &RAMP ID = 'c_ash', T=400., F=1.362 /
97 &RAMP ID = 'c_ash', T=500., F=1.461 /
98 &RAMP ID = 'c_ash', T=600., F=1.548 /
99 &RAMP ID = 'c_ash', T=700., F=1.625 /
100 &RAMP ID = 'c_ash', T=800., F=1.694 /
101 &RAMP ID = 'c_ash', T=900., F=1.758 /
102 &RAMP ID = 'c_ash', T=1000., F=1.818 /
103 &RAMP ID = 'c_ash', T=1100., F=1.873 /
104 &RAMP ID = 'c_ash', T=1200., F=1.925 /
105
106 &PART ID='plants', SAMPLING_FACTOR=1, SURF_ID='wet_vegetation', PROP_ID='needle_image', COLOR='FOREST_GREEN'
107   QUANTITIES='PARTICLE_TEMPERATURE','PARTICLE_MASS','PARTICLE_DIAMETER', STATIC=.TRUE. /
108
109 &INIT PART_ID='plants', XB=-0.25, 0.25, 0.17, 0.23 0.25, 1.75 , N_PARTICLES=4000, MASS_PER_VOLUME=42.16, DE
110
111 &PROP ID='needle_image', SMOKEVIEW_ID='TUBE', SMOKEVIEW_PARAMETERS='L=0.005', 'D=0.05' /
112
113 &PROP ID='Heat_Flux_Gauge', GAUGE_TEMPERATURE=50.0 /
114
115
116
117 &DEVC ID='1', QUANTITY='GAUGE_HEAT_FLUX', XYZ=0.01, 0.1, 0.25, IOR=2.0/behind vgs      dev1
118 &DEVC ID='2', QUANTITY='GAUGE_HEAT_FLUX', XYZ=0.01, 0.1, 1.0, IOR=2.0/                         dev2
119 &DEVC ID='3', QUANTITY='GAUGE_HEAT_FLUX', XYZ=0.01, 0.1, 1.5, IOR=2.0/                         dev3
120 &DEVC ID='4', QUANTITY='GAUGE_HEAT_FLUX', XYZ=0.01, 0.1, 2.0, IOR=2.0/meet de lijnbrander output dev4
121
122 &DEVC ID='x=-0.3_0.0', QUANTITY='TEMPERATURE', XYZ=-0.25, 0.15, 0.0, IOR=2.0/x=-0.3 LINE dev5
123 &DEVC ID='x=-0.3_0.1', QUANTITY='TEMPERATURE', XYZ=-0.25, 0.15, 0.1, IOR=2.0/x=-0.3 LINE dev6
124 &DEVC ID='x=-0.3_0.2', QUANTITY='TEMPERATURE', XYZ=-0.25, 0.15, 0.2, IOR=2.0/x=-0.3 LINE dev7
125 &DEVC ID='x=-0.3_0.3', QUANTITY='TEMPERATURE', XYZ=-0.25, 0.15, 0.3, IOR=2.0/x=-0.3 LINE dev8
126 &DEVC ID='x=-0.3_0.4', QUANTITY='TEMPERATURE', XYZ=-0.25, 0.15, 0.4, IOR=2.0/x=-0.3 LINE dev9
127 &DEVC ID='x=-0.3_0.5', QUANTITY='TEMPERATURE', XYZ=-0.25, 0.15, 0.5, IOR=2.0/x=-0.3 LINE dev10
128 &DEVC ID='x=-0.3_0.6', QUANTITY='TEMPERATURE', XYZ=-0.25, 0.15, 0.6, IOR=2.0/x=-0.3 LINE dev11
129 &DEVC ID='x=-0.3_0.7', QUANTITY='TEMPERATURE', XYZ=-0.25, 0.15, 0.7, IOR=2.0/x=-0.3 LINE dev12
130 &DEVC ID='x=-0.3_0.8', QUANTITY='TEMPERATURE', XYZ=-0.25, 0.15, 0.8, IOR=2.0/x=-0.3 LINE dev13
131 &DEVC ID='x=-0.3_0.9', QUANTITY='TEMPERATURE', XYZ=-0.25, 0.15, 0.9, IOR=2.0/x=-0.3 LINE dev14

```



```

268 &DEVC ID='z=1.1_-0.75', QUANTITY='TEMPERATURE', XYZ=-0.75, 0.15, 1.1, IOR=2.0/z=0.75 LINE dev166
269 &DEVC ID='z=1.1_-0.65', QUANTITY='TEMPERATURE', XYZ=-0.65, 0.15, 1.1, IOR=2.0/z=0.75 LINE dev167
270 &DEVC ID='z=1.1_-0.55', QUANTITY='TEMPERATURE', XYZ=-0.55, 0.15, 1.1, IOR=2.0/z=0.75 LINE dev168
271 &DEVC ID='z=1.1_-0.45', QUANTITY='TEMPERATURE', XYZ=-0.45, 0.15, 1.1, IOR=2.0/z=0.75 LINE dev169
272 &DEVC ID='z=1.1_-0.35', QUANTITY='TEMPERATURE', XYZ=-0.35, 0.15, 1.1, IOR=2.0/z=0.75 LINE dev170
273 &DEVC ID='z=1.1_-0.25', QUANTITY='TEMPERATURE', XYZ=-0.25, 0.15, 1.1, IOR=2.0/z=0.75 LINE dev171
274 &DEVC ID='z=1.1_-0.15', QUANTITY='TEMPERATURE', XYZ=-0.15, 0.15, 1.1, IOR=2.0/z=0.75 LINE dev172
275 &DEVC ID='z=1.1_-0.05', QUANTITY='TEMPERATURE', XYZ=-0.05, 0.15, 1.1, IOR=2.0/z=0.75 LINE dev173
276 &DEVC ID='z=1.1_0.05', QUANTITY='TEMPERATURE', XYZ=0.05, 0.15, 1.1, IOR=2.0/z=0.75 LINE dev174
277 &DEVC ID='z=1.1_0.15', QUANTITY='TEMPERATURE', XYZ=0.15, 0.15, 1.1, IOR=2.0/z=0.75 LINE dev175
278 &DEVC ID='z=1.1_0.25', QUANTITY='TEMPERATURE', XYZ=0.25, 0.15, 1.1, IOR=2.0/z=0.75 LINE dev176
279 &DEVC ID='z=1.1_0.35', QUANTITY='TEMPERATURE', XYZ=0.35, 0.15, 1.1, IOR=2.0/z=0.75 LINE dev177
280 &DEVC ID='z=1.1_0.45', QUANTITY='TEMPERATURE', XYZ=0.45, 0.15, 1.1, IOR=2.0/z=0.75 LINE dev178
281 &DEVC ID='z=1.1_0.55', QUANTITY='TEMPERATURE', XYZ=0.55, 0.15, 1.1, IOR=2.0/z=0.75 LINE dev179
282 &DEVC ID='z=1.1_0.65', QUANTITY='TEMPERATURE', XYZ=0.65, 0.15, 1.1, IOR=2.0/z=0.75 LINE dev180
283 &DEVC ID='z=1.1_0.75', QUANTITY='TEMPERATURE', XYZ=0.75, 0.15, 1.1, IOR=2.0/z=0.75 LINE dev181
284 &DEVC ID='z=1.1_0.85', QUANTITY='TEMPERATURE', XYZ=0.85, 0.15, 1.1, IOR=2.0/z=0.75 LINE dev182
285 &DEVC ID='z=1.1_0.95', QUANTITY='TEMPERATURE', XYZ=0.95, 0.15, 1.1, IOR=2.0/z=0.75 LINE dev183
286 &DEVC ID='z=1.1_1.05', QUANTITY='TEMPERATURE', XYZ=1.05, 0.15, 1.1, IOR=2.0/z=0.75 LINE dev184
287 &DEVC ID='z=1.1_1.15', QUANTITY='TEMPERATURE', XYZ=1.15, 0.15, 1.1, IOR=2.0/z=0.75 LINE dev185
288 &DEVC ID='z=1.1_1.2', QUANTITY='TEMPERATURE', XYZ=1.25, 0.15, 1.1, IOR=2.0/z=0.75 LINE dev186
289
290
291
292 &DEVC XB=-1.75,1.75,-0.25,1.5,0,3 , QUANTITY='DENSITY', ID='fuel_gas_mass', SPATIAL_STATISTIC='VOLUME_INTEGRAL'
293 &DEVC XB=-1.75,1.75,-0.25,1.5,0,3 , QUANTITY='DENSITY', ID='water_vapor_mass', SPATIAL_STATISTIC='VOLUME_INTEGRAL'
294 &DEVC XB=-1.75,1.75,-0.1,1.5,0,3 , QUANTITY='MPUV', PART_ID='plants', ID='solid_mass', SPATIAL_STATISTIC='VOLUME_INTEGRAL'
/
295
296
297 &OBST ID='Adiabatic_wall', XB=-1.25, 1.25, 0.0, 0.1, 0.0, 3.5, RGB=211,211,211, , SURF_ID='WALL', TRANSPARENCY=0.6/ adiabatic Wall
298
299 &OBST ID='Adiabatic_side_wall_left', XB=-0.45, -0.35, 0.1, 0.3, 0.0, 1 RGB=211,211,211, SURF_ID='WALL', TRANSPARENCY=0.6/ adiabatic Wall
300 &OBST ID='Adiabatic_side_wall_right', XB=0.35, 0.45, 0.1, 0.3, 0.0, 1 RGB=211,211,211, SURF_ID='WALL', TRANSPARENCY=0.6/ adiabatic Wall
301
302 &OBST XB=-0.25, 0.25, 0.17, 0.27, 0.0, 0.15, COLOR='RED', TRANSPARENCY=5, SURF_IDS='BRAND', 'WALL', 'WALL', /
303
304
305 &VENT MB='XMIN', SURF_ID='OPEN' /
306 &VENT MB='XMAX', SURF_ID='OPEN' /
307 &VENT MB='YMIN', SURF_ID='OPEN' /
308 &VENT MB='YMAX', SURF_ID='OPEN' /
309 &VENT MB='ZMAX', SURF_ID='OPEN' /
310
311 &BNDF QUANTITY='GAUGE_HEAT_FLUX'/
312
313 &SLCF PBX=0.0, QUANTITY='TEMPERATURE', CELL_CENTERED=.TRUE. /shows temp of X plane in center
314 &SLCF PBY=0.15, QUANTITY='TEMPERATURE', CELL_CENTERED=.TRUE. /shows temp of Y plane in center
315 &SLCF PBZ=0.4, QUANTITY='TEMPERATURE', CELL_CENTERED=.TRUE. /shows temp of Z plane in center
316
317
318
319 &TAIL /

```

B.2 GCI Calculation Code Matlab

```

1 clear all
2
3 %% Refinement ratio
4 %definition Mesh1 = coarse, Mesh2= medium, Mesh3= fine
5 r21 = 4/2; %coarse medium mesh
6 r32 = 2/1;%medium fine mesh
7

```

```

8
9 %% Import results
10 %import mesh 1 COARSE
11 Mesh1=importdata("1000 HRRPUA\kleiner mesh in cm\dynamisch\4 cm point of interest\
12 ValidationStraling_devc.csv"); %coarse mesh 4cm
13 header1 = Mesh1.colheaders;
14 Mesh1= Mesh1.data;
15 Mesh1Table = array2table(Mesh1);
16 Mesh1Table.Properties.VariableNames = header1;
17 Mesh1Table = Mesh1Table(1:1000, :);
18
19 %import mesh 2 MEDIUM
20 Mesh2=importdata("1000 HRRPUA\kleiner mesh in cm\dynamisch\2 cm point of interest\2\
21 ValidationStraling_devc.csv"); %medium mesh 2cm
22 header2 = Mesh2.colheaders;
23 Mesh2= Mesh2.data;
24 Mesh2Table = array2table(Mesh2);
25 Mesh2Table.Properties.VariableNames = header2;
26
27
28 %import mesh 3 FINE
29 Mesh3=importdata("1000 HRRPUA\kleiner mesh in cm\dynamisch\1cm point of interest\
30 ValidationStraling_devc.csv"); %fine mesh 1cm
31 header3 = Mesh3.colheaders;
32 Mesh3= Mesh3.data;
33 Mesh3Table = array2table(Mesh3);
34 Mesh3Table.Properties.VariableNames = header3;
35
36
37
38 disp('import\u2022done');
39 %% Average temperatures of lines Mesh1 COARSE
40
41 %coarse vertical line 1 at x=-0.3
42 M1V1T = Mesh1Table(:,6:41);
43 M1V1median = median(M1V1T);
44 M1V1 = table2array(M1V1median);
45 M1V1 = reshape(M1V1, [], 1);
46
47 %coarse vertical line 2 at x=0
48 M1V2T = Mesh1Table(:,42:77);
49 M1V2median = median(M1V2T);
50 M1V2 = table2array(M1V2median);
51 M1V2 = reshape(M1V2, [], 1);
52
53 %coarse vertical line 3 at x=0.3
54 M1V3T = Mesh1Table(:,78:113);
55 M1V3median = median(M1V3T);
56 M1V3 = table2array(M1V3median);
57 M1V3 = reshape(M1V3, [], 1);
58
59
60 %coarse horizontal line 1 at z=0.7
61 M1H1T = Mesh1Table(:,114:137);
62 M1H1median = median(M1H1T);
63 M1H1 = table2array(M1H1median);
64 M1H1 = reshape(M1H1, [], 1);
65
66 %coarse horizontal line 2
67 M1H2T = Mesh1Table(:,138:161);
68 M1H2median = median(M1H2T);
69 M1H2 = table2array(M1H2median);
70 M1H2 = reshape(M1H2, [], 1);
71
72 disp('mesh\u20221\u2022coarse\u2022lines\u2022done');
73 %% average temperatures of lines mid
74
75 %mid vertical line 1

```

```

76 M2V1T = Mesh2Table(:,6:41);
77 M2V1median = median(M2V1T);
78 M2V1 = table2array(M2V1median);
79 M2V1 = reshape(M2V1, [], 1);
80
81
82 %mid vertical line 2
83 M2V2T = Mesh2Table(:,42:77);
84 M2V2median = median(M2V2T);
85 M2V2 = table2array(M2V2median);
86 M2V2 = reshape(M2V2, [], 1);
87
88 %mid vertical line 3
89 M2V3T = Mesh2Table(:,78:113);
90 M2V3median = median(M2V3T);
91 M2V3 = table2array(M2V3median);
92 M2V3 = reshape(M2V3, [], 1);
93
94
95 %mid horizontal line 1
96 M2H1T = Mesh2Table(:,114:137);
97 M2H1median = median(M2H1T);
98 M2H1 = table2array(M2H1median);
99 M2H1 = reshape(M2H1, [], 1);
100
101 %mid horizontal line 2
102 M2H2T = Mesh2Table(:,138:161);
103 M2H2median = median(M2H2T);
104 M2H2 = table2array(M2H2median);
105 M2H2 = reshape(M2H2, [], 1);
106
107 disp('mesh_2_medium_lines_done');
108 %% average temperatures of lines Fine
109
110 %fine vertical line 1
111 M3V1T = Mesh3Table(:,6:41);
112 M3V1median = median(M3V1T);
113 M3V1 = table2array(M3V1median);
114 M3V1 = reshape(M3V1, [], 1);
115
116 %fine vertical line 2
117 M3V2T = Mesh3Table(:,42:77);
118 M3V2median = median(M3V2T);
119 M3V2 = table2array(M3V2median);
120 M3V2 = reshape(M3V2, [], 1);
121
122 %fine vertical line 3
123 M3V3T = Mesh3Table(:,78:113);
124 M3V3median = median(M3V3T);
125 M3V3 = table2array(M3V3median);
126 M3V3 = reshape(M3V3, [], 1);
127
128
129 %fine horizontal line 1
130 M3H1T = Mesh3Table(:,114:137);
131 M3H1median = median(M3H1T);
132 M3H1 = table2array(M3H1median);
133 M3H1 = reshape(M3H1, [], 1);
134
135 %fine horizontal line 2
136 M3H2T = Mesh3Table(:,138:161);
137 M3H2median = median(M3H2T);
138 M3H2 = table2array(M3H2median);
139 M3H2 = reshape(M3H2, [], 1);
140
141 disp('mesh_3_fine_lines_done');
142 %% Calculating the P (apparent order of accuracy)

```

```

144 %P of vertical line 1
145 %P_V1 = log((M1V1-M2V1)./(M2V1-M3V1)) / log(r21);
146 P_V1 = (M1V1-M2V1) / (M2V1-M3V1);
147 den = log(2);
148 if P_V1 <= 0
149     error('Invalid GCI calculation: log argument is negative or zero.');
150 end
151 nonZeroCols = any(P_V1 ~= 0, 1); %checks non zero values in each column
152 P_V1 = P_V1(:, nonZeroCols);
153 P_V1 = abs(P_V1);
154 P_V1=log(P_V1)/den;
155 P_V1 = mean(P_V1);
156 disp 'done'

157
158
159 %vertical 2
160 P_V2 = (M1V2-M2V2) / (M2V2-M3V2);
161
162 if any((M1V2-M2V2) / (M2V2-M3V2) < 0)
163     warning('Non-monotonic convergence V2 detected. Check your results.');
164 end
165 nonZeroCols = any(P_V2 ~= 0, 1); %checks non zero values in each column
166 P_V2 = P_V2(:, nonZeroCols);
167 P_V2 = abs(P_V2);
168 P_V2=log(P_V2)/den;
169 P_V2 = mean(P_V2);

170
171 %vertical 3
172 P_V3 = (M1V3-M2V3) / (M2V3-M3V3);
173
174 if any((M1V3-M2V3) / (M2V3-M3V3) < 0)
175     warning('Non-monotonic convergence V3 detected. Check your results.');
176 end
177
178 nonZeroCols = any(P_V3 ~= 0, 1); %checks non zero values in each column
179 P_V3 = P_V3(:, nonZeroCols);
180
181 P_V3 = abs(P_V3);
182 P_V3 = log(P_V3)/den;
183 P_V3 = mean(P_V3);

184
185
186 %P of horizontal line 1
187 P_H1 = (M1H1-M2H1) / (M2H1-M3H1);
188
189 if any((M1H1-M2H1) / (M2H1-M3H1) < 0)
190     warning('Non-monotonic convergence H1 detected. Check your results.');
191 end
192 nonZeroCols = any(P_H1 ~= 0, 1); %checks non zero values in each column
193 P_H1 = P_H1(:, nonZeroCols);
194
195 P_H1 = abs(P_H1);
196 P_H1 = log(P_H1)/den;
197 P_H1 = mean(P_H1);

198
199 %horizontal 2
200 P_H2 = (M1H2-M2H2) / (M2H2-M3H2);
201
202 if any((M1H2-M2H2) / (M2H2-M3H2) < 0)
203     warning('Non-monotonic convergence H2 detected. Check your results.');
204 end
205 nonZeroCols = any(P_H2 ~= 0, 1); %checks non zero values in each column
206 P_H2 = P_H2(:, nonZeroCols);
207 P_H2 = abs(P_H2);
208 P_H2 = log(P_H2)/den;
209 P_H2 = mean(P_H2);

210
211

```

```

212 %whole average p of coarse medium grid
213 P_avg = (abs(P_V1+P_V2+P_V3+P_H1+P_H2))/5 ;
214
215 disp('P_calculation done');
216
217 %% calculating the epsilon aka the relative error this is of the coarse medium M21
218 %medium coarse mesh
219
220 eps21V1 = ((M2V1-M1V1)./M2V1);
221 eps21V2 = ((M2V2-M1V2)./M2V2);
222 eps21V3 = ((M2V3-M1V3)./M2V3);
223
224 eps21H1 = ((M2H1-M1H1)./M2H1);
225 eps21H2 = ((M2H2-M1H2)./M2H2);
226
227 disp('relative error M21 done');
228
229 %% GCI Calculation of Coarse Medium M21
230
231 %vertical 1
232 r1 = r21^P_avg;
233 GCI21V1= (1.25/(r1-1)) * abs(eps21V1);
234 GCI21V1 = median(GCI21V1);
235
236 %vertical 2
237 r2 = r21^P_avg;
238 GCI21V2= (1.25/(r2-1)) * abs(eps21V2);
239 GCI21V2 = median(GCI21V2);
240
241 %vertical 3
242 r3 = r21^P_avg;
243 GCI21V3= (1.25/(r3-1)) * abs(eps21V3);
244 GCI21V3 = median(GCI21V3);
245
246 %horizontal 1
247 r4 = r21^P_avg;
248 GCI21H1= (1.25/(r4-1)) * abs(eps21H1);
249 GCI21H1 = median(GCI21H1);
250
251 %horizontal 2
252 r5 = r21^P_avg;
253 GCI21H2= (1.25/(r5-1)) * abs(eps21H2);
254 GCI21H2 = median(GCI21H2);
255
256 %overall GCI
257 GCI_M21 =(GCI21V1+GCI21V2+GCI21V3+GCI21H1+GCI21H2);
258 GCI_M21 = 0.2* GCI_M21;
259 GCI_M21pr = GCI_M21*100
260
261 disp('GCI M21 done');
262
263 %% GCI calculation with overall average p M21
264 r_Pavg = 2^P_avg
265 %vertical 1
266 GCI21V1_Pavg= (1.25/(r_Pavg-1)) * abs(eps21V1);
267
268 %vertical 2
269 GCI21V2_Pavg= (1.25/(r_Pavg-1)) * abs(eps21V2);
270
271 %vertical 3
272 GCI21V3_Pavg= (1.25/(r_Pavg-1)) * abs(eps21V3);
273
274 %horizontal 1
275 GCI21H1_Pavg= (1.25/(r_Pavg-1)) * abs(eps21H1);
276
277 %horizontal 2
278 GCI21H2_Pavg= (1.25/(r_Pavg-1)) * abs(eps21H2);
279

```

```

280 %overall GCI
281 GCI_M21_Pavg = (1/5)*(GCI21V1_Pavg+GCI21V2_Pavg+GCI21V3_Pavg+GCI21H1_Pavg+GCI21H2_Pavg);
282 GCI_M21pr_Pavg = GCI_M21_Pavg*100
283
284 disp('GCI21 with average P taken done');
285 %%
286
287 %% calculating the epsilon aka the relative error this is of the medium fine M32
288 %fine medium mesh
289
290 eps32V1 = ((M3V1-M2V1)./M3V1);
291 eps32V2 = ((M3V2-M2V2)./M3V2);
292 eps32V3 = ((M3V3-M2V3)./M3V3);
293
294 eps32H1 = ((M3H1-M2H1)./M3H1);
295 eps32H2 = ((M3H2-M2H2)./M3H2);
296
297 disp('relative error M32 done');
298 %% GCI Calculation of Medium Fine M32
299
300 %vertical 1
301 GCI21V1= (1.25/(r1-1)) * abs(eps32V1);
302
303 %vertical 2
304 GCI21V2= (1.25/(r2-1)) * abs(eps32V2);
305
306 %vertical 3
307 GCI21V3= (1.25/(r3-1)) * abs(eps32V3);
308
309 %horizontal 1
310 GCI21H1= (1.25/(r4-1)) * abs(eps32H1);
311
312 %horizontal 2
313 GCI21H2= (1.25/(r5-1)) * abs(eps32H2);
314
315 %overall GCI
316 GCI_M32 = (1/5)*(GCI32V1+GCI32V2+GCI32V3+GCI32H1+GCI32H2);
317 GCI_M32pr = GCI_M31*100
318
319 disp('GCI M32 done');
320 %% GCI calculation with overall average p M21
321 r_Pavg = 2^P_avg;
322 %vertical 1
323 GCI21V1_Pavg= (1.25/(r_Pavg-1)) * abs(eps21V1);
324
325 %vertical 2
326 GCI21V2_Pavg= (1.25/(r_Pavg-1)) * abs(eps21V2);
327
328 %vertical 3
329 GCI21V3_Pavg= (1.25/(r_Pavg-1)) * abs(eps21V3);
330
331 %horizontal 1
332 GCI21H1_Pavg= (1.25/(r_Pavg-1)) * abs(eps21H1);
333
334 %horizontal 2
335 GCI21H2_Pavg= (1.25/(r_Pavg-1)) * abs(eps21H2);
336
337 %overall GCI
338 GCI_M21_Pavg = (1/5)*(GCI21V1_Pavg+GCI21V2_Pavg+GCI21V3_Pavg+GCI21H1_Pavg+GCI21H2_Pavg);
339 GCI_M21pr_Pavg = GCI_M21_Pavg*100
340
341 disp('GCI M32 with average P taken done');

```

B.3 Matlab Code for Creating Average Temperature Image

```

1 %% import video for screen average

```

```

2 | temperatureVideo = "1000_HRRPUA\kleiner mesh in cm\dynamisch\2 cm point of interest\video\
3 | ValidationStraling01.mp4"; % Change this to your file
4 |
5 | TempVideo1 = VideoReader(temperatureVideo);
6 |
7 | % Get video dimensions
8 | frameHeight = TempVideo1.Height;
9 | frameWidth = TempVideo1.Width;
10 | numFrames = TempVideo1.NumFrames;
11 |
12 | averageFrame = zeros(frameHeight, frameWidth, 3, 'double'); % Assuming RGB video
13 |
14 | frameCount = 0;
15 | while hasFrame(TempVideo1)
16 |     frame = double(readFrame(TempVideo1)); % Read frame and convert to double
17 |     averageFrame = averageFrame + frame;
18 |     frameCount = frameCount + 1;
19 | end
20 |
21 |
22 | % Compute the average image
23 | averageFrame = averageFrame / frameCount;
24 |
25 | % Convert back to uint8 format for display
26 | averageImage = uint8(averageFrame);
27 |
28 | % Display the average image
29 | imshow(averageImage);
30 | title('Average Temperature Image');
31 |
32 | % Optionally, save the output
33 | imwrite(averageImage, 'average_temperature_image.png');

```

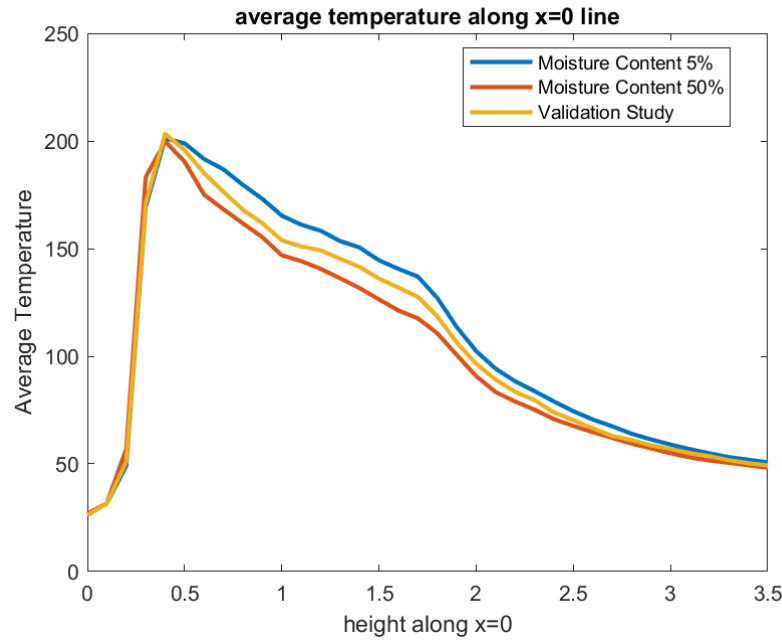


Figure 98: Average Temperatures Recorded along $x=0$

C Application Studies

C.1 Moisture Simulations

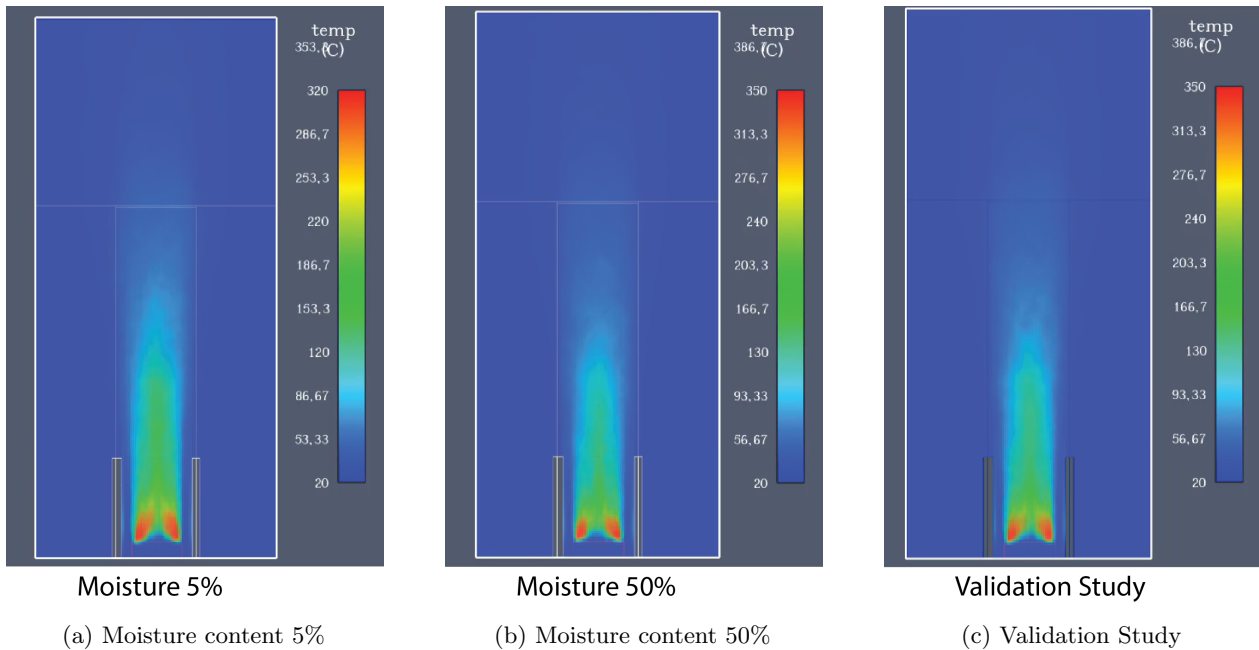
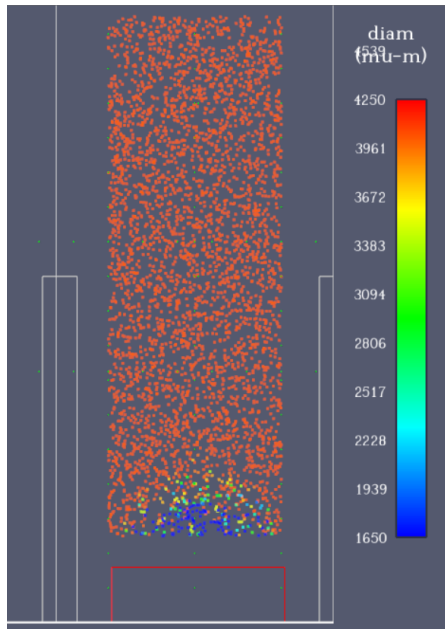
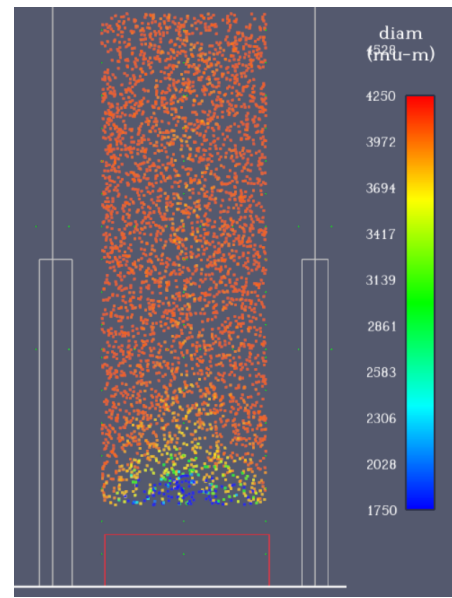


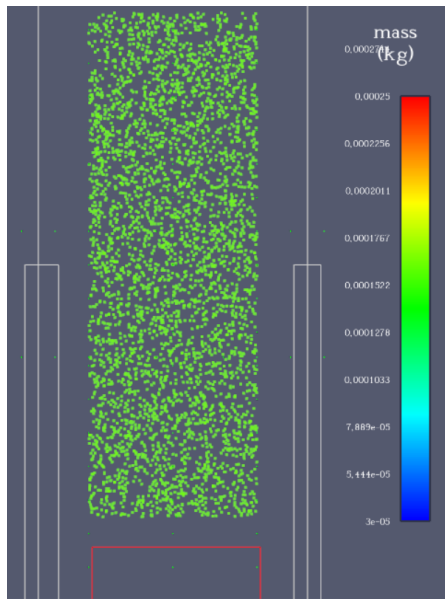
Figure 99: Average temperature image different moisture levels



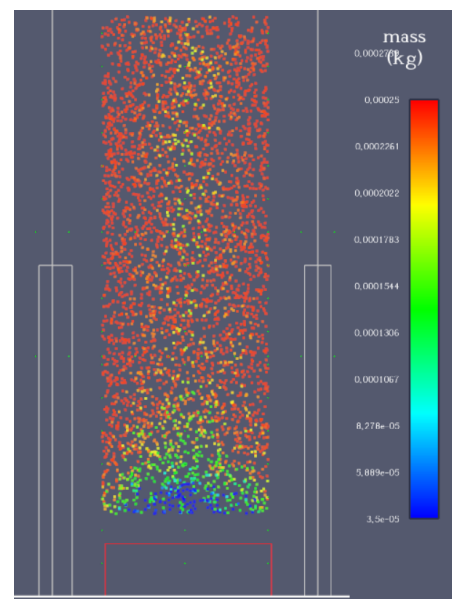
(a) Moisture content 5% - Particle Diameter at 350 sec



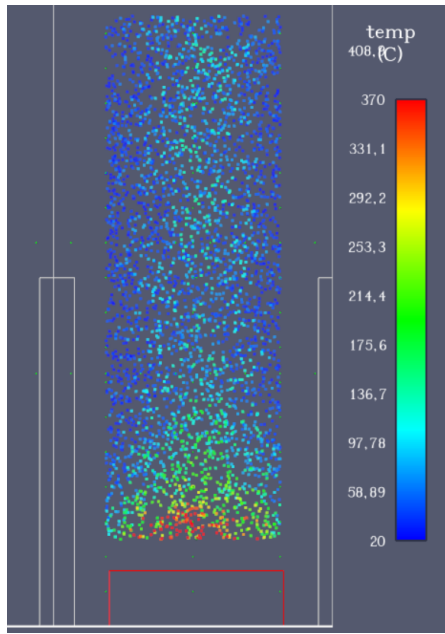
(b) Moisture content 50% - Particle Diameter at 350 sec



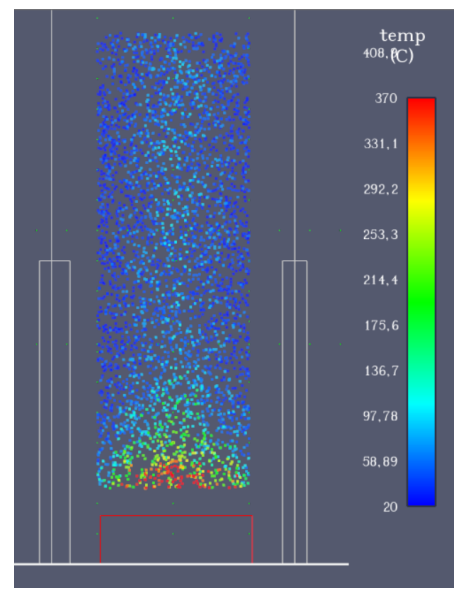
(a) Moisture content 5% - Particle Mass at 350 sec



(b) Moisture content 50% - Particle Mass at 350 sec

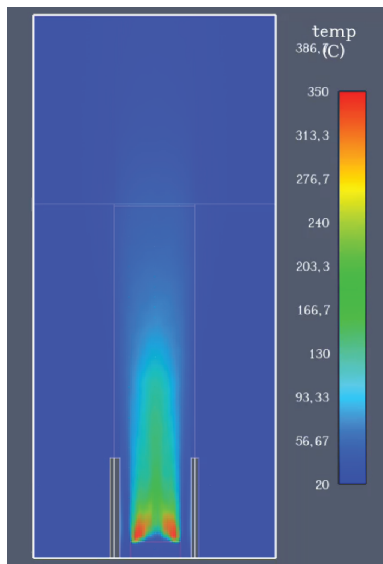


(a) Moisture content 5% - Particle Temperature at 350 sec

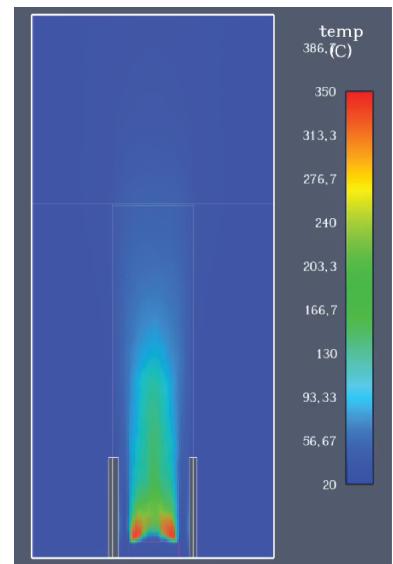


(b) Moisture content 50% - Particle Temperature at 350 sec

C.2 Leaf Area Simulations

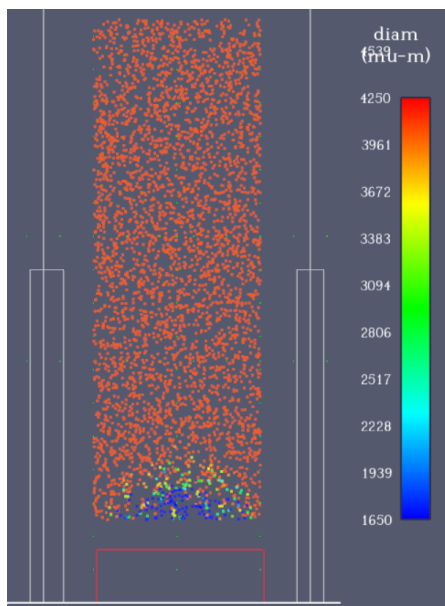


Small Leaf

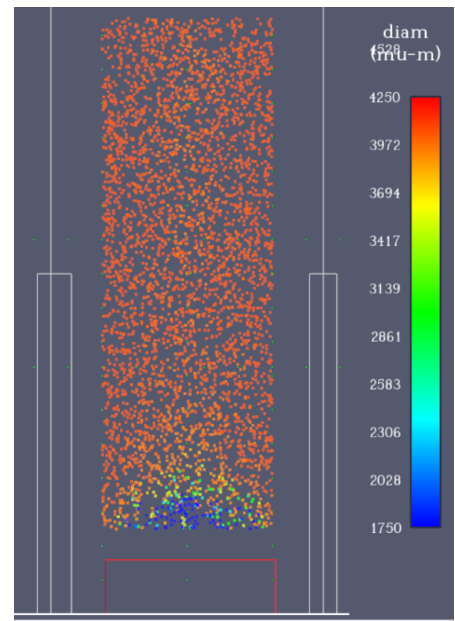


Large Leaf

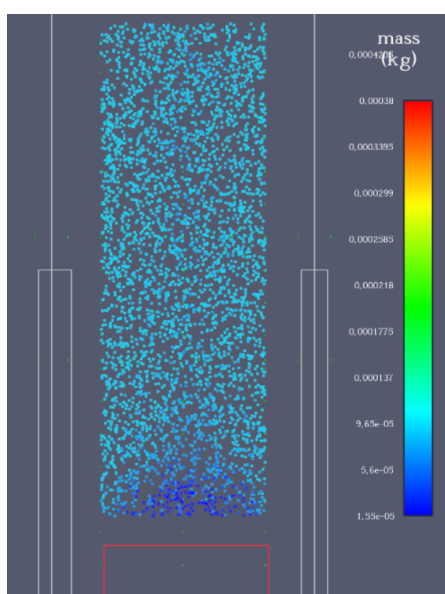
Figure 103: Average temperature image different moisture levels



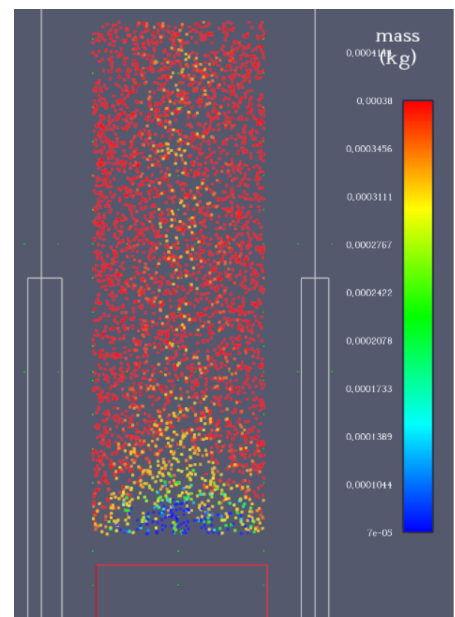
(a) Small Leaf - Particle Diamter at 350 sec



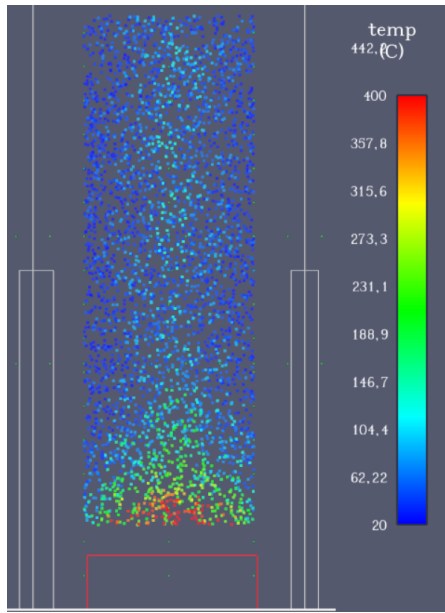
(b) Large leaf - Particle Diameter at 350 sec



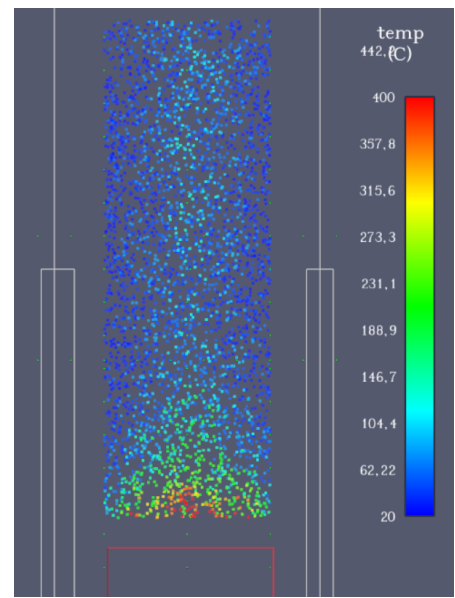
(a) Small leaf - Particle Mass at 350 sec



(b) Large leaf - Particle Mass at 350 sec



(a) Small leaf - Particle Temperature at 350 sec

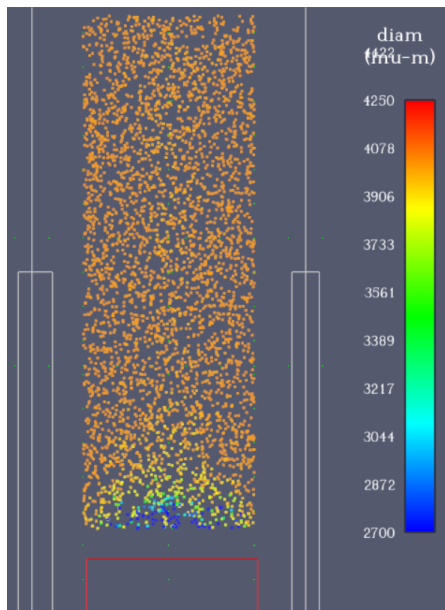


(b) Moisture content 50% - Particle Temperature at 350 sec

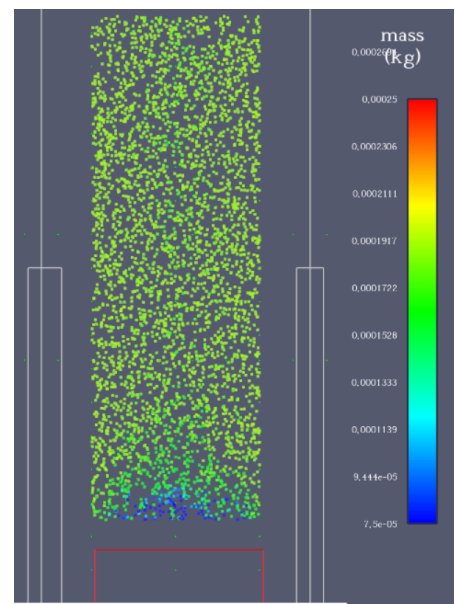
C.3 Vegetation Density

C.4 Lower Ignition Temperature

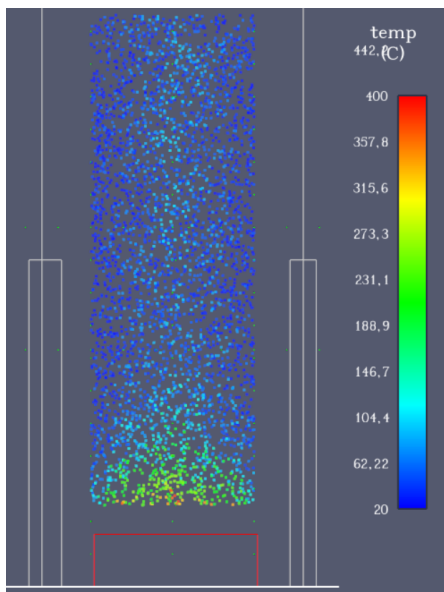
C.5 Removing Line Burner



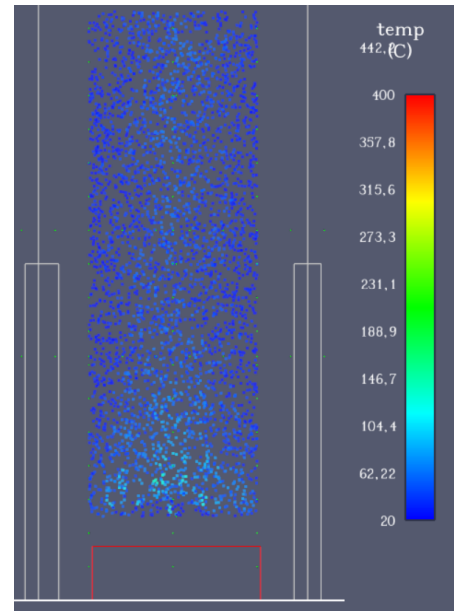
(a) Removing Lineburner - Particle Diameter at 350 sec



(b) LineBurner - Particle Mass at 350 sec



(a) Removing Lineburner - Particle temperature at 150 sec



(b) Removing Lineburner - Particle temperature at 180 sec

C.6 Elementary Effects Matlab Code

```

1  %% The input parameters, add all different simulations done!
2
3 StudyNames = {'Validation'; 'Low_Moisture'; 'High_Moisture'; 'Small_Leaf'; 'Large_Leaf';
4 'Low_Density'; 'High_Density'; 'Burning_Temperature'}
5 MoistureContent = [22.51; 5; 50; 22.51; 22.51; 22.51; 22.51; 22.51];
6 LeafArea = [0.05; 0.05; 0.05; 0.025; 0.10; 0.05; 0.05; 0.05];
7 PlantDensity = [42.16; 42.16; 42.16; 42.16; 42.16; 20; 80; 42.16];
8 BurningTemperature = [268; 268; 268; 268; 268; 268; 268; 200];
9
10 input_params_table = table(MoistureContent, LeafArea, PlantDensity, BurningTemperature);
11 input_params_table_with_names = table(StudyNames, MoistureContent, LeafArea, PlantDensity,
12 BurningTemperature);
13
14 num_params = size(input_params_table, 2); % (2 looks at columns) returns the total number of
15 changed parameters
16 num_runs = size(input_params_table, 1); % (1 looks at rows) the total number of
17 simulations which have been completed
18
19
20 %% importing the output values
21 output_folder = '01_output_folder_for_EE'; % Select the folder manually because the path doesn't work for
22 output_files = dir(fullfile(output_folder, '*.mat'));
23
24 output_files = dir(fullfile(output_folder, '*.mat')); % Get all .mat files in the folder
25
26 num_runs = length(output_files); % Number of files (simulations)
27 output_tables = cell(num_runs, 1); % Initialize cell array to store tables
28
29 % Load each .mat file in the loop
30 for i = 1:num_runs
31     file_path = fullfile(output_folder, output_files(i).name);

```

```

32 % Load .mat file (this returns a structure)
33 data = load(file_path);
34
35 % Get the table name(s) inside the .mat file
36 table_names = fieldnames(data); % Extract variable names in the file
37
38 % Extract the first variable (assuming it's a table)
39 output_tables{i} = data.(table_names{1});
40
41 % Display confirmation
42 fprintf('Loaded: %s\n', output_files(i).name);
43
44 end
45
46 % Convert tables to arrays and remove the first column (Datetime) because
47 % this will influence the output
48 output_values = cellfun(@(x) table2array(x(:, 2:end)), output_tables, 'UniformOutput', false);
49
50 output_matrix = vertcat(output_values{:}); % Convert the cleaned cell array to a numerical
51 matrix otherwise it doesn't work
52
53 %% My input table needs to match the number of my output matrix
54 % Extract number of rows for each output table
55 num_output_rows = cellfun(@(x) size(x, 1), output_tables);
56 disp(num_output_rows); % Check the row count for each simulation
57 % Create an expanded input table by repeating each row according to output row count
58 input_params_table_expanded = repelem(input_params_table, num_output_rows, 1);
59
60 %check if they match
61 disp(size(input_params_table_expanded)); % Should match total rows in output_matrix
62 disp(size(output_matrix)); % Output should match input
63
64 %% combine the temperature outputs so it becomes a readable table
65 % Define which columns contain temperature values (e.g., columns 1 to 50)
66 temperature_columns = 5:160; % Adjust this based on your data structure
67
68 % Compute an overall temperature metric to median temp
69 T_median = median(output_matrix(:, temperature_columns), 2); % Median Temperature
70 output_combined = T_median; % Replace with T_max or T_median if preferred
71
72 % Remove old temperature columns and replace them with the combined value
73 output_matrix(:, temperature_columns(1)) = output_combined; % Store in first temp column
74 output_matrix(:, temperature_columns(2:end)) = []; % Remove extra columns
75
76 %%
77 % The input parameters need to be normalized for the EE method
78 % Extract numerical input parameters
79 input_params = table2array(input_params_table_expanded); % Convert table to array
80
81 % Compute min and max for each parameter
82 X_min = min(input_params);
83 X_max = max(input_params);
84
85 % Normalize input parameters
86 input_params_norm = (input_params - X_min) ./ (X_max - X_min);
87
88 % Convert back to table (optional, to keep structured data)
89 input_params_table_norm = array2table(input_params_norm, 'VariableNames', input_params_table.Properties.VariableNames);
90
91 % Normalized input table for EE method
92 disp(input_params_table_norm);
93
94 % Define step size (should be within [0,1] normalized space)
95 Delta = 0.1;
96
97 %%
98 % Convert the normalized input parameters table to an array for computation
99 input_params_array = table2array(input_params_table_norm);

```

```

100
101 % Get the number of parameters and outputs
102 num_params = size(input_params_array, 2); % Number of varied parameters
103 num_outputs = size(output_matrix, 2); % Number of output variables
104 num_runs = size(output_matrix, 1); % Number of simulations
105
106
107 % Initialize Elementary Effects matrix
108 EE = zeros(num_runs, num_params, num_outputs);
109 % Compute Elementary Effects for each parameter and output
110 for i = 1:num_params % Loop over parameters
111     for j = 1:num_runs % Loop over runs
112         % Identify the perturbed input row (by checking variations)
113         for k = 1:num_runs
114             if input_params_array(j, i) ~= input_params_array(k, i) && sum(input_params_array(j, :) ~= input_params_array(k, :)) == 1
115                 for o = 1:num_outputs
116                     EE(j, i, o) = (output_matrix(k, o) - output_matrix(j, o)) / Delta;
117                 end
118             end
119         end
120     end
121 end
122
123
124 % Remove zero rows (cases where no proper comparison was found)
125 EE(EE == 0) = NaN; % Set to NaN for better averaging
126
127 % Compute Mean and Standard Deviation of Elementary Effects
128 mu = squeeze(nanmean(abs(EE), 1)); % Mean of absolute EE (sensitivity measure)
129 sigma = squeeze(nanstd(EE, 0, 1)); % Standard deviation (variability measure)
130
131 % Display results
132 disp('Mean Elementary Effects (mu):');
133 disp(mu);
134
135 disp('Standard Deviation (sigma):');
136 disp(sigma);

```